(2)

THEORETICAL AND EXPERIMENTAL STUDY OF THERMOACOUSTIC ENGINES

Richard Raspet, Henry E. Bass and W. Pat Arnott
Physical Acoustics Research Group
University of Mississippi
University, Mississippi 38677

FINAL REPORT

THE OFFICE OF NAVAL RESEARCH
CONTRACT #N00014-89-J-3087

PARGUM REPORT 92-03

DECEMBER 1992

UNCLASSIFIED
SECURITY CLASSIFICATION OF THIS PAGE

REPORT DOCUMENTATION PAGE

Form Approved OMB No. 0704-0188

1a. REPORT SECURITY CLASSIFICATION: Unclassified	1b. RESTRICTIVE MARKINGS
2a. SECURITY CLASSIFICATION AUTHORITY	3. DISTRIBUTION/AVAILABILITY OF REPORT: Approval for public release; distribution unlimited
2b. DECLASSIFICATION/DOWNGRADING SCHEDULE	
4. PERFORMING ORGANIZATION REPORT NUMBER(S): PARGUM 92-03	5. MONITORING ORGANIZATION REPORT NUMBER(S)
6a. NAME OF PERFORMING ORGANIZATION: University of Mississippi; 6b. OFFICE SYMBOL (If applicable)	7a. NAME OF MONITORING ORGANIZATION: Office of Naval Research
6c. ADDRESS (City, State, and ZIP Code): Dept. of Physics & Astronomy, University of Mississippi, University, MS 38677	7b. ADDRESS (City, State, and ZIP Code): Physics Division, Code 1112, Arlington, VA 22217-5660
8a. NAME OF FUNDING/SPONSORING ORGANIZATION; 8b. OFFICE SYMBOL (If applicable)	9. PROCUREMENT INSTRUMENT IDENTIFICATION NUMBER: N00014-89-J-3087
8c. ADDRESS (City, State, and ZIP Code)	10. SOURCE OF FUNDING NUMBERS

PROGRAM ELEMENT NO.	PROJECT NO.	TASK NO.	WORK UNIT ACCESSION NO.
61153N11		uri5005	

11. TITLE (Include Security Classification)

Theoretical and Experimental Study of Thermoacoustic Engines

12. PERSONAL AUTHOR(S)

Richard Raspet, Henry E. Bass and W. Pat Arnott

13a. TYPE OF REPORT	13b. TIME COVERED	14. DATE OF REPORT (Year, Month, Day)	15. PAGE COUNT
Final	FROM 89/7/1 TO 92/9/30	92/12/31	

16. SUPPLEMENTARY NOTATION

17. COSATI CODES			18. SUBJECT TERMS (Continue on reverse if necessary and identify by block number)
FIELD	GROUP	SUB-GROUP	Thermoacoustics, thermoacoustic refrigerator, heat driven sound source
20	01		

19. ABSTRACT (Continue on reverse if necessary and identify by block number)

A three year study of thermoacoustic engines operating as prime movers and refrigerators was completed. The major thrusts of this effort was the use and theoretical description of ceramic honeycomb structures as the active element in thermoacoustic engines. An air-filled demonstration prime mover was constructed and demonstrated at Acoustical Society of America and IEE meetings. A helium-filled test prime mover was designed and built and is being employed in studies of the threshold of oscillation as a function of temperature difference and pressure. In addition, acoustically based theories of the thermoacoustic engine have been developed and tested for a parallel plate stack at the Naval Postgraduate School and for a honeycomb stack at the University of Mississippi. Most of this work is described in detail in the attached publications. In this report we will give an overview of the research completed to date and its relationship to work performed at the Naval Postgraduate School and to future work at the University of Mississippi.

20. DISTRIBUTION/AVAILABILITY OF ABSTRACT	21. ABSTRACT SECURITY CLASSIFICATION
☒ UNCLASSIFIED/UNLIMITED ☐ SAME AS RPT. ☐ DTIC USERS	Unclassified

22a. NAME OF RESPONSIBLE INDIVIDUAL	22b. TELEPHONE (Include Area Code)	22c. OFFICE SYMBOL
Logan E. Hargrove, ONR Physics Division	(703) 696-4221	ONR Code 1112

DD Form 1473, JUN 86 *Previous editions are obsolete.*

SECURITY CLASSIFICATION OF THIS PAGE
UNCLASSIFIED

TABLE OF CONTENTS

THEORETICAL AND EXPERIMENTAL STUDY OF THERMOACOUSTIC ENGINES

ABSTRACT

A three year study of thermoacoustic engines operating as prime movers and refrigerators was completed. The major thrusts of this effort was the use and theoretical description of ceramic honeycomb structures as the active element in thermoacoustic engines. An air–filled demonstration prime mover was constructed and demonstrated at Acoustical Society of America and IEEE meetings. A helium–filled test prime mover was designed and built and is being employed in studies of the threshold of oscillation as a function of temperature difference and pressure. In addition, acoustically based theories of the thermoacoustic engine have been developed and tested for a parallel plate stack at the Naval Postgraduate School (NPS) and for a honeycomb stack at the University of Mississippi (UM). Most of this work is described in detail in the attached publications. In this report we will give an overview of the research completed to date and its relationship to work performed at NPS and to future work at UM.

THEORETICAL AND EXPERIMENTAL STUDY OF THERMOACOUSTIC ENGINES

INTRODUCTION

Thermoacoustic engines are devices which convert heat energy to acoustic energy or acoustic energy to a heat transfer. The acoustic wave serves as the pump to compress and displace the working fluid. In a prime mover, a section of a standing wave tube is occupied by a stack, a porous material with an impressed temperature gradient. The hot end of the stack faces the pressure antinode. The entropy and vorticity modes modify the standing acoustic wave such that the temperature change lags the compression and work is done on the gas and the acoustic wave is amplified.

In a refrigerator, the acoustic wave is driven by an electroacoustic driver (or by a thermoacoustic prime mover) and the stack carries the opposite temperature gradient from the prime mover. In this case the acoustic wave transfers energy from the cool end of the stack to the hot end where heat exchangers remove the heat. A detailed description of thermoacoustics is contained in Ref. 1.

Previous analytical work with realistic thermoacoustic engines has relied on Runge–Kutta integration to evaluate the behavior of the entire standing wave tube. In Section I we will briefly describe our efforts to develop an acoustic or impedance based method for an element by element analysis of thermoacoustic engines. The attached publications provide a detailed description of this analysis.[2]

Two types of stacks have been employed in thermoacoustic devices, parallel plates or a section of the tube wall. The former type was constructed either by parallel linear plates or by a spiral shaped by winding up thin sheets of plastic material. Sections of closed tubes with large temperature gradients have been observed to resonate naturally.

The Sondhauss tube results when blown glass develops a temperature gradient while Taconic oscillations are observed when glass tubes reach from room temperature to cryogenic temperatures.

A portion of our effort was to extend the acoustic based formulation of thermoacoustics to other pore geometries based on previous experiments at UM on the analysis of sound propagation in porous media. In particular, we have employed rigid ceramic catalytic converter cores as the stack material. These cores are attractive as stack material since they provide a regular cross section and are cheap and easy to form. In addition, the two–dimensional matrix may reduce turbulence effects relative to the parallel plate arrangement at high amplitudes.

The development of an acoustic based formulation for different shapes (particularly rectangular pores) is described in Section II. Details of this analysis and background work on acoustic propagation in rectangular porous materials are presented in Refs. 3, 4 and 5.

The formulation developed in Ref. 3 was used to design a helium–filled prime mover with a minimum onset temperature difference. The prime mover was constructed and measurements of onset temperature difference versus pressure are in progress. This work is described in Section III.

Section IV describes the application of impedance measurements to the air–filled demonstration prime mover.[6] These measurements illustrate the power of acoustic analysis and measurement techniques to thermoacoustic problems.

Section V summarizes our accomplishments in this three year effort and briefly describes future work.

I. AN ACOUSTICS BASED STUDY OF THE THERMOACOUSTIC PRIME MOVER BELOW ONSET

Henry Bass worked with Anthony A. Atchley, Thomas Hofler and Hsiao–Tseng Lin at NPS in developing and testing an acoustic based formulation of a thermoacoustic prime mover.[2] A counterpropagating plane wave description of the stack was developed based on Zwikker and Kosten's analysis of sound propagation in porous rigid media. The thermoacoustic effects and the impressed temperature gradient lead to different complex wave numbers for propagation with the temperature gradient and against it.

This theory was compared to measurements of the Q factor of the resonate tube versus temperature difference at different pressures. Good agreement was achieved. The worst discrepancies occurred for low temperature gradients when the acoustic description should be best. Apparently the thermoacoustic effects at higher temperature gradients dominate this source of error.

II. GENERAL FORMULATION OF THERMOACOUSTICS FOR ARBITRARY STACK CROSS SECTIONS

Basic research on the acoustic description of regular rectangular ceramic catalytic cores[4,5] was extended to thermoacoustic calculations.[3] The effect of the pore shape on the interaction of the acoustic mode with the vorticity and thermal mode is given by the function $F(x,y,\lambda)$ which satisfies

$$F(x,y;\lambda) + (R^2/i\lambda^2)\,\Delta_t F(x,y;\lambda) = 1\ , \qquad (1)$$

subject to the boundary condition of $F(x,y;\lambda) = 0$ at the pore walls. R is a characteristic transverse dimension of the pore and λ is the shear wave number, $\lambda = R_0(\rho_0\omega/\eta)^{1/2}$, or the thermal disturbance number, $\lambda_T = R(\rho_0\omega c_p/\kappa)^{1/2}$. Use of the Prandtl number,

$N_{pr} = \eta c_p/\kappa$, gives $\lambda_T = \lambda(N_{pr})^{1/2}$. Since we are interested in average values, the $F(x,y,\lambda)$ are averaged over the pore cross section to form $F(\lambda)$. The functional form of $F(\lambda)$ was determined for square, rectangular, triangular, and circular pores as well as for parallel slits.

The average pressure and particle velocity differential equations in the pore are then used to form an impedance differential equation:

$$\frac{dZ(z)}{dz} = ik(z)\, Z_{int}(z) \left(1 - \frac{Z(z)^2}{Z_{int}(z)^2} \right) + 2\alpha(z)\, Z(z) \tag{2}$$

where

$$\alpha(z) = \frac{\beta T_{0z}}{2} \left(\frac{F(\lambda_T)/F(\lambda) - 1}{1 - N_{pr}} \right), \tag{3}$$

$$k(z) = \left(\frac{\omega}{c} \right)^2 \frac{1}{F(\lambda)} \left[\gamma = (\gamma - 1)\, F(\lambda_T) \right], \tag{4}$$

and

$$Z_{int}(z) = \rho_0 \omega / [\Omega\, F(\lambda)\, k] . \tag{5}$$

Since the gas properties vary with temperature along the stack, Eq. (2) must be evaluated by numerical integration. The heat and work flows in the stack have also been evaluated in terms of $F(\lambda)$ and $F(\lambda_T)$. These equations are used to determine the steady state condition for the thermoacoustic devices.

In a refrigerator, the operating parameters are varied until the heat flow in the stack is constant as a function of position. This determines the temperature profile in the stack.

Calculation of the $F(\lambda)$ for the various pore shapes demonstrates that the parallel plate is the optimum shape for the short stack approximation for linear acoustic waves.

III. SPECIFIC IMPEDANCE MEASUREMENTS OF A PRIME MOVER

A. Prime Mover Impedance Measurements[6]

The experimental arrangement used is shown in Fig. 1. A prime mover was mounted vertically and an impedance tube was attached at the bottom via a flange. The prime mover was built originally for use as a demonstration device and for practice in fabricating the elements. A section of resonator made of copper pipe of length 20.96 cm and inner radius 4.32 cm, and capped at the top, was the first element. High temperature heat tape was wrapped around the entire section followed by a 1 inch layer of heat insulating material. Heat was transported by conduction to the next element which was the hot heat exchanger. A type K thermocouple was placed inside the hot exchanger to monitor the temperature. The stack (or thermoacoustic engine) which supports the temperature gradient was the next element and will be discussed below. Heat was removed at the cold exchanger by water from a the lab sink. Another section of resonator, which was wrapped with water–circulating tubing, was the next element. This section was 44.45 cm long and of radius 4.32 cm.

The heat exchangers were made by laminating with epoxy copper sheets spaced by aluminum sheets. The copper–aluminum laminate was then turned to a cylindrical shape using a lathe. The cylindrical boundary was clad with a shell of copper about 2.5 mm thick by using an electroplating technique. The heat exchanger was then machined into a disk form and inserted into a flanged holder for attachment to the other elements. The

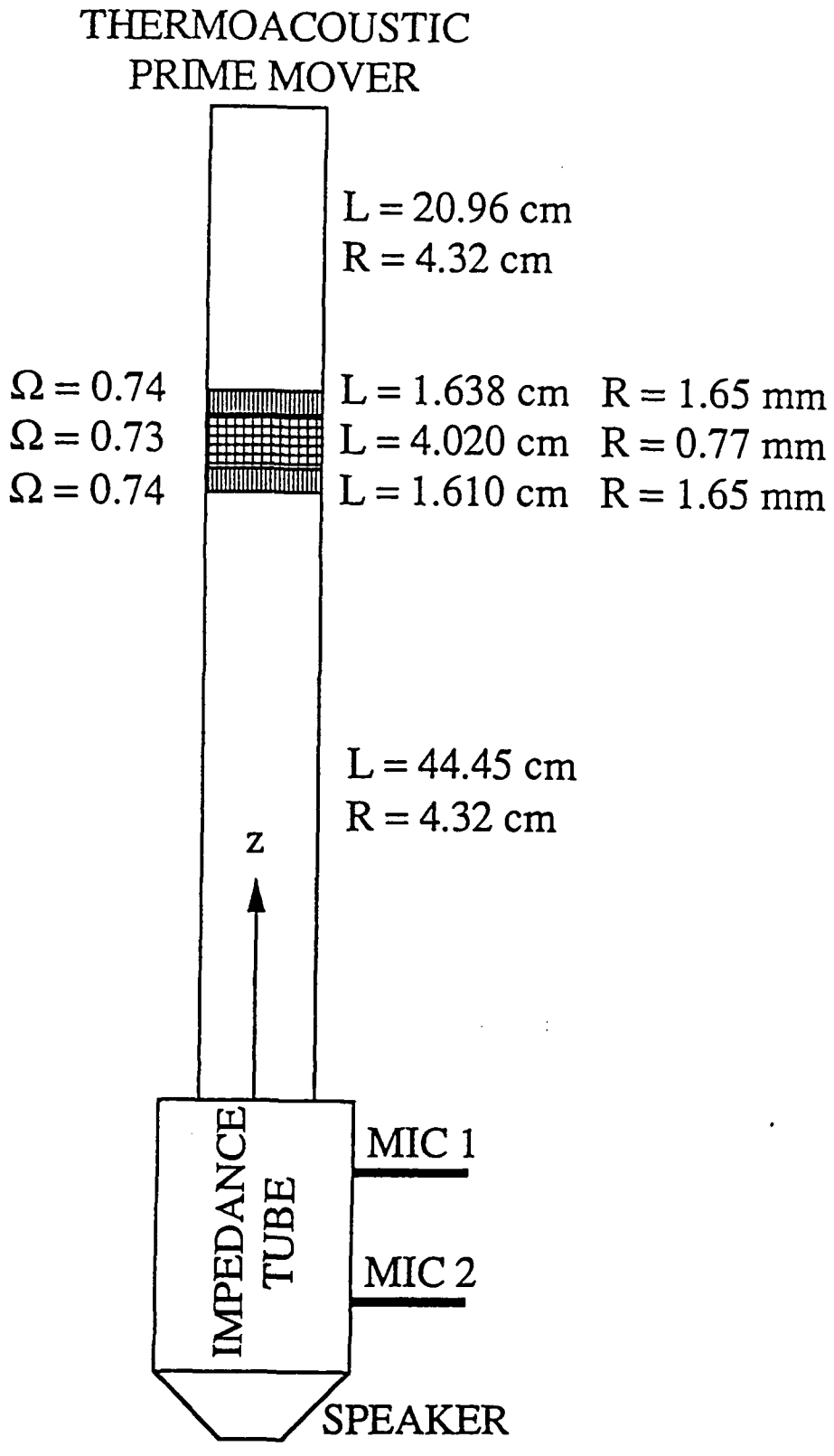

Figure 1. Demonstration thermoacoustic oscillator and analysis impedance tube.

aluminum was etched away using a dilute hydrochloric acid solution. The resulting heat exchanger was made entirely of copper with plate to plate spacing of the copper strips equal to 1.65 mm. The cold heat exchanger flange included an open tank for water circulation around the periphery of the plates. The hot and cold exchangers were 1.638 cm and 1.610 cm long, and had open to total volume ratios of $\Omega = 0.74$.

The stack was a ceramic cylindrical sample of a monolithic catalyst support. Reference 4 describes the analysis of some acoustic properties of the catalyst supports. It is a section of a porous medium in which the open pores have square boundaries of semi–width 0.77 mm, and are straight tubes in the z direction (Fig. 1). The ceramic sample had a radius of 7.3 cm. To attach it to the heat exchangers, a ring of inner radius 4.32 cm, outer radius 7.3 cm, and depth 3.2 mm was removed from the ceramic sample. This left a protruding central portion. Copper rings of thickness 3.2 mm, inner radius 4.32 cm, and outer radius of 12 cm were supported between the ends of the ceramic piece using threaded rod stand–offs. Holes were drilled in the copper disks to match the heat exchanger flange holes.

An impedance tube with an inner radius of 7.3 cm was attached at the bottom of the prime mover. Microphones were placed 5 cm from the bottom of the prime mover and the speaker below (10 cm separation). The impedance tube[7] is generally used to determine the specific acoustic impedance (or pressure divided by particle velocity) at z=0 in Fig. 1. Denote by P_1, V_1, and v_1 the pressure, volume velocity, and particle velocity at $z = 0$ in the impedance tube of cross–sectional area $A_1 = 167.5$ cm^2. Denote by subscript 2 the corresponding quantities for the prime mover. Assuming conservation of pressure and volume velocity at the interface, $P_1/V_1 = P_2/V_2$. The quantity measured using the impedance tube was $Z_1 = P_1/v_1 = A_1 P_1/V_1 = A_1 P_2/V_2 = A_1 P_2/(v_2 A_2)$. The desired quantity $Z_2 = P_2/v_2$ was thus determined from $Z_2 = Z_1 A_2/A_1$. Neglect of interfacial effects of the impedance tube to prime mover radius

discontinuity is a low frequency approximation. The prime mover was evaluated using swept sine wave analysis at sufficiently low amplitudes that negligible heat was transported thermoacoustically. The measured impedance can become a function of the amplitude of driving pressure signal at high levels due to the alteration of the static temperature gradient by thermoacoustic streaming.[8]

The real and imaginary parts of the measured specific acoustic impedance as a function of the temperature difference are shown in Figs. 2a and 2b. The real part becomes negative at some frequencies, indicating the possibility of having an active system with reflection coefficients greater than one.[9] When the impedance tube is removed, which of course changes the prime mover termination impedance, sound at a nominal frequency of 115 Hz is produced for $\Delta T \geq 176$ K. The expression for radiation specific acoustic impedance[10] at the mouth of the prime mover is $Z_{rad}(\omega) = -\rho_0 c[(k_0 R/2)^2 - i\, 0.6\, k_0 R]$ where $k_0 = \omega/c$, ω is the radian frequency, ρ_0 is the ambient air density, c is the adiabatic sound speed of air, and R = 4.32 cm is the tube radius. The minus sign occurs because of our choice for the positive direction of z in the coordinated system on Fig. 1. Radiation impedance is represented by dashed lines in Figs. 2a and 2b. One immediate check of the measurements is that the initial operating point (115 Hz, ΔT = 176 K) given by the plus symbol occurs, for both the real and imaginary parts of the radiation impedance, at the intersection of the calculated and measured impedance values.

B. Conclusions

Specific acoustic impedance measurements were made as a function of the temperature gradient across the stack. Among other uses, these measurements are helpful for evaluating the possibility of using the prime mover as a sound source. Another interpretation of Fig. 2 is, for example, that the plane wave reflection coefficient

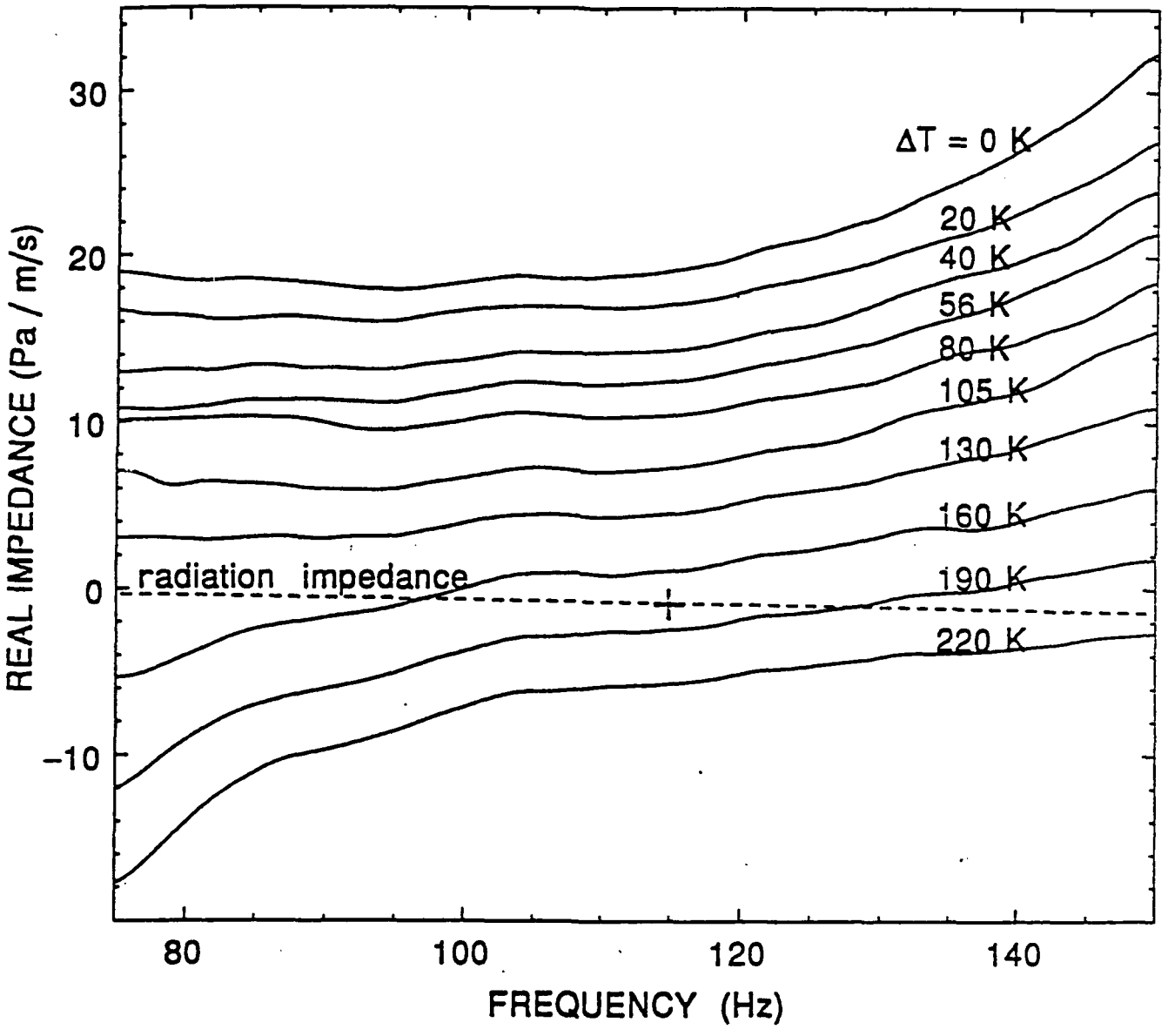

Figure 2a. Real part of the specific acoustic impedance at the mouth of the prime mover.

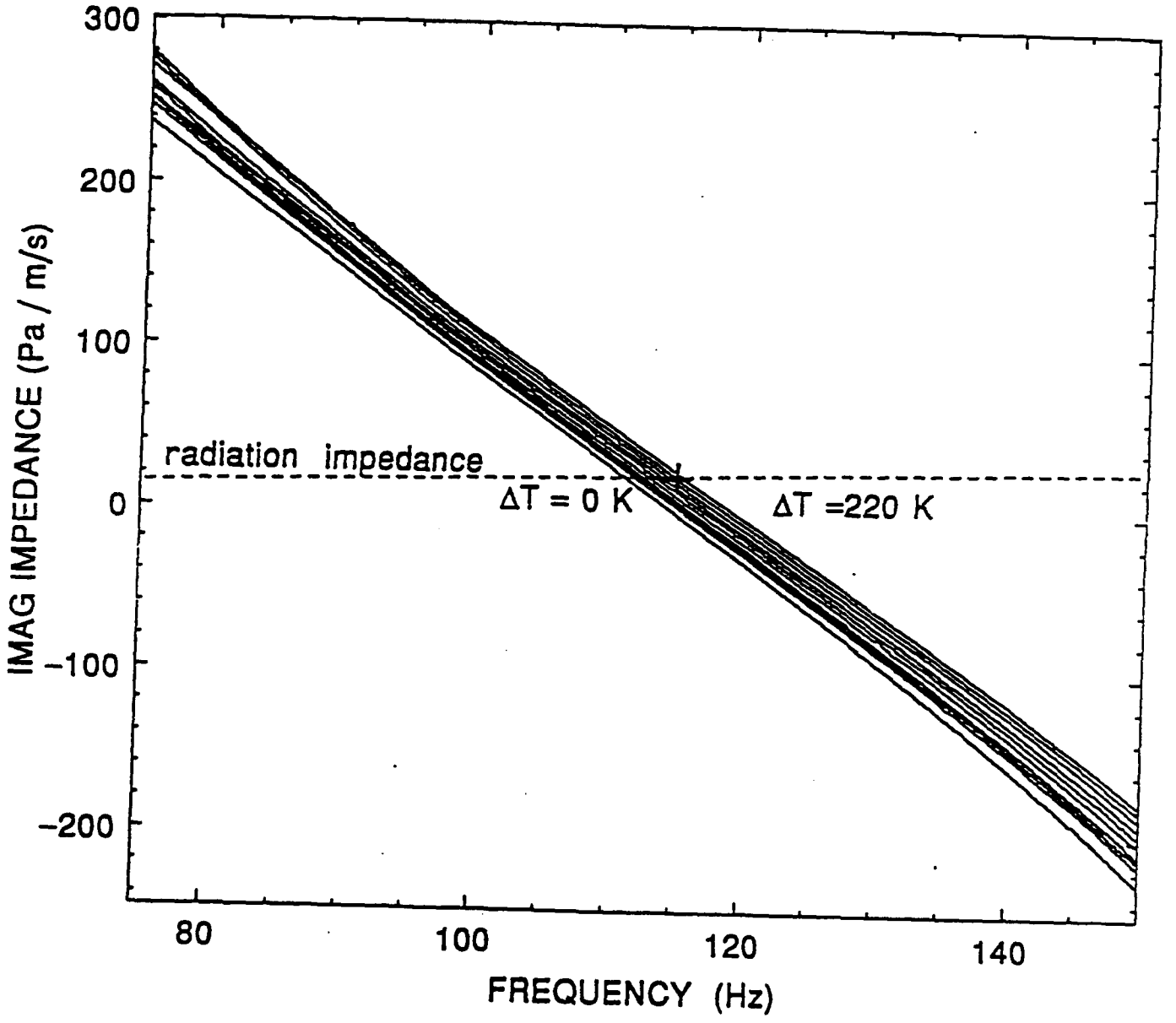

Figure 2b. Imaginary part of the specific acoustic impedance.

at 80 Hz and ΔT = 160 K is > 1 for waves incident in an infinite length tube of the same diameter as the prime mover but in the location of the impedance tube in Fig. 1. For prime movers far above the onset of sound production, or for strongly driven thermoacoustic refrigerators, the temperature distribution from hot to cold is not simply the static distribution established by the thermal conductivity of the gas and stack. The presence of the strong acoustic wave influences its thermal surroundings[8] by heat transport and in this sense the thermoacoustic oscillation is an example of a self–interacting wave process.

IV. ONSET MEASUREMENTS IN AN OPTIMIZED HELIUM–FILLED PRIME MOVER

The theory described in Section II and in Ref. 3 was used to design a helium–filled thermoacoustic engine (see Fig. 3). The design goal for this tube was to produce sound at as small a temperature gradient as possible. After construction, the thermoacoustic engine is being tested to compare the predicted onset gradient to the measured.

In initial tests the tube was filled with helium to 3 kPa. Figure 4 shows the computed stability curve for the fundamental frequency near 308 Hz and the 1st harmonic near 605 Hz. Ambient pressure is the horizontal axis. Temperature difference between hot and cold ends is on the vertical axis. For temperatures below the boundary between stable and unstable no gas oscillations occur. Thermal boundary layer thickness $\delta_T = (2k/\rho_0\omega c_p)^{1/2} \propto \omega^{-1/2} P_0^{-1/2}$ where P_0 is the ambient pressure in the tube. For fixed tube length as in the thermoacoustic engine, the boundary layer thickness can be adjusted by changing P_0. For low P_0, the boundary layer is much thicker than the pore size in the stack and heat exchangers so gas viscosity chokes the flow. For P_0 = 173 kPa the boundary layer thickness is optimal for thermoacoustic effects and the lowest onset temperature of around 180°C occurs. One factor that greatly contributes to

SCALE DRAWING OF UM TAE:

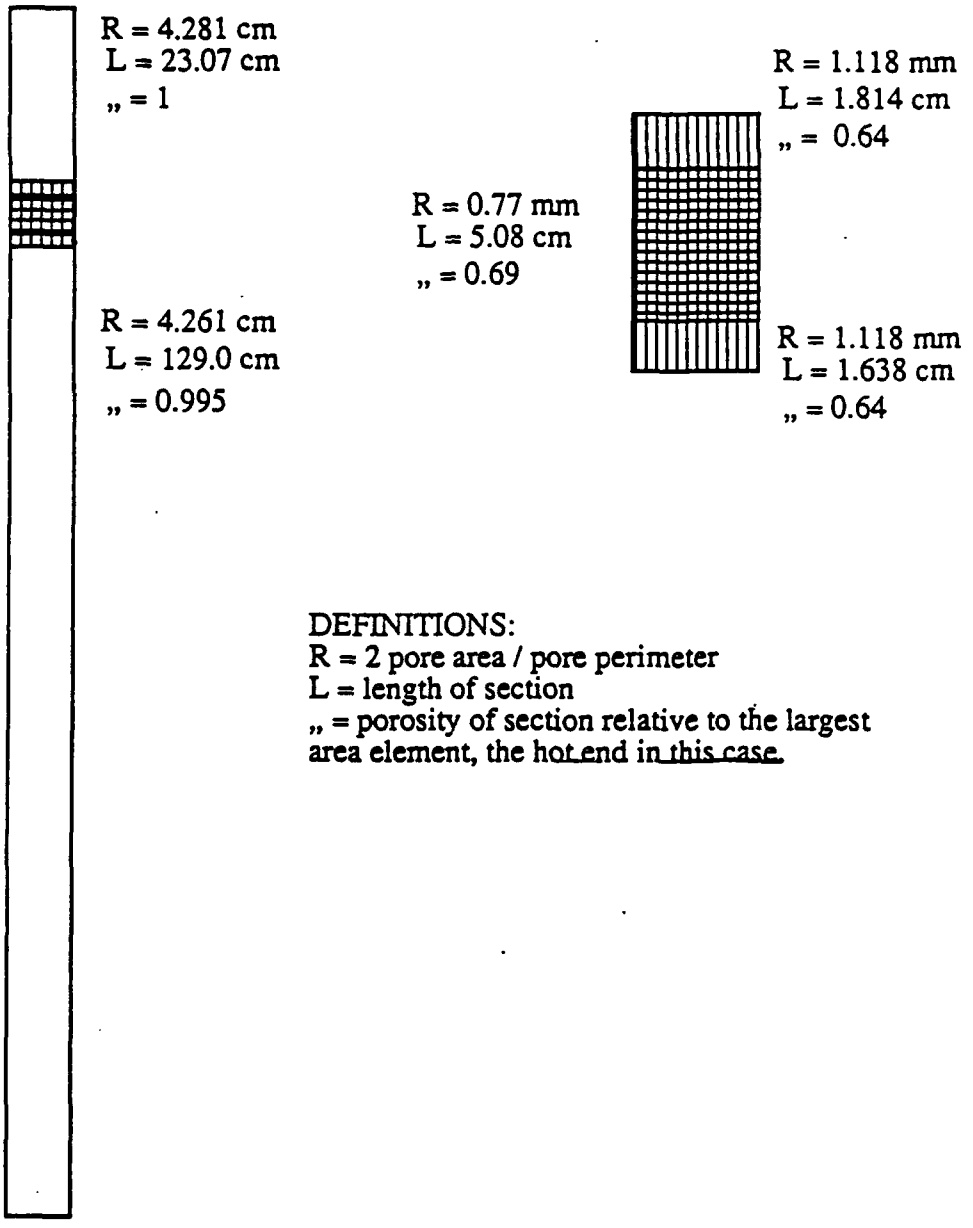

DEFINITIONS:
R = 2 pore area / pore perimeter
L = length of section
„ = porosity of section relative to the largest area element, the hot end in this case.

Figure 3. Scale drawing for the fundamental and first harmonic for the UM TAE.

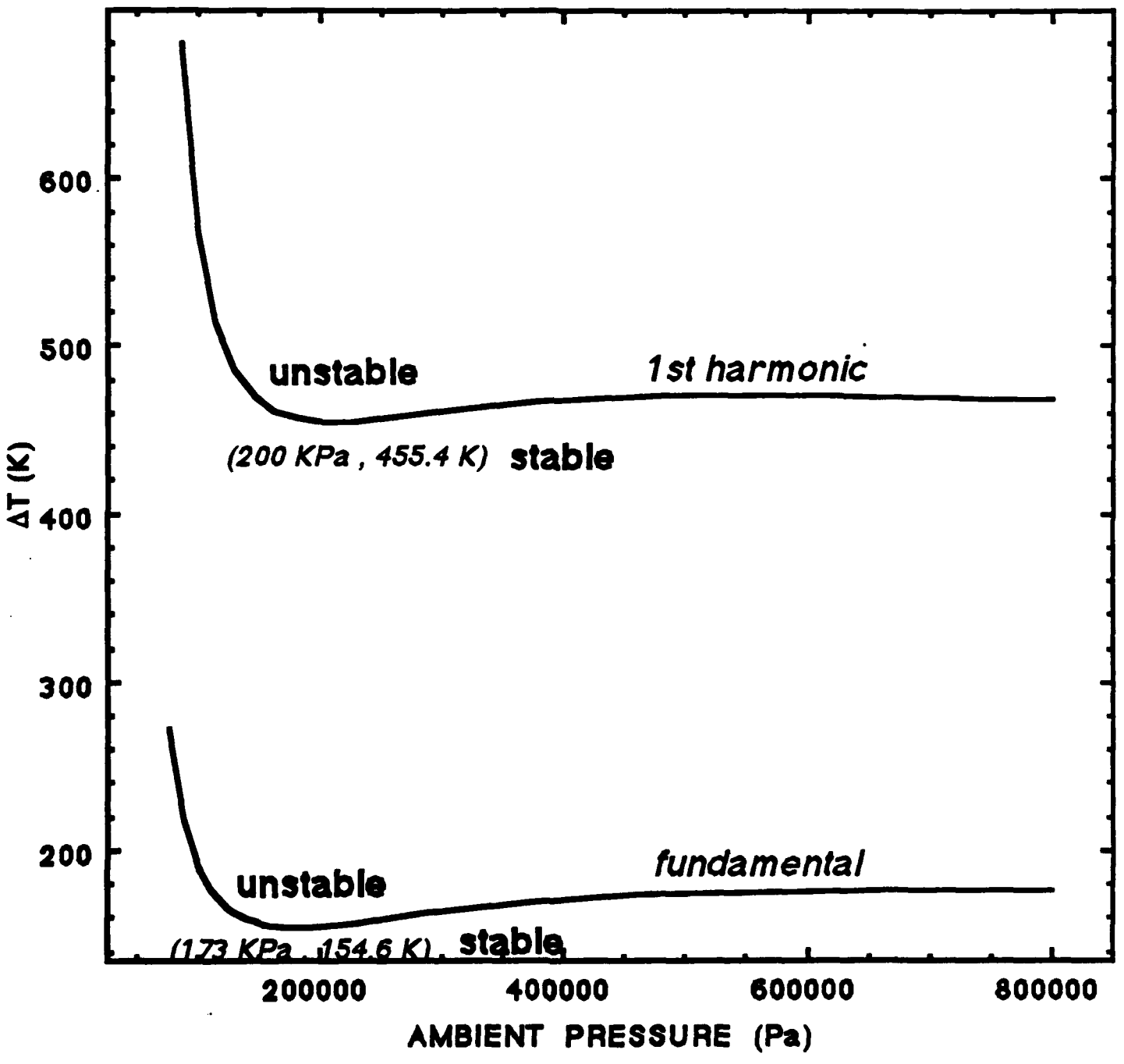

Figure 4. Stability curves for the fundamental and first harmonic for the UM TAE.

minimizing the onset temperature is the location of the stack and heat exchangers relative to the lengths of the hot and cold ends. When the elements are too close to the hot end gas particle displacement is small so the required temperature gradient becomes prohibitively large. When you try to do work on the gas it responds by changing pressure but only a small particle displacement occurs. However as the elements move too close to the center of the tube where a pressure node occurs the work done approaches zero. When you try to do work on the gas at this point in the standing wave the gas responds by undergoing a large displacement, but only a small pressure change occurs. Somewhere between the pressure node at the center and the particle velocity node at the end is an optimal location for the location of the elements. The optimal location is closer to the end where particle velocity is less so that losses due to gas viscosity are minimal. The thermoacoustic engine was designed to optimize the location of the elements.

Since $\delta_T \propto T_0^{0.8}\, \omega^{-1/2}\, P_0^{-1/2}$ it seems odd at first glance that the minimum of the first harmonic would be at a higher pressure than the fundamental. The temperature dependence is in part due to ambient density and in part to thermal conductivity. Supposing there to exist *an* optimal boundary layer thickness, then as ω is increased, P_0 should decrease to balance the equation. However, there is *no* single optimal boundary layer thickness for the tube. Viscous losses can be defeated by aiming at thin boundary layers. The stack location helps to minimize viscous losses for the fundamental, but not the first harmonic. Additionally, particle displacement is smaller at higher frequencies so the necessary temperature gradient $|T_{0z}|$ to make $\Gamma > 1$ for onset increases. (The pressure in the standing wave changes from maximum to minimum over a shorter distance as the frequency increases.) At a frequency double the fundamental, the ambient pressure must diminish by a factor of $2^{1/2}$ to get the same optimal boundary layer thickness. But the average temperature $(T_H + T_C)/2$ must increase by a factor of

2. To offset the temperature increase, the ambient pressure must increase by a factor of $2^{0.8}$. Thus it is reasonable that the ambient pressure must increase by a net amount approximately equal to $2^{0.3}$ to achieve the boundary layer thickness for optimal thermoacoustic pumping of the wave. In order to experimentally observe both modes, the thermoacoustic engine should be heated to a temperature in the unstable region of the 1st harmonic with the Q of the resonant cavity so low that there is no oscillation of the fundamental. When the Q is increased, both modes should oscillate .

Figure 5a is the 1/Q curve for the fundamental and 1st harmonic for a pressure of 173 kPa. When $1/Q = 0$ the thermoacoustic engine is at the perilous boundary between stability and instability. For ΔT above the onset value 154.6 K for the fundamental, the time evolution of the pressure follows the form $\exp(\pi f_0 t/|Q|)$ until nonlinearity becomes apparent. The exponential growth factor for the fundamental has a maximum at ΔT = 800 K. For higher temperatures the ambient temperature in the hot end causes the ambient sound speed, which is $c \propto T_0^{1/2}$, to increase. As a rough guide for computing the resonant frequency of the tube, note that resonance should occur for $2k_{0c}L_c + 2k_{0h}L_h = 2\pi$ or alternatively $f_0 = 1/[2(L_c/c_c + L_h/c_h)]$ where L_c and c_c are the lengths and sound speeds of the cold section, etc. Thus as c_h increases we can view this as an effective shortening of the hot end, which puts the elements closer to a velocity node with concomitant decrease of effectiveness. We can also understand the increase of the resonant frequency with temperature shown in Fig. 5b from the equation for f_0. Dispersion effects in the thermoacoustic elements are somewhat apparent in this figure in that the frequency of the first harmonic is not twice the fundamental. This difference is much more noticeable in the original numbers from which these files were made.

Figure 6 shows the experimental onset temperature gradient compared to the theoretical gradient. The cold heat exchanger is maintained at T_0 = 20°C. The experimental values show good agreement with the theoretical curve, but shifted upward

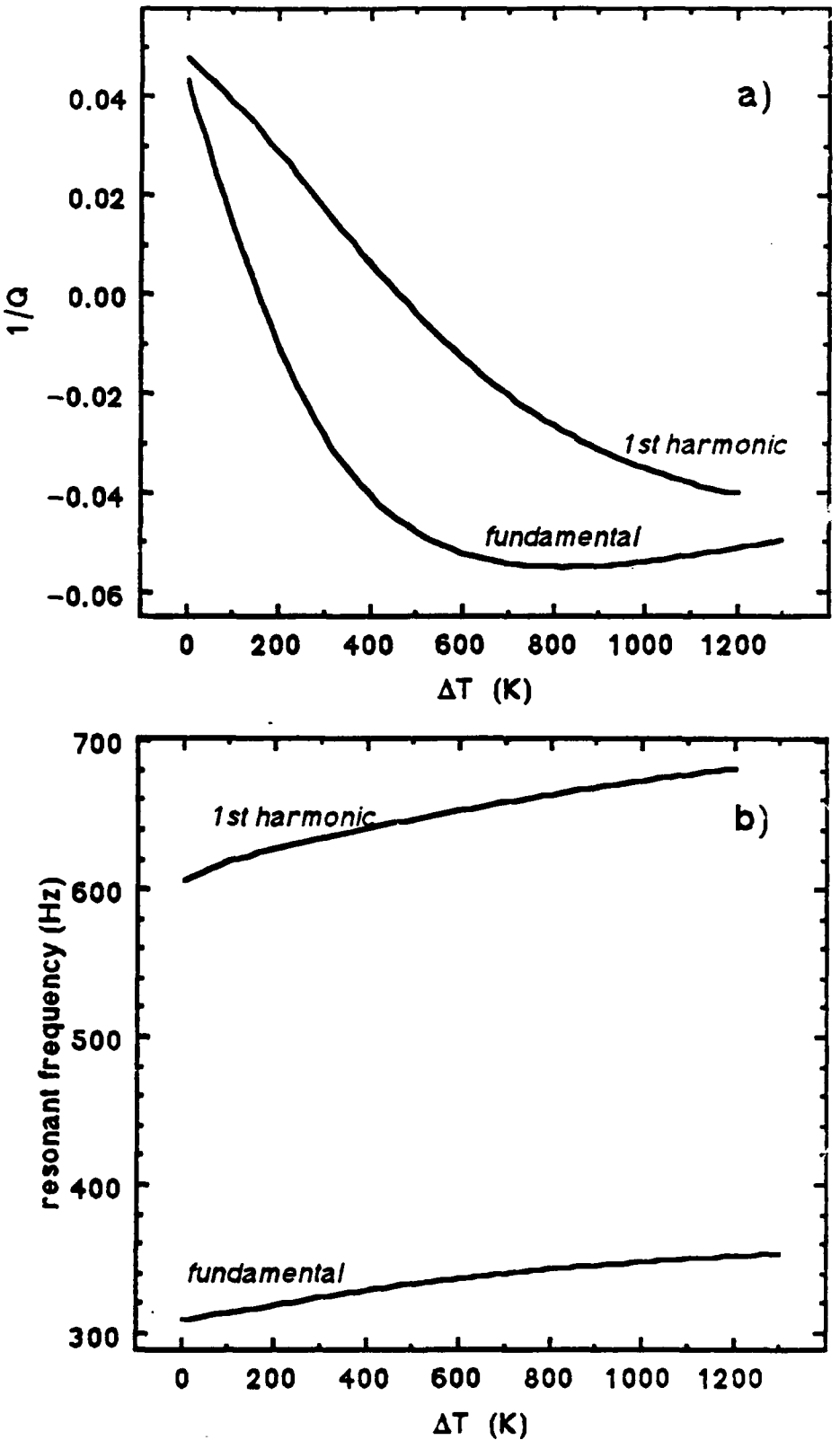

Figure 5. a) Quality factor; b) Resonant frequency for UM TAE with ambient pressure 173 kPa.

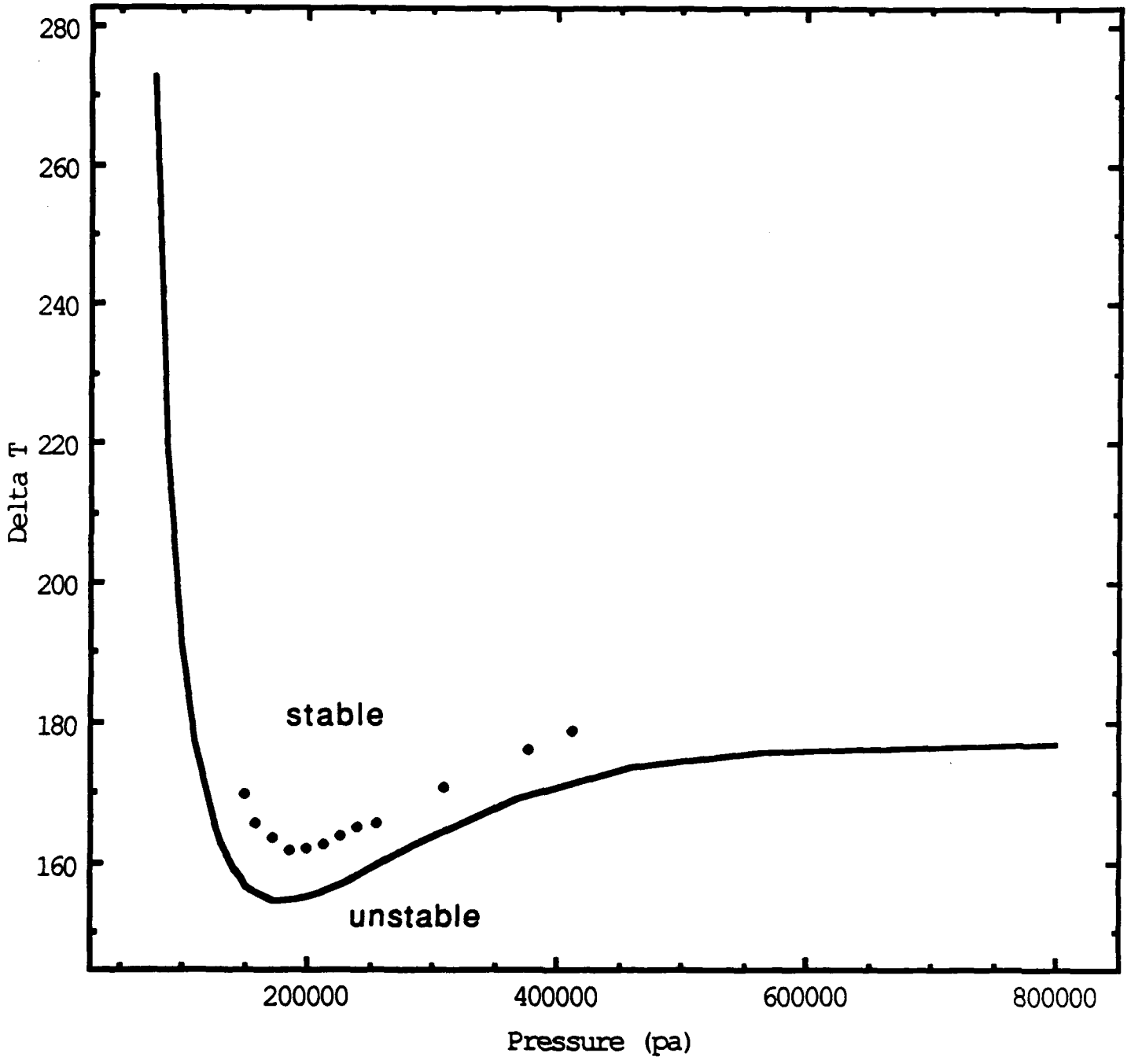

Figure 6. The experimental onset temperature gradient compared to the theoretical gradient.

by approximately 4°C. Thermocouples placed on the exterior of the tube show a temperature gradient along the length of the tube from the cold heat exchanger to the cold end. This reverse gradient could account for this shift.

New experiments are being performed with more uniform cooling of the tube and with thermocouples placed in the stack. These improvements should reduce the error.

V. SUMMARY AND CONCLUSION

The three year study of thermoacoustic devices has been highly successful although we have not accomplished all we hoped. Ceramic catalytic converter cores have been used as the stack material in air–filled and helium–filled thermoacoustic prime movers. A general theory for thermoacoustic engines based on the theory of acoustic propagation in porous materials has been developed for a single layer model for a parallel plate stack[2] and for arbitrary pore shapes using numerical integration.[3] The results of these theories agree well with onset data in thermoacoustic prime movers as well as impedance tube measurements.[6]

It was originally planned to build a thermoacoustically driven refrigerator in the third year of this study. We have not built this device yet but it will not be difficult to design and build. The helium–filled thermoacoustic engine is modular in construction so that additional elements can be easily incorporated. The computer program contained in Appendix A will be used to optimize the design of the engine–refrigerator so that nonlinear effects will be minimized.

The work of the past three years forms a good basis for future work in the physics of thermoacoustic refrigerators and engines.

VI. REFERENCES

1. G.W. Swift, "Thermoacoustic engines," J. Acoust. Soc. Am. **84** (4), 1145–1180 (1988).

2. Anthony A. Atchley, Henry E. Bass, Thomas J. Hofler, and Hsiao–Tseng Lin, "Study of thermoacoustic prime mover below onset of self–oscillation," J. Acoust. Soc. Am. **91** (2), 734–743 (1992).

3. W. Pat Arnott, Henry E. Bass and Richard Raspet, "General formulation of thermoacoustics for stacks having arbitrarily shaped pore cross sections," J. Acoust. Soc. Am. **90** (6), 3228–3237 (1991).

4. Heui–Seol Roh, W. Patrick Arnott, and James M. Sabatier, "Measurement and calculation of acoustic propagation constants in arrays of small air–filled rectangular tubes," J. Acoust. Soc. Am. **89** (6), 2617–2624 (1991).

5. W. Patrick Arnott, James M. Sabatier, and Richard Raspet, "Sound propagation in capillary–tube–type porous media with small pores in the capillary walls," J. Acoust. Soc. Am. **90** (6), 3299–3306 (1991).

6. W. Pat Arnott, Henry E. Bass, and Richard Raspet, "Specific acoustic impedance measurements of an air–filled thermoacoustic prime mover," J. Acoust. Soc. Am. **92**, 3432–3434 (1992).

7. A.F. Seybert and D.F. Ross, "Experimental determination of acoustic properties using a two–microphone random–excitation technique," J. Acoust. Soc. Am. **61**, 1362–1370 (1977).

8. J. Wheatley, T. Hofler, G.W. Swift, and A. Migliori, "An intrinsically irreversible thermoacoustics heat engine," J. Acoust. Soc. Am. **74**, 153–170 (1983).

9. A.D. Pierce, *Acoustics: An Introduction to Its Physical Principles and Applications,* (American Institute of Physics, New York, 1989), p. 109.

10. L.E. Kinsler, A.R. Frey, A.B. Coppens, and J.V. Sanders, *Fundamentals of Acoustics,* 3rd ed., (John Wiley and Sons, New York, 1982), p. 202.

APPENDIX A

FORTRAN PROGRAM FOR ANALYSIS OF THE THERMOACOUSTIC ENGINE

APPENDIX: FORTRAN PROGRAM FOR ANALYSIS OF THE UM TAE EXECUTION FILE FOR THE THERMOACOUSTIC ENGINE CODE. THE CODE IS ON MY ACCOUNT ON THE IBM 3084, CMS OPERATING SYSTEM MACHINE. ACCESS: LOGIN PAARNOTT, PASSWORD FROGGY.

```
&IF &INDEX NE 0 &GOTO -HEREWEGO
&TYPE ENTER THE NAME OF THE PARAMS FILE WHICH DESCRIBES THE TAE.
&READ ARGS
-HEREWEGO
VMFCLEAR
 COPYFILE &1 PARAMS A TEMP PARAMS A (REPLACE
 EXEC GLOBALS
 FILEDEF 1 DISK T DATA A
 FILEDEF 2 DISK TEMP PARAMS A
 FILEDEF 15 DISK PRESS DATA A (RECFM V
 FILEDEF 16 DISK WORKFLOW DATA A (RECFM V
 FILEDEF 17 DISK HEATFLOW DATA A (RECFM V
 FILEDEF 18 DISK IMPED3D DATA A (RECFM V
 FILEDEF 19 DISK IMPED DATA A (RECFM V
 FILEDEF 20 DISK ENTHALPY DATA A (RECFM V
 FILEDEF 21 DISK WORKDRIV DATA A (RECFM V
 FILEDEF 27 DISK QUALREC DATA A
 FILEDEF 28 DISK RESFREQ DATA A
 FILEDEF 29 DISK QUALFACT DATA A
 FILEDEF 30 DISK POSVSDT DATA A
 FILEDEF 37 DISK QUALREC DATAEIG A
 FILEDEF 38 DISK RESFREQ DATAEIG A
 FILEDEF 39 DISK QUALFACT DATAEIG A
 FILEDEF 41 DISK T0Z DATA A
 FILEDEF 42 DISK REIMPED DATA A (RECFM V
 FILEDEF 43 DISK IMIMPED DATA A (RECFM V
 FILEDEF 44 DISK STABCURV DATA A (RECFM V
* PROGRAM FOR COMPUTING PROPAGATION CONSTANTS....
*LOAD TAEUTIL ( CLEAR NOMAP START
* GENERAL PROGRAM FOR COMPUTING Z,P,HEAT,WORK.
*LOAD TAEHE2 ( CLEAR NOMAP START
* GENERAL PROGRAM, FINITE DIFF IN STACK, FOR COMPUTING Z,P,HEAT,WORK.
*LOAD TAEHE3 ( CLEAR NOMAP START
* GENERAL PROGRAM, FINITE DIFF IN STACK, FOR COMPUTING Z,P,HEAT,WORK.
* GAS ABSORPTION IS INCLUDED IN THE OPEN TUBE SECTIONS.
*LOAD TAEHE3V2 ( CLEAR NOMAP START
* GENERAL PROGRAM, RUNGE KUTTA IN STACK, FOR COMPUTING Z,P,HEAT,WORK.
*LOAD TAERUNGE ( CLEAR NOMAP START
* GENERAL PROGRAM, RUNGE KUTTA IN STACK, FOR COMPUTING Z,P,HEAT,WORK.
* CAN ALSO COMPUTE TRAVELING WAVES. SOMEWHAT OPTIMIZED.
*LOAD TAEHEUNG ( CLEAR NOMAP START
* GENERAL PROGRAM FOR COMPUTING Z,P,HEAT,WORK. BASED ON DF/DLAMBDA.
*LOAD TAEHE4 ( CLEAR NOMAP START
* PROGRAM FOR COMPUTING THE Q FROM COMPLEX EIGENFREQUENCY.
*LOAD TAEHEQ ( CLEAR NOMAP START
* PROGRAM FOR COMPUTING THE Q FROM COMPLEX EIGENFREQUENCY.
* USES INPUT FROM TAEHE3 AS INPUT TO START THINGS OFF WITH.
*LOAD TAEHEQ2 ( CLEAR NOMAP START
* ALL RUNGE-KUTTA PROGRAMS ABOVE HERE ARE NOT CORRECTED.
* PROGRAM FOR COMPUTING THE Q AS A FUNCTION OF TEMPERATURE IN AN EASY
* WAY. USES RUNGE KUTTA INTEGRATION.
* SECOND PROGRAM IS A COMPLEX NUMBER VERSION TO GET THE COMPLEX EIG FRE.
*LOAD TAEAUTO ( CLEAR NOMAP START
*LOAD TAECAUTO ( CLEAR NOMAP START
* VERSION OF TAECAUTO FOR AIR FILLED TUBES.
* LOAD TAECAIR ( CLEAR NOMAP START
* TO PLOT 1/Q AND RES VERSUS LAMBDA, USING TAECAIR, FOR A PRIMEMOVER.
* LOAD TAECBALT ( CLEAR NOMAP START
* TAECMONT: PROGRAM BASED ON TAECAUTO TO COMPUTE THE Q AND RESFREQ FOR
```

* THE MONTEREY TUBE. TAKES INTO ACCOUNT THE DEPENDENCE ON TEMPERATURE
* WHEN COMPUTING THE THERMAL CONDUCTIVITY OF THE STACK.
*LOAD TAECMONT (CLEAR NOMAP START
* UMTAE FORTRAN : PROGRAM FOR DESIGN OF THE UMTAE. USED TAECAUTO AS THE
* STARTING PROGRAM.
*LOAD UMTAE (CLEAR NOMAP START
* UMTAECH: CHECK OF UMTAE WITH MONTEREY DATA
*LOAD UMTAECH (CLEAR NOMAP START
* PROGRAM FROM TAECBALT FOR COMPUTING THE RESPONSE OF THE DEMO TAE IN AIR
*LOAD TAEAIRD (CLEAR NOMAP START
* UMTAEV2 FORTRAN : PROG FOR DESIGN OF THE UMTAE. USED TAECAUTO AS THE
* STARTING PROGRAM.
LOAD UMTAEV2 (CLEAR NOMAP START
ERASE TEMP PARAMS A
ERASE FILE SCRATCH A
FILEDEF * CLEAR
&EXIT

TAE PARAMETER FILE. ACTUAL #S OF THE UMTAE TUBE.

TAE PARAMETER FILE. ACTUAL #S OF THE UMTAE TUBE.
DEFINE THE TUBE FROM RIGHT TO LEFT. AT LEFT ONE USUALLY HAS THE DRIVER.
MINIMUM FREQUENCY, MAXIMUM FREQUENCY, (HZ), AND NUMBER OF FREQ. POINTS.
250.000 400. 300
TERMINATION AT THE RIGHT END OF THE TUBE.
ONE OF RIGID, FREE, OR INFIN. INFIN IS AN INFINITE TUBE.
RIGID
AMBIENT PRESSURE IN THE TUBE AND THE DRIVER PRESSURE AMPLITUDE FOR ALL
FREQUENCIES. PRESSURE IN PASCAL, DRIVER DISPLACEMENT IN METERS.
3.00D5 1.D-8
NUMBER OF SECTIONS IN THE TAE. E.G. AN OPEN SECTION, RGH HEAT EXCH,
STACK, LEFT HEAT EXCH, AND ANOTHER OPEN SECTION WOULD BE 5. INTEGER.
5
******** DEFINITION OF SECTION 1 **********
SECTION TYPE, ONE OF OPENTU, HEXCH, OR STACK.
OPENTU
ELEMENT TYPE. HAS MEANING ONLY FOR HEXCH OR STACK SECTION TYPES.
ONE OF RECT, CYL, OR SLIT, DEFINING THE TYPE OF PORES.
SLIT
NUMBER OF LAYERS THIS SECTION IS BROKEN UP INTO.
1<= NUMLAY <= 100 PRACTICALLY.
1
LENGTH OF THE SECTION.
METERS.
23.07D-2
TEMPERATURE OF THE RCH END OF THE SECTION. FOR AN ISOTHERMAL SECTION
SUCH AS OPEN TUBE OR HEAT EXCHANGERS, USE TRGH = TLEFT. KELVIN.
293.000000000000000
TEMPERATURE AT THE LEFT END OF THE SECTION.
SEE NOTE ABOVE. KELVIN.
293.
RATIO OF 2 PORE AREA TO PORE PERIMETER (M). FOR: CYL=RADIUS, SLIT=
WIDTH, RECT=2SW A/(1+A) A>1=SIDES ASPECT RATIO, SW=SHORTEST SEMIWIDTH.
4.281D-2
ASPECT RATIO OF THE PORE. VALID FOR RECTANGULAR PORES ONLY.
NECESSARY AS A GENERAL RULE.
1.0D0
POROSITY OF THE SECTION. FOR OPEN TUBE, USE POROSITY = 1.
FOR OTHER TYPES OF SECTIONS, POROSITY <=1.
1.D0
END OF SECTION 1. **********
******** DEFINITION OF SECTION 2 **********

```
SECTION TYPE, ONE OF OPENTU, HEXCH, OR STACK.
          HEXCH
ELEMENT TYPE. HAS MEANING ONLY FOR HEXCH OR STACK SECTION TYPES.
ONE OF RECT, CYL, OR SLIT, DEFINING THE TYPE OF PORES.
          SLIT
NUMBER OF LAYERS THIS SECTION IS BROKEN UP INTO.
1<= NUMLAY <= 100 PRACTICALLY.
          1
LENGTH OF THE SECTION.
METERS.
          1.814D-2
TEMPERATURE OF THE RGH END OF THE SECTION. FOR AN ISOTHERMAL SECTION
SUCH AS OPEN TUBE OR HEAT EXCHANGERS, USE TRGH = TLEFT. KELVIN.
          293.
TEMPERATURE AT THE LEFT END OF THE SECTION.
SEE NOTE ABOVE. KELVIN.
          293.
RATIO OF 2 PORE AREA TO PORE PERIMETER (M). FOR: CYL=RADIUS, SLIT=
WIDTH, RECT=2SW A/(1+A) A>1=SIDES ASPECT RATIO, SW=SHORTEST SEMIWIDTH.
          1.118D-3
ASPECT RATIO OF THE PORE. VALID FOR RECTANGULAR PORES ONLY.
NECESSARY AS A GENERAL RULE. ASPECT RATIO => 1 ALWAYS.
          1.0D0
POROSITY OF THE SECTION. FOR OPEN TUBE, USE POROSITY = 1.
FOR OTHER TYPES OF SECTIONS, POROSITY <=1.
          .64D0
END OF SECTION 2. ************************************************************
******** DEFINITION OF SECTION 3 ************************************
SECTION TYPE, ONE OF OPENTU, HEXCH, OR STACK.
          STACK
ELEMENT TYPE. HAS MEANING ONLY FOR HEXCH OR STACK SECTION TYPES.
ONE OF RECT, CYL, OR SLIT, DEFINING THE TYPE OF PORES.
          RECT
NUMBER OF LAYERS THIS SECTION IS BROKEN UP INTO.
1<= NUMLAY <= 100 PRACTICALLY. (WAS 20 AT ONE TIME)
          25
LENGTH OF THE SECTION.
METERS.
          5.08D-2
TEMPERATURE OF THE RGH END OF THE SECTION. FOR AN ISOTHERMAL SECTION
SUCH AS OPEN TUBE OR HEAT EXCHANGERS, USE TRGH = TLEFT. KELVIN.
          293.
TEMPERATURE AT THE LEFT END OF THE SECTION.
SEE NOTE ABOVE. KELVIN.
          293.
RATIO OF 2 PORE AREA TO PORE PERIMETER (M). FOR: CYL=RADIUS, SLIT=
WIDTH, RECT=2SW A/(1+A) A>1=SIDES ASPECT RATIO, SW=SHORTEST SEMIWIDTH.
          .77D-3
ASPECT RATIO OF THE PORE. VALID FOR RECTANGULAR PORES ONLY.
NECESSARY AS A GENERAL RULE. ASPECT RATIO => 1 ALWAYS.
          1.0D0
POROSITY OF THE SECTION. FOR OPEN TUBE, USE POROSITY = 1.
FOR OTHER TYPES OF SECTIONS, POROSITY <=1.
          .69D0
END OF SECTION 3. ************************************************************
******** DEFINITION OF SECTION 4 ************************************
SECTION TYPE, ONE OF OPENTU, HEXCH, OR STACK.
          HEXCH
```

```
ELEMENT TYPE. HAS MEANING ONLY FOR HEXCH OR STACK SECTION TYPES.
ONE OF RECT, CYL, OR SLIT, DEFINING THE TYPE OF PORES.
          SLIT
NUMBER OF LAYERS THIS SECTION IS BROKEN UP INTO.
1<= NUMLAY <= 100 PRACTICALLY.
          1
LENGTH OF THE SECTION.
METERS.
          1.638D-2
TEMPERATURE OF THE RGH END OF THE SECTION. FOR AN ISOTHERMAL SECTION
SUCH AS OPEN TUBE OR HEAT EXCHANGERS, USE TRGH = TLEFT. KELVIN.
          293.
TEMPERATURE AT THE LEFT END OF THE SECTION.
SEE NOTE ABOVE. KELVIN.
          293.
RATIO OF 2 PORE AREA TO PORE PERIMETER (M). FOR: CYL=RADIUS, SLIT=
WIDTH, RECT=2SW A/(1+A) A>1=SIDES ASPECT RATIO, SW=SHORTEST SEMIWIDTH.
          1.118D-3
ASPECT RATIO OF THE PORE. VALID FOR RECTANGULAR PORES ONLY.
NECESSARY AS A GENERAL RULE. ASPECT RATIO => 1 ALWAYS.
          1.0D0
POROSITY OF THE SECTION. FOR OPEN TUBE, USE POROSITY = 1.
FOR OTHER TYPES OF SECTIONS, POROSITY <=1.
          .640D0
END OF SECTION 4. ************************************************************
******** DEFINITION OF SECTION 5 ************************************
SECTION TYPE, ONE OF OPENTU, HEXCH, OR STACK.
          OPENTU
ELEMENT TYPE. HAS MEANING ONLY FOR HEXCH OR STACK SECTION TYPES.
ONE OF RECT, CYL, OR SLIT, DEFINING THE TYPE OF PORES.
          SLIT
NUMBER OF LAYERS THIS SECTION IS BROKEN UP INTO.
1<= NUMLAY <= 100 PRACTICALLY.
          1
LENGTH OF THE SECTION.
METERS.
          1.29
TEMPERATURE OF THE RGH END OF THE SECTION. FOR AN ISOTHERMAL SECTION
SUCH AS OPEN TUBE OR HEAT EXCHANGERS, USE TRGH = TLEFT. KELVIN.
          293.
TEMPERATURE AT THE LEFT END OF THE SECTION.
SEE NOTE ABOVE. KELVIN.
          293.
RATIO OF 2 PORE AREA TO PORE PERIMETER (M). FOR: CYL=RADIUS, SLIT=
WIDTH, RECT=2SW A/(1+A) A>1=SIDES ASPECT RATIO, SW=SHORTEST SEMIWIDTH.
          4.261D-2
ASPECT RATIO OF THE PORE. VALID FOR RECTANGULAR PORES ONLY.
NECESSARY AS A GENERAL RULE. ASPECT RATIO => 1 ALWAYS.
          1.0D0
POROSITY OF THE SECTION. FOR OPEN TUBE, USE POROSITY = 1.
FOR OTHER TYPES OF SECTIONS, POROSITY <=1.
          .995D0
END OF SECTION 5. ************************************************************
```

FORTRAN CODE FOR THE UM TAE.

The main program is the only part of this program that is specific to the UM TAE.

```
************************************************************************
**SUBROUTINE SETVAL * GET THE INPUT PARAMETERS FROM AN EXTERNAL FILE**
************************************************************************
   SUBROUTINE SETVAL
```

```
* VARIABLES WHICH DEFINE THE TAE.
      CHARACTER*70 SECTYP(100),ETYPE(100),TERMIN
      INTEGER NUMLAY(100),NUMSEC,NUMFRE
      REAL*8 DELEM(100),TRGH(100),TLEFT(100),RATIO(100)
     *,ASPECT(100),POROS(100),
     * THCOND(100),HECAP(100),PAMB,FREMIN,FREMAX,DDRIVE
      INTEGER J
      CHARACTER DUMMY
      COMMON /VARS1/ SECTYP,ETYPE,TERMIN
      COMMON /VARS2/ NUMLAY,NUMSEC,NUMFRE
      COMMON /VARS3/ DELEM,TRGH,TLEFT,RATIO,
     *  ASPECT,POROS,THCOND,HECAP,PAMB,FREMIN,FREMAX,DDRIVE
    1 FORMAT (A1)
    2 FORMAT (A70)
      REWIND 2
      READ (2,1) DUMMY
      READ (2,1) DUMMY
      READ (2,1) DUMMY
            READ (2,*) FREMIN,FREMAX,NUMFRE
      READ (2,1) DUMMY
      READ (2,1) DUMMY
            READ (2,2) TERMIN
      CALL NOPAD(TERMIN)
      READ (2,1) DUMMY
      READ (2,1) DUMMY
            READ (2,*) PAMB,DDRIVE
      READ (2,1) DUMMY
      READ (2,1) DUMMY
            READ (2,*) NUMSEC
                  DO 10 J=NUMSEC,1,-1
      READ (2,1) DUMMY
      READ (2,1) DUMMY
            READ (2,2) SECTYP(J)
      CALL NOPAD(SECTYP(J))
      READ (2,1) DUMMY
      READ (2,1) DUMMY
            READ (2,2) ETYPE(J)
      CALL NOPAD(ETYPE(J))
      READ (2,1) DUMMY
      READ (2,1) DUMMY
            READ (2,*) NUMLAY(J)
      READ (2,1) DUMMY
      READ (2,1) DUMMY
            READ (2,*) DELEM(J)
      READ (2,1) DUMMY
      READ (2,1) DUMMY
            READ (2,*) TRGH(J)
      READ (2,1) DUMMY
      READ (2,1) DUMMY
            READ (2,*) TLEFT(J)
      READ (2,1) DUMMY
      READ (2,1) DUMMY
            READ (2,*) RATIO(J)
      READ (2,1) DUMMY
      READ (2,1) DUMMY
            READ (2,*) ASPECT(J)
      READ (2,1) DUMMY
      READ (2,1) DUMMY
            READ (2,*) POROS(J)
      READ (2,1) DUMMY
      THCOND(J)=0.D0
   10 HECAP(J)=0.0D0
      REWIND 2
      RETURN
```

```
      END
*****************************************************************
* SUBROUTINE NOPAD * GETS RID OF BLANKS IN NAMES  ***********
*****************************************************************
      SUBROUTINE NOPAD(NAME)
      CHARACTER*70 OLD,NEW,NAME
      CHARACTER*1 O(70),N(70)
      INTEGER I,J
      EQUIVALENCE (OLD,O(1))
      EQUIVALENCE (NEW,N(1))
      OLD=NAME
      NEW='
     *                    '
      J=0
      DO 10 I=1,70
      N(I)=' '
      IF (O(I) .NE.' ') THEN
      J=J+1
      N(J)=O(I)
      END IF
   10 CONTINUE
      NAME=NEW
      RETURN
      END
*****************************************************************
* SUBROUTINE WFLOW * COMPUTE THE WORK FLOW AT Z  **********
*****************************************************************
      SUBROUTINE WFLOW(P1,Z,W2)
      REAL*8 W2
      COMPLEX*16 P1,Z
      W2=CDABS(P1)**2 * DIMAG((0.D0,1.D0)/Z) / 2.D0
      RETURN
      END
*****************************************************************
* SUBROUTINE QFLOW * COMPUTE THE HEAT FLOW AT Z.  **********
* I HAVE ASSUMED THE COEFFICIENT OF THERMAL EXPANSION BETA=1/TEMP. **
*****************************************************************
      SUBROUTINE QFLOW(POROS,P1,Z,FLAM,FLAMT,W,DENS,T0Z,KGAS,KSOLID,Q2)
      REAL*8 POROS,DENS,T0Z,KGAS,KSOLID,Q2,NPR,CP,GAMMA
      COMPLEX*16 P1,Z,FLAM,FLAMT,W
      COMMON /PHYCON/ GAMMA,NPR,CP
      Q2=POROS*CDABS(P1)*CDABS(P1)/2.D0
      Q2=Q2*DIMAG((0.D0,1.D0)*(DCONJG(FLAMT)/FLAM-1.D0)/
     *  (POROS*Z*(1.D0+NPR) ) -
     *  T0Z * DENS * CP*(FLAM*NPR +DCONJG(FLAMT) ) /
     *  (POROS**2 * W*(CDABS(FLAM*Z))**2*(1.D0-NPR**2)))-
     *  T0Z*(POROS*KGAS + (1.D0-POROS)*KSOLID)
      RETURN
      END
*****************************************************************
* SUBROUTINE DERIVS * COMPUTE THE DERIVATIVES DZ/DZ AND DP/DZ FOR
* THE RUNGE-KUTTA WORK.
*****************************************************************
      SUBROUTINE DERIVS(ZETA,ZINT,ALPRIM,P,Z,DPDZ,DZDZ)
      COMPLEX*16 ZETA,ZINT,ALPRIM,P,Z,DPDZ,DZDZ,I,FAC,FAC2
      I = (0.D0,1.D0)
      FAC = Z/ZINT
      FAC = (1.D0 - FAC*FAC)
      FAC2 = I * ZETA * ZINT
      DZDZ = FAC2 * FAC + 2.D0 * ALPRIM * Z
*     FAC = I * ZETA * (ZINT - Z*Z/ZINT)
*     DZDZ = FAC + 2.D0 * ALPRIM * Z
      DPDZ = FAC2 * P / Z
      RETURN
```

```
      END
*****************************************************************
* SUB STAKPM * GET THE MANY PARAMETERS WHICH ARE TEMPERATURE DEPENDENT
* IN THE STAK.  USED FOR RUNGE KUTTA INTEGRATION.
* THE STACK IS ASSUMED TO HAVE POROUS WALLS.
*****************************************************************
      SUBROUTINE STAKPM(ETYPE,W,POROUS,PAMB,T,T0Z,DENS,RATIO,ASPECT,
     *            FLAM,FLAMT,ZETA,ALPRIM,ZINT)
      CHARACTER*70 ETYPE
      REAL*8 POROUS,PAMB,T,T0Z,DENS,RATIO,ASPECT
      COMPLEX*16 FLAM,FLAMT,ZETA,ALPRIM,ZINT,W,LAMBDA,LAMBDT
* POROUS WALL VARIABLES.
      REAL*8 PORTOT,PORWAL,DWALL,WFACT
      COMPLEX*16 XI
* SUPPORTING ROLE VARIABLES.
      REAL*8 SSPEED,VISC,CP,NPR,GAMMA
      COMMON /PHYCON/ GAMMA,NPR,CP
* SET THE POROUS WALL CONSTANTS FOR THE 200 CELL CERAMIC.
* TO TURN OFF THE POROUS WALL CALCULATION JUST LET XI=1.D0 BELOW.
      PORWAL = 0.49D0
      DWALL = 100.D-6
      PORTOT = POROUS*(1.D0 + 2.D0*PORWAL*DWALL/RATIO)
      WFACT = GAMMA*(PORTOT-POROUS)/(2.D0*POROUS)
* BEGIN
      CALL VDCHE(T,PAMB,VISC,DENS,SSPEED,KGAS)
      CALL GETLAM(DENS,VISC,W,RATIO,LAMBDA)
      LAMBDT = DSQRT(NPR) * LAMBDA
       IF (ETYPE.EQ.'RECT') THEN
        CALL FRECT(ASPECT,LAMBDA,FLAM)
        CALL FRECT(ASPECT,LAMBDT,FLAMT)
       ELSE IF (ETYPE.EQ.'CYL') THEN
        CALL FCYL(LAMBDA,FLAM)
        CALL FCYL(LAMBDT,FLAMT)
       ELSE IF (ETYPE.EQ.'SLIT') THEN
        CALL FSLIT(LAMBDA,FLAM)
        CALL FSLIT(LAMBDT,FLAMT)
       ELSE
        STOP
       END IF
      CALL WNHEX(FLAMT,FLAM,W,SSPEED,ZETA)
      ZINT = DENS*W / (POROUS * FLAM * ZETA)
      XI = GAMMA - (GAMMA-1.D0)*FLAMT
      XI = 1.D0 + WFACT / XI
      ZETA = ZETA * XI
      ZINT = ZINT / XI
       ALPRIM = T0Z * (FLAMT / FLAM - 1.D0) / (2.D0 * T * (1.D0 - NPR))
      RETURN
      END
*****************************************************************
* SUBROUTINE ZPTRAN * DO THE IMPEDANCE TRANSLATION THEOREM ****
* * DO ALSO THE PRESSURE TRANSLATION THEOREM ****
* THIS VERSION IS FOR THE HEAT EXCHANGERS AND OPEN TUBE SECTIONS.
*****************************************************************
      SUBROUTINE ZPTRAN(ZINT,SN,CS,Z,ZMD,P1,P1MD)
      COMPLEX*16 Z,ZMD,ZINT,SN,CS,CT,P1,P1MD,FAC
      CT = CS / SN
      FAC = ZINT / Z
      ZMD = ZINT * ( CT - (0.D0,1.D0)*FAC ) /
     * ( FAC*CT - (0.D0,1.D0) )
       P1MD = P1 * ( CS - (0.D0,1.D0) * FAC * SN )
      RETURN
      END
*****************************************************************
* SUBROUTINE ZRIGID ** IMPEDANCE OF A RIGID TERMINATION.
```

```
*************************************************************************
      SUBROUTINE ZRIGID(DENS,SSPEED,VISC,W,Z)
      REAL*8 DENS,SSPEED,VISC,NPR,GAMMA,CP
      COMPLEX*16 Z,W,FAC
      COMMON /PHYCON/ GAMMA,NPR,CP
      FAC = CDSQRT( DENS*SSPEED**2 / (W*VISC) )
      Z = (1.D0,1.D0)*DENS*SSPEED*FAC*DSQRT(NPR)/(DSQRT(2.D0)*(GAMMA -
     *          1.0D0))
      RETURN
      END
*************************************************************************
* SUBROUTINE WNTUBE ** WAVENUMBERS FOR WAVES IN THE OPEN TUBE PARTS.
*************************************************************************
      SUBROUTINE WNTUBE(LAMBDA , W , SSPEED , K)
      REAL*8 SSPEED,GAMMA,NPR,LAMBDA,FAC1,CP
      COMPLEX*16 K,W
      COMMON /PHYCON/ GAMMA,NPR,CP
      FAC1 = ( 1.D0 + (GAMMA - 1.D0) / DSQRT(NPR) ) /  DSQRT(2.D0)
      K = W/SSPEED * ( 1.D0 + (1.D0 , 1.D0) * FAC1 / LAMBDA )
      RETURN
      END
*************************************************************************
* SUBROUTINE FTUBE * COMPUTES F(LAMBDA) FOR THE RESONANT TUBE.
*************************************************************************
      SUBROUTINE FTUBE(LAMBDA,FLAM)
      COMPLEX*16 LAMBDA,FLAM
      FLAM = 1.D0 - (1.D0,1.D0) * DSQRT(2.0D0) / LAMBDA
      RETURN
      END
*************************************************************************
* SUBROUTINE WNHEX ** WAVENUMBERS FOR WAVES IN THE HEAT EXCHANGERS.
*************************************************************************
      SUBROUTINE WNHEX(FLAMT , FLAM , W , SSPEED , K)
      REAL*8 SSPEED,GAMMA,NPR,CP
      COMPLEX*16 FLAMT,FLAM,K,W
      COMMON /PHYCON/ GAMMA,NPR,CP
      K = W/SSPEED * CDSQRT( (GAMMA - (GAMMA - 1.D0)*FLAMT) / FLAM )
      RETURN
      END
*************************************************************************
* SUBROUTINE VDCHE ** VISCOSITY, DENSITY, AND SOUND SPEED OF HELIUM
* AS A FUNCTION OF TEMPERATURE AND AMBIENT PRESSURE. ALSO THE THERMAL
* CONDUCTIVITY.
*************************************************************************
      SUBROUTINE VDCHE(TABS , PAMB , VISC , DENS , SSPEED,KGAS)
      REAL*8 TABS,PAMB,VISC,DENS,SSPEED,GAMMA,NPR,CP,KGAS
      COMMON /PHYCON/ GAMMA,NPR,CP
      DENS = PAMB * 4.0D-3 / ( TABS * 8.3143D0 )
* MY EXPRESSION FOR VISCOSITY.
      VISC = 1.887D-5 * (TABS / 273.15D0)**0.6567D0
* MY EXPRESSION FOR THERMAL CONDUCTIVITY:  NPR = CONSTANT.
      KGAS = VISC * CP / NPR
* SWIFT'S EXPRESSION FOR VISCOSITY.
*     VISC = 5.131D-7 * TABS**.6441D0
* SWIFT'S EXPRESSION FOR THERMAL CONDUCTIVITY. NPR NOT CONSTANT.
*     KGAS = 0.0044 * TABS**.6441D0
*     NPR = VISC * CP / KGAS
      SSPEED = 972.8D0 * DSQRT(TABS / 273.15D0)
      RETURN
      END
*************************************************************************
* SUBROUTINE FSLIT *** COMPUTES F(LAMBDA) FOR PARALLEL SLITS.
*************************************************************************
      SUBROUTINE FSLIT(LAMBDA , FLAM)
```

```
      COMPLEX*16 LAMBDA,FLAM,SQRMI,ARGUM,CTANH,AR
      SQRMI = (1.0D0 , -1.0D0) / DSQRT( 2.0D0 )
      AR = SQRMI * LAMBDA
      ARGUM = CDEXP(-AR)
      AR = AR / 2.D0
      CTANH = ( 1.D0 - ARGUM ) / ( 1.D0 + ARGUM )
      FLAM = 1.0D0 - CTANH / AR
      RETURN
      END
*****************************************************************************
* SUBROUTINE FCYL **** COMPUTES F(LAMBDA) FOR CYLINDRICAL PORES.
*****************************************************************************
      SUBROUTINE FCYL(LAMBDA , FLAM)
      COMPLEX*16 FLAM,SQRI,CBS(2),J0,J1,ARGUM,LAMBDA
      INTEGER N
      N=2
      SQRI = (1.0D0 , 1.0D0) / DSQRT( 2.0D0 )
      ARGUM = SQRI * LAMBDA
      CALL DCBJNS( ARGUM , N , CBS )
      J0 = CBS(1)
      J1 = CBS(2)
      FLAM = 1.0D0 - ( 2.0D0 * J1 ) / ( ARGUM * J0 )
      RETURN
      END
*****************************************************************************
* SUBROUTINE FRECT **** COMPUTES F(LAMBDA) FOR RECTANGULAR PORES.
* OPTIMIZED BY RANDY ZAGAR, 21 NOVEMBER 1991.
*****************************************************************************
      SUBROUTINE FRECT(ASPECT, LAMBDA, FLAM)
      REAL*8    PISQ, ASPECT, ASPSQ
      REAL*8    XN, XM, FAC, TMN, TNM, TMM
      REAL*8    TTERM, SSUM
      INTEGER   M, N, SUMMAX
      COMPLEX*16 SUM, FLAM, YMN, YNM, YMM
      COMPLEX*16 FAC1, LAMBDA, TERM
      DATA      PISQ/9.869604404D0/
      DATA      FAC/6.57022864D-1/
C
      FAC1  = PISQ / (LAMBDA * (1.D0 + ASPECT))**2
      FAC1R = DREAL(FAC1)
      FAC1I = DIMAG(FAC1)
C
      ASPSQ  = ASPECT * ASPECT
      SUMMAX = 51
      SUM    = (0.D0, 0.D0)
C
      DO 30 M = 1, SUMMAX, 2
        XM = DFLOAT(M)
        XM = XM * XM
C
        TMM = XM * (ASPSQ + 1.D0)
        YMM = DCMPLX(1.D0 - FAC1I * TMM, FAC1R * TMM)
        SUM = SUM + 1.D0 / (YMM * XM * XM)
C
        DO 40 N = M+2, SUMMAX, 2
          XN = DFLOAT(N)
          XN = XN * XN
C
          TMN = (ASPSQ * XM + XN)
          YMN = DCMPLX(1.0D0 - FAC1I * TMN, FAC1R * TMN)
C
          TNM = (ASPSQ * XN + XM)
          YNM = DCMPLX(1.0D0 - FAC1I * TNM, FAC1R * TNM)
C
```

```
      TERM = (1.D0/YMN + 1.D0/YNM) / (XM * XN)
      TTERM = TERM * DCONJG(TERM)
      SSUM  = SUM * DCONJG(SUM)
C
* GUARANTEED ACCURACY FOR THE SUM TO EXPONENT/2. E.G. SUM = SUM + ERROR
* WHERE 1.D-EXPONENT/2 = ERROR/SUM.  COMPARES ON THIS LEVEL OF ACCURACY
* WITH FRECTO.
      IF (TTERM .LT. (SSUM*1.0D-10)) GOTO 30
C
         SUM = SUM + TERM
40     CONTINUE
30    CONTINUE
      FLAM = SUM * FAC
      RETURN
      END
*************************************************************************
*  SUBROUTINE FRECTO **** COMPUTES F(LAMBDA) FOR RECTANGULAR PORES.
*  OLD SLOWER VERSION.
*************************************************************************
      SUBROUTINE FRECTO(ASPECT , LAMBDA , FLAM)
      REAL*8 PI,ASPECT,ASPSQ
      REAL*8 F,XN,XM,FAC
      INTEGER M,N,SUMMAX
      COMPLEX*16 SUM,FLAM,YMN,LAMBDA,FAC1
*  SUMMAX MUST BE AN ODD NUMBER!!!!!!!!!!!!!!!!!!!.
      PI = 4.0D0 * DATAN(1.0D0)
      FAC1 = PI * PI / ( LAMBDA * ( 1.0D0 + ASPECT ) )**2
      FAC = 64.0D0 / PI**4
      ASPSQ = ASPECT * ASPECT
      SUMMAX = 51
      SUM = (0.0D0 , 0.0D0)
      DO 30 M=SUMMAX,1,-2
      XM = DFLOAT(M)
      XM = XM*XM
      DO 40 N=SUMMAX,1,-2
      XN = DFLOAT(N)
      XN = XN*XN
      YMN = 1.D0 + (0.D0,1.D0) * FAC1 * ( ASPSQ * XM + XN )
40    SUM = SUM + 1.0D0 / ( XM * XN * YMN )
30    CONTINUE
      FLAM = SUM * FAC
      RETURN
      END
*************************************************************************
*  SUBROUTINE QUAFAC COMPUTES THE QUALITY FACTOR AND RESONANT FREQU.
*************************************************************************
      SUBROUTINE QUAFAC(AMP,FREQ,Q,RESFRE)
      REAL*8 Q,RESFRE,AMP(2000),FREQ(2000),MAXAMP,FREHAF,AMPHAF
       REAL*8 AMP2(2000),FREQ2(2000),XC(3),BL(3),BU(3),XSCALE(3)
      REAL*8 XGUESS(3),FVALUE,FSCALE(3),RPARAM(7)
      INTEGER J,JRES,JHALF,NUMDAT,JCOUNT,N,ISTART,IBTYPE,IPARAM(7)
      COMMON /QCALC/ AMP2,FREQ2,NUMDAT
      EXTERNAL FUNCT1
      N = 3
      IPARAM(1) = 0
      IBTYPE=0
      ISTART=0
      MAXAMP = 0.D0
      JCOUNT = 0
       DO 10 J=1,2000
      IF (AMP(J) .GT. MAXAMP) THEN
      MAXAMP=AMP(J)
      RESFRE = FREQ(J)
      JRES = J
```

```
      END IF
   10 CONTINUE
      AMPHAF=MAXAMP/DSQRT(2.D0)
      DO 20 J=1,2000
      IF (AMP(J) .GT. AMPHAF) THEN
      FREHAF = (FREQ(J)+FREQ(J-1))/2.D0
      Q = 0.5D0 * RESFRE / (RESFRE - FREHAF)
      JHALF = J
      GOTO 30
      END IF
   20 CONTINUE
   30 DO 40 J=JHALF-1,JRES + (JRES-JHALF) + 1
      JCOUNT = JCOUNT + 1
      AMP2(JCOUNT) = AMP(J)
   40 FREQ2(JCOUNT) = FREQ(J)
      NUMDAT = JCOUNT
      XGUESS(1) = MAXAMP
      XGUESS(2) = RESFRE
      XGUESS(3) = Q
      DO 50 J=1,3
      XSCALE(J)=1.D0
      FSCALE(J)=1.D0
      BL(J) = XGUESS(J) * .5D0
   50 BU(J) = XGUESS(J) * 2.D0
      CALL DBCONF(FUNCT1, N , XGUESS , IBTYPE , BL , BU ,
     *     XSCALE , FSCALE , IPARAM , RPARAM , XC , FVALUE)
      MAXAMP = XC(1)
      RESFRE = XC(2)
      Q = XC(3)
      RETURN
      END
*************************************************************************
****************************** SUBROUTINE FUNCT1 FOR IMSL OPTIMIZATION
*************************************************************************
      SUBROUTINE FUNCT1(N , XC , RMSERR)
      REAL*8 AMP(2000),FREQ(2000),XC(3),RMSERR,MAXSQ,F0,Q,F
      INTEGER NUMDAT,J
      COMMON /QCALC/ AMP,FREQ,NUMDAT
      MAXSQ = XC(1)*XC(1)
      F0 = XC(2)
      Q = XC(3)
      RMSERR = 0.D0
      DO 10 J=1,NUMDAT
      F = FREQ(J)
      RMSERR = ( MAXSQ / (1.D0 + (2.D0*Q*(F-F0)/F0)**2 )
     *     - AMP(J)*AMP(J))**2 + RMSERR
   10 CONTINUE
      RETURN
      END
*************************************************************************
****************************** SUBROUTINE GETLAM ********************
****************************** LAMBDA ***********************************
      SUBROUTINE GETLAM(DENS , VISC , W , R , LAMBDA)
      REAL*8 DENS,VISC,R
      COMPLEX*16 LAMBDA,W
      LAMBDA = R * CDSQRT( DENS * W / VISC )
      RETURN
      END
*************************************************************************
*************************************************************************
* VERSION 3.0 FOR HELIUM BY PAT ARNOTT, 16 FEB 91 ********************
* THIS VERSION USES RUNGE KUTTA SOLUTION FOR THE DE INSIDE OF THE STAK.
* TRANSLATION THEOREMS ARE USED IN OPEN TUBE AND HEAT EXCHANGERS.
* W THE RADIAN FREQUENCY IS ASSUMED COMPLEX EVERYWHERE.
```

```
************************************************************************
      SUBROUTINE TAE(FMIN,FMAX,NFREQ,F0EST)
      COMPLEX*16 W,LAMBDA,LAMBDT,FOFW,FPLUS,SQRI,KA
* GENERIC VARIABLES SUCH AS PHYSICAL PROPERTIES OF THE GAS.
      REAL*8 SSPEED,VISC,CP,NPR,GAMMA,KGAS,KSOLID,ARES
* Z DEPENDENT ARRAYS....
      PARAMETER (N=5000)
      REAL*8 DENS(N),TAVE(N),T0Z(N),POROUS(N),DSUB(N),ZCOOR(N),Q2(N),
     *     W2(N)
      COMPLEX*16 ALPHA(N),K(N),COMDEN(N),FLAM(N),FLAMT(N),Z(N),P1(N)
      LOGICAL INSTAK(N)
* VARIABLES WHICH DEFINE THE TAE.
      CHARACTER*70 SECTYP(100),ETYPE(100),TERMIN
      INTEGER NUMLAY(100),NUMSEC,NUMFRE,PLOTN
      REAL*8 DELEM(100),TRGH(100),TLEFT(100),RATIO(100),FRENEW
     *,ASPECT(100),POROS(100),
     * THCOND(100),HECAP(100),PAMB,FREMIN,FREMAX,DDRIVE,PAMBTM
* DEFINE SOME GLOBAL VARIABLES.
      REAL*8 PI,TWOPI,FMIN,FMAX
      INTEGER NFREQ
* EXTRA VARIABLES NECESSARY FOR RUNGE KUTTA EVALUATION OF THE PROBLEM.
      COMPLEX*16 K1,K2,K3,K4,M1,M2,M3,M4,DPDZ,DZDZ,TFUN
      COMPLEX*16 ZETA,ALPRIM,ZINT,AR,SN,CS
      REAL*8 TNS,TNSM1,F0EST,LEQUIV,RGAS,LSUM,OPL
      INTEGER I,J,JUP,JLOW,NUMTOT,NS
      COMMON /PHYCON/ GAMMA,NPR,CP
      COMMON /VARS1/ SECTYP,ETYPE,TERMIN
      COMMON /VARS2/ NUMLAY,NUMSEC,NUMFRE
      COMMON /VARS3/ DELEM,TRGH,TLEFT,RATIO,
     *  ASPECT,POROS,THCOND,HECAP,PAMB,FREMIN,FREMAX,DDRIVE
      COMMON /OUTPUT/ P1,Z,Q2,W2,ZCOOR,INSTAK
* ESTABLISH SOME OFTEN USED CONSTANTS.
      PI = 4.D0 * DATAN(1.D0)
      TWOPI = 2.D0 * PI
      NPR = 2.D0 / 3.D0
      GAMMA = 5.D0 / 3.D0
       RGAS = 8.3143D0 * 1000.0D0 / 4.D0
       CP = 2.5D0 * 8.3143D0 / 4.D-3
      KSOLID = 0.16
      SQRI = (1.D0,1.D0) / DSQRT(2.D0)
* GET DETAILS OF THE TAE.
      CALL SETVAL
      ARES = PI * RATIO(NUMSEC)**2
* ESTIMATE THE RESONANT FREQUENCY FROM THE LENGTH AND SOUND SPEED DIST.
      LSUM=0.D0
      OPL = 0.0
      DO 1 J=1,NUMSEC
      LEQUIV = DELEM(J) * POROS(J)
*     LEQUIV = DELEM(J)
      LSUM = LSUM + LEQUIV
      SSPEED=DSQRT(GAMMA*RGAS*TLEFT(J))*(3.D0+TRGH(J)/TLEFT(J))/4.D0
1     OPL = OPL + SSPEED*LEQUIV
      F0EST = OPL / (2.D0 * LSUM**2)
* COUNT THE NUMBER OF BINS USED.....
      NUMTOT = 0
      DO 10 J=1,NUMSEC
10    NUMTOT = NUMTOT + NUMLAY(J)
      NUMTOT = NUMTOT + 1
      FMIN = FREMIN
      FMAX = FREMAX
      NFREQ = NUMFRE
      RETURN
*     AMBIENT PRESSURE VARIATION IS HARDWIRED IN HERE.
      ENTRY TAE1(W,FOFW,FPLUS,PAMBTM)
```

```
      PAMB = PAMBTM
*  GET THE SPECIFIC ACOUSTIC IMPEDANCE AND PRESSURE AT ALL POINTS.
*  START AT THE RIGHT AND MOVE TO THE LEFT.
      IF (TERMIN .EQ. 'RIGID') THEN
       CALL VDCHE(TRGH(NUMSEC),PAMB,VISC,DENS(NUMTOT),SSPEED,KGAS)
       CALL ZRIGID(DENS(NUMTOT),SSPEED,VISC,W,Z(NUMTOT))
      ELSE IF (TERMIN .EQ. 'FREE') THEN
       CALL VDCHE(TRGH(NUMSEC),PAMB,VISC,DENS(NUMTOT),SSPEED,KGAS)
       CALL GETLAM(DENS(NUMTOT),VISC,W,RATIO(NUMSEC),LAMBDA)
       CALL WNTUBE(LAMBDA,W,SSPEED,K(NUMTOT))
       KA = K(NUMTOT) * RATIO(NUMSEC)
       Z(NUMTOT) = SSPEED*DENS(NUMTOT)*KA*(KA/4.D0 - (0.0D0,0.6D0))
      ELSE IF (TERMIN .EQ. 'INFIN') THEN
       CALL VDCHE(TRGH(NUMSEC),PAMB,VISC,DENS(NUMTOT),SSPEED,KGAS)
       CALL GETLAM(DENS(NUMTOT),VISC,W,RATIO(NUMSEC),LAMBDA)
       CALL FTUBE(LAMBDA,FLAM(NUMTOT))
       CALL WNTUBE(LAMBDA,W,SSPEED,K(NUMTOT))
       Z(NUMTOT) = DENS(NUMTOT) * W / (FLAM(NUMTOT) * K(NUMTOT))
      ELSE
       STOP
      END IF
      P1(NUMTOT) = 1.D0
*  APPLY THE IMPEDANCE AND PRESSURE TRANSLATION THEOREMS EVERYWHERE.
*  WORK FROM RIGHT TO LEFT.
      DO 40 I=NUMSEC,1,-1
      JUP = 0
      DO 50 J=I+1,NUMSEC
50    JUP = JUP + NUMLAY(J)
      JUP = NUMTOT - JUP - 1
      JLOW = JUP - NUMLAY(I) + 1
      DSUB(JUP)  = DELEM(I) / NUMLAY(I)
      POROUS(JUP) = POROS(I)
*  IMPEDANCE TRANSLATE FOR THE OPEN TUBE OR HEAT EXCHANGER SECTIONS.
      IF (SECTYP(I).EQ.'OPENTU' .OR. SECTYP(I).EQ.'HEXCH') THEN
       CALL VDCHE(TRGH(I),PAMB,VISC,DENS(JUP),SSPEED,KGAS)
       TAVE(JUP) = TRGH(I)
       T0Z(JUP) = 0.0D0
       ALPHA(JUP) = (0.D0,0.D0)
       CALL GETLAM(DENS(JUP),VISC,W,RATIO(I),LAMBDA)
       LAMBDT = DSQRT(NPR) * LAMBDA
       IF (SECTYP(I).EQ.'OPENTU') THEN
        CALL FTUBE(LAMBDA,FLAM(JUP))
        CALL FTUBE(LAMBDT,FLAMT(JUP))
        CALL WNTUBE(LAMBDA,W,SSPEED,K(JUP))
*        CALL FCYL(LAMBDA,FLAM(JUP))
*        CALL FCYL(LAMBDT,FLAMT(JUP))
*        CALL WNHEX(FLAMT(JUP),FLAM(JUP),W,SSPEED,K(JUP))
*  OTHERWISE, THE TUBE SECTION IS A HEAT EXCHANGER.  FIND ITS GEOMETRY.
       ELSE IF (SECTYP(I).EQ.'HEXCH') THEN
        IF (ETYPE(I).EQ.'RECT') THEN
         CALL FRECT(ASPECT(I),LAMBDA,FLAM(JUP))
         CALL FRECT(ASPECT(I),LAMBDT,FLAMT(JUP))
        ELSE IF (ETYPE(I).EQ.'CYL') THEN
         CALL FCYL(LAMBDA,FLAM(JUP))
         CALL FCYL(LAMBDT,FLAMT(JUP))
        ELSE IF (ETYPE(I).EQ.'SLIT') THEN
         CALL FSLIT(LAMBDA,FLAM(JUP))
         CALL FSLIT(LAMBDT,FLAMT(JUP))
        ELSE
         STOP
*        AN ERROR ON THE INPUT OF ETYPE(I) HAS OCCURED.
        END IF
        CALL WNHEX(FLAMT(JUP),FLAM(JUP),W,SSPEED,K(JUP))
       END IF
```

```
      COMDEN(JUP)=DENS(JUP)/FLAM(JUP)
      ZINT = COMDEN(JUP) * W / ( K(JUP) * POROUS(JUP) )
      AR = K(JUP) * DSUB(JUP)
      SN = CDSIN(AR)
      CS = CDCOS(AR)
      DO 60 J=JUP,JLOW,-1
      INSTAK(J)=.FALSE.
      DENS(J)=DENS(JUP)
      TAVE(J)=TAVE(JUP)
      T0Z(J) = T0Z(JUP)
      POROUS(J)=POROUS(JUP)
      ALPHA(J) = ALPHA(JUP)
      FLAM(J) = FLAM(JUP)
      FLAMT(J) = FLAMT(JUP)
      K(J) = K(JUP)
      COMDEN(J) = COMDEN(JUP)
      DSUB(J) = DSUB(JUP)
      CALL ZPTRAN(ZINT,SN,CS,Z(J+1),Z(J),P1(J+1),P1(J))
60    CONTINUE
      ELSE IF (SECTYP(I).EQ.'STACK') THEN
* IMPEDANCE TRANSLATE FOR THE STACK SECTIONS.
      T0Z(JUP)=(TRGH(I) - TLEFT(I)) / DELEM(I)
      NS = 0
      DO 70 J=JUP,JLOW,-1
      INSTAK(J)=.TRUE.
      NS = NS + 1
      TNS = TRGH(I) - (TRGH(I) - TLEFT(I)) * DFLOAT(NS)
     *            / DFLOAT(NUMLAY(I))
      TNSM1 = TRGH(I) - (TRGH(I) - TLEFT(I)) * DFLOAT(NS-1)
     *            / DFLOAT(NUMLAY(I))
      TAVE(J) = (TNS + TNSM1) / 2.D0
      POROUS(J) = POROUS(JUP)
      DSUB(J) = DSUB(JUP)
      T0Z(J) = T0Z(JUP)
* START THE RUNGE-KUTTA
      CALL STAKPM(ETYPE(I),W,POROUS(J),PAMB,TNSM1,T0Z(J),DENS(J),
     2    RATIO(I),ASPECT(I),FLAM(J),FLAMT(J),ZETA,ALPRIM,ZINT)
      CALL DERIVS(ZETA,ZINT,ALPRIM,P1(J+1),Z(J+1),DPDZ,DZDZ)
      K1 = -DSUB(J)*DPDZ
      M1 = -DSUB(J)*DZDZ
      P1(J) = P1(J+1) + K1/2.D0
      Z(J)  = Z(J+1) + M1/2.D0
      CALL STAKPM(ETYPE(I),W,POROUS(J),PAMB,TAVE(J),T0Z(J),DENS(J),
     2    RATIO(I),ASPECT(I),FLAM(J),FLAMT(J),ZETA,ALPRIM,ZINT)
      CALL DERIVS(ZETA,ZINT,ALPRIM,P1(J),Z(J),DPDZ,DZDZ)
      K2 = -DSUB(J)*DPDZ
      M2 = -DSUB(J)*DZDZ
      P1(J) = P1(J+1) + K2/2.D0
      Z(J)  = Z(J+1) + M2/2.D0
      CALL DERIVS(ZETA,ZINT,ALPRIM,P1(J),Z(J),DPDZ,DZDZ)
      K3 = -DSUB(J)*DPDZ
      M3 = -DSUB(J)*DZDZ
      P1(J) = P1(J+1) + K3
      Z(J)  = Z(J+1) + M3
      CALL STAKPM(ETYPE(I),W,POROUS(J),PAMB,TNS,T0Z(J),DENS(J),
     2    RATIO(I),ASPECT(I),FLAM(J),FLAMT(J),ZETA,ALPRIM,ZINT)
      CALL DERIVS(ZETA,ZINT,ALPRIM,P1(J),Z(J),DPDZ,DZDZ)
      K4 = -DSUB(J)*DPDZ
      M4 = -DSUB(J)*DZDZ
      P1(J) = P1(J+1) + (K1+2.D0*K2+2.D0*K3+K4)/6.D0
      Z(J) = Z(J+1) + (M1+2.D0*M2+2.D0*M3+M4)/6.D0
      COMDEN(J)=DENS(J)/FLAM(J)
      ALPHA(J) = ALPRIM
70    CONTINUE
```

```
      ELSE
*  AN ERROR ON INPUT OF SECTYP HAS OCCURED.
       STOP
      END IF
40    CONTINUE
*  THE IMPEDANCE IS NOW KNOWN AT ALL SPOTS IN THE TAE.
*  GET THE ACOUSTIC PRESSURE, ZCOOR, WORK AND HEAT FLUXES.
*       ZCOOR(1) = 0.0D0
       IF (TERMIN.EQ.'INFIN') THEN
        TFUN =  1.D0 / P1(1)
       ELSE
        TFUN  =  (0.D0,-1.D0) * W * Z(1) * DDRIVE / P1(1)
       END IF            ! TERMIN.EQ.'INFIN' CONDITIONAL.
       P1(1) = TFUN * P1(1)
*      CALL WFLOW(P1(1),Z(1),W2(1))
       DO 80 J=1,NUMTOT-1
       P1(J+1) = P1(J+1) * TFUN
*      ZCOOR(J+1) = ZCOOR(J) + DSUB(J)
*      CALL WFLOW(P1(J+1),Z(J+1),W2(J+1))
*      CALL QFLOW(POROUS(J),P1(J),Z(J),FLAM(J),FLAMT(J),W,
*     *           DENS(J),T0Z(J),KGAS,KSOLID,Q2(J))
80     CONTINUE
*      J = NUMTOT-1
*      CALL QFLOW(POROUS(J),P1(J+1),Z(J+1),FLAM(J),FLAMT(J),W,
*     *        DENS(J),T0Z(J),KGAS,KSOLID,Q2(NUMTOT))
*      DO 81 J=1,NUMTOT
*      Q2(J) = Q2(J) * ARES
*81    W2(J) = W2(J) * ARES
*  THE SIGN OF Z(1) WAS CHANGED ON 8-12-91.  THE IMPEDANCE LOOKING TO
*  THE RIGHT HAS TO BE EQUAL TO MINUS THE IMPEDANCE LOOKING TO THE LEFT
*  AND THE MINUS SIGN COMES FROM THE DIRECTION OF PARTICLE VELOCITY.
       FOFW = SQRI * CDSQRT(DENS(1)**3 * SSPEED**4 * NPR / (W*VISC) )/
      *     (GAMMA - 1.D0)  + Z(1)
       FPLUS = FOFW - 2.D0 * Z(1)
       RETURN
       END
*************************************************************************
*  SUBROUTINE CHANGE.  USED TO INSERT A NUMBER INTO A LINE OF A
*  SEQUENTIAL FILE.
*************************************************************************
       SUBROUTINE CHANGE(FNUM,LNUM,TO)
       INTEGER FNUM,LNUM,J
       CHARACTER*80 LINE
1      FORMAT(A80)
       REAL*8 TO
       OPEN(3,FILE='SCRATCH')
       REWIND(3)
       REWIND(FNUM)
        DO 10 J=1,5000
       READ(FNUM,1,END=20) LINE
       IF (J.NE.LNUM) THEN
       WRITE(3,1) LINE
       ELSE
       WRITE(3,*) TO
       END IF
10     CONTINUE
20     ENDFILE 3
       REWIND(3)
       REWIND(FNUM)
        DO 30 J=1,5000
       READ(3,1,END=40) LINE
30     WRITE(FNUM,1) LINE
40     ENDFILE FNUM
       REWIND(3)
```

```
      REWIND(FNUM)
      RETURN
      END
*************************************************************************
* PROGRAM :  EVALUATE TAE FOR A RANGE OF PARAMETERS.
* VERSION EXPLICITELY FOR THE UMTAE.
* PAT ARNOTT, 22 MARCH 1991, MOD 11-15-91.
* DETERMINES THE STABILITY CURVE FOR THE FIRST TWO MODES AS A FUNCTION
* OF THE AMBIENT PRESSURE. INCLUDES FINITE WALL POROSITY IN THE STACK.
*************************************************************************
      PROGRAM UMTAE2
* VARIABLES USED TO GET THE Q.
      REAL*8 AMPLIT(2000),FREQU(2000),QUAL,RESFRE,RESOLD,QOLD
      REAL*8 QOLD2,TOLD2,RSOLD2,TOLD
* VARIABLES RETURNED FROM TAE.
      REAL*8 FREMIN,FREMAX,F0EST
      INTEGER NUMFRE
* LOCAL VARIABLES TO THE MAINLINE.....
      REAL*8 PAMB,PMIN,PMAX,TMIN
      REAL*8 TRGH,TONSET,PI,TWOPI,TEST,TESTF,TNOLD,TNOLD2
      INTEGER ITRGH,PLOTN,IFREQ,NTIMES,NPAMBS,NPRESS,MODE
      COMPLEX*16 W,WNEW,FOFW,DFOFW,FOFWPE,WPEW,EPSIL
      COMPLEX*16 FPLUS,DUMB,WMEW,FOFWME,WCORR,WSTART
* DEFINE THE VARIABLE FOR THE OUTPUT COMMON BLOCK.
      PARAMETER (N=5000)
      REAL*8 Q2(N),W2(N),ZCOOR(N)
      COMPLEX*16 Z(N),P1(N)
      LOGICAL INSTAK(N)
      COMMON /OUTPUT/ P1,Z,Q2,W2,ZCOOR,INSTAK
* PRELIMINARIES.
      PI = 4.D0 * DATAN(1.D0)
      TWOPI = 2.D0 * PI
* SET UP THE AMBIENT PRESSURE LOOP.....
      PMIN = 2.00D5
      PMAX = 8.0D5
      PMIN = DSQRT(PMIN)
      PMAX = DSQRT(PMAX)
      NPAMBS=16
* SET UP THE MODE LOOP.....
      DO 18 MODE=2,2
      IF (MODE.EQ.2) THEN
        TMIN = 603.D0
      ELSE
        TMIN = 403.D0
      END IF
      DO 17 NPRESS=14,NPAMBS
        WCORR = (3151.633184D0,-67.8178943D0)/(3152.921237D0,-66.734D0)
      PLOTN = 0
      QUAL=30.D0
      PAMB = PMIN + (PMAX-PMIN) * DFLOAT(NPRESS) / DFLOAT(NPAMBS)
      PAMB = PAMB*PAMB
* HOP ON THE TEMPERATURE CALCULATIONS.....
      DO 10 ITRGH=INT(TMIN),1593,20
      EPSIL = 1.D-8
      NTIMES=0
      TRGH = DFLOAT(ITRGH)
      CALL CHANGE(2,28,TRGH)
      CALL CHANGE(2,31,TRGH)
      CALL CHANGE(2,56,TRGH)
      CALL CHANGE(2,59,TRGH)
      CALL CHANGE(2,84,TRGH)
      PLOTN = PLOTN + 1
      CALL TAE(FREMIN,FREMAX,NUMFRE,F0EST)
      F0EST = F0EST*DFLOAT(MODE)
```

```
      WRITE (*,111) FOEST
  111   FORMAT(' RESONANT FREQUENCY ESTIMATE FROM OPL ',F9.3)
*     IF (PLOTN.NE.1) FREMIN = RESFRE*(1.D0 - 0.5D0 / QUAL)
* START THE COMPLEX EIGENFREQUENCY ALGORITHM WITH THE DRIVEN SYSTEM Q.
      IF ((QUAL.LT.200.D0).AND.((QUAL.GT.0.D0).AND.(PLOTN.LT.7))) THEN
      DO 100 IFREQ=1,NUMFRE
      IF (NUMFRE.EQ.1) THEN
       FREQ = FREMIN
      ELSE
      FREQ = FREMIN + (FREMAX-FREMIN)*DFLOAT(IFREQ)/DFLOAT(NUMFRE-1)
      END IF
      FREQ=FREQ*DFLOAT(MODE)
      W = TWOPI * FREQ
      CALL TAE1(W,FOFW,FPLUS,PAMB)
      AMPLIT(IFREQ)=CDABS(P1(1))
  100 FREQU(IFREQ) = FREQ
* GET THE Q AND RESONANT FREQUENCY USING THE CONSTANT AMPLIT DRIVER
* RESPONSE.
      CALL QUAFAC(AMPLIT,FREQU,QUAL,RESFRE)
       WRITE (29,1010) RESFRE,QUAL,TRGH-293.D0
       WRITE (27,*) TRGH-293.D0,1.D0/QUAL
      WRITE (28,*) TRGH-293.D0,RESFRE
      WRITE (*,1010) RESFRE,QUAL,TRGH-293.D0
 1010 FORMAT(' ROTE: RES FREQ=',F9.3,' Q=',F9.3,' DELTAT=',F9.3,' K')
      ELSE  ! LINEARLY INTERPOLATE TO GET A START FOR QUAL AND RESFRE.
* 1/QUAL AND RESFRE ARE ASSUMED TO BE LINEAR IN DELTA T.
      QUAL=1.D0/QOLD+(QOLD-QOLD2)*(TRGH-TOLD)/((TOLD2-TOLD)*QOLD2*QOLD)
      QUAL = 1.D0 / QUAL
      RESFRE= RESOLD + (RSOLD2-RESOLD)*(TRGH-TOLD)/(TOLD2-TOLD)
      END IF ! THIS ENDS THE INITIAL SEARCH FOR A START Q AND RESFRE.
*  NOW GET THE COMPLEX EIGENFREQUENCY FOR COMPARISON.
* INITIAL GUESS FOR THE NEWTON'S TECHNIQUE OF ROOT DETERMINATION.
      W = TWOPI * RESFRE * (1.D0 - (0.D0,0.5D0)/QUAL)
      WSTART = W
      IF (((MODE.EQ.2).AND.(PLOTN.NE.1)).OR.(MODE.EQ.1)) W = W * WCORR
      WRITE (*,*) DREAL(W)/TWOPI,-DREAL(W)/(2.D0*DIMAG(W))
  110 CALL TAE1(W,FOFW,FPLUS,PAMB)
      NTIMES=NTIMES+1
      WPEW = W * (1.D0 + EPSIL)
      WMEW = W * (1.D0 - EPSIL)
      CALL TAE1(WPEW,FOFWPE,DUMB,PAMB)
      CALL TAE1(WMEW,FOFWME,DUMB,PAMB)
      DFOFW = (FOFWPE - FOFWME) /  (2.D0 * EPSIL)
      WNEW = W - 100.D0 * FOFW / DFOFW
      EPSIL = (WNEW - W)*2.D-4/(WNEW+W)
*     TEST = CDABS((WNEW-W)/(WNEW+W))
      TESTF = CDABS(FOFW/FPLUS)
*     IF ((TEST .GT. 1.D-4) .OR. (TESTF .GT. 1.D-4))  THEN
      IF (TESTF .GT. 1.D-5)  THEN
       W = WNEW
       GOTO 110
      ELSE            ! COMPLEX EIGENFREQUENCY HAS BEEN FOUND.
       W = (W + WNEW) / 2.D0
       WCORR = W / WSTART
       WRITE (*,*) NTIMES
       WRITE (*,*) FOFW
      END IF          ! TEST .GT. OR TESTF.GT CONDITIONAL.
* GET THE Q AND RESONANT FREQUENCY.
      RESFRE = DREAL(W) / TWOPI
      QUAL = -DREAL(W)/(2.D0 * DIMAG(W))
      WRITE (39,1011) RESFRE,QUAL,TRGH-293.D0,PAMB
      WRITE (37,*) TRGH-293.D0,1.D0/QUAL
      WRITE (38,*) TRGH-293.D0,RESFRE
      WRITE (*,1011) RESFRE,QUAL,TRGH-293.D0,PAMB
```

```
1011  FORMAT(' EIG: F0',F9.3,' Q',F9.3,' DT',F9.3,' K',' PAMB',F10.2)
* DETERMINE IF ONSET HAS BEEN ACHIEVED: IF SO, GET DT AND RESFRE, NEXTP
   IF (PLOTN .EQ. 1) THEN
      RESOLD = RESFRE
      QOLD  = QUAL
      TOLD  = TRGH
   ELSE
      IF (QOLD*QUAL .LT. 0.D0) THEN
*        INTERPOLATE TO GET THE ONSET DELTA T.
         TONSET = TOLD + (TRGH - TOLD)/(1.D0 - QOLD/QUAL)
         WRITE (44,*) PAMB,TONSET-293.D0,MODE
         WRITE (*,1117) PAMB,TONSET-293.D0,MODE
1117  FORMAT(' AMBIENT PRES ',F10.2,' ONSET DELTAT',F9.3,' MODE',I3)
         GOTO 17
        ELSE       ! RESET OLD PARAMETERS TO NEW PARAMETERS.
         RSOLD2 = RESOLD
         QOLD2  = QOLD
         TOLD2  = TOLD
         RESOLD = RESFRE
         QOLD  = QUAL
         TOLD  = TRGH
      END IF       ! ONSET CONDITIONAL.
   END IF          ! PLOTN .EQ. 1
10  CONTINUE          ! TEMPERATURE LOOP INCREMENT
   TNOLD2=TNOLD
   TNOLD=TONSET
17  CONTINUE          ! PRESSURE LOOP INCREMENT
18  CONTINUE          ! MODE LOOP INCREMENT
   END
```

MAINLINE USED TO COMPUTE THE RESONANT FREQUENCY AND QUALITY FACTOR CURVES.

```
**************************************************************************
* PROGRAM :  EVALUATE TAE FOR A RANGE OF PARAMETERS.
* VERSION EXPLICITELY FOR THE UMTAE.
* PAT ARNOTT, 22 MARCH 1991, MOD 11-15-91.
* DETERMINES THE STABILITY CURVE FOR THE FIRST TWO MODES AS A FUNCTION
* OF THE AMBIENT PRESSURE. INCLUDES FINITE WALL POROSITY IN THE STACK.
* PROGRAM USED TO DETERMINE THE Q AND RESFRE OF THE UMTAE VS TEMPERATURE
**************************************************************************
   PROGRAM UMTAE2
* VARIABLES USED TO GET THE Q.
   REAL*8 AMPLIT(2000),FREQU(2000),QUAL,RESFRE,RESOLD,QOLD
   REAL*8 QOLD2,TOLD2,RSOLD2,TOLD
* VARIABLES RETURNED FROM TAE.
   REAL*8 FREMIN,FREMAX,F0EST
   INTEGER NUMFRE
* LOCAL VARIABLES TO THE MAINLINE.....
   REAL*8 PAMB,PMIN,PMAX,TMIN
   REAL*8 TRGH,TONSET,PI,TWOPI,TEST,TESTF,TNOLD,TNOLD2
   INTEGER ITRGH,PLOTN,IFREQ,NTIMES,NPAMBS,NPRESS,MODE
   COMPLEX*16 W,WNEW,FOFW,DFOFW,FOFWPE,WPEW,EPSIL
   COMPLEX*16 FPLUS,DUMB,WMEW,FOFWME,WCORR,WSTART
* DEFINE THE VARIABLE FOR THE OUTPUT COMMON BLOCK.
   PARAMETER (N=5000)
   REAL*8 Q2(N),W2(N),ZCOOR(N)
   COMPLEX*16 Z(N),P1(N)
   LOGICAL INSTAK(N)
   COMMON /OUTPUT/ P1,Z,Q2,W2,ZCOOR,INSTAK
* PRELIMINARIES.
   PI = 4.D0 * DATAN(1.D0)
   TWOPI = 2.D0 * PI
* SET UP THE AMBIENT PRESSURE LOOP.....
   PMIN = 1.73D5
   PMAX = 1.73D5
```

```
      TMIN = 293.D0
      NPAMBS=1
*  SET UP THE MODE LOOP.....
      DO 18 MODE=2,2
      DO 17 NPRESS=1,NPAMBS
        WCORR = (3151.633184D0,-67.8178943D0)/(3152.921237D0,-66.734D0)
      PLOTN = 0
      QUAL=30.D0
      PAMB = PMIN + (PMAX-PMIN) * DFLOAT(NPRESS) / DFLOAT(NPAMBS)
*  HOP ON THE TEMPERATURE CALCULATIONS.....
      DO 10 ITRGH=INT(TMIN),1593,20
      EPSIL = 1.D-8
      NTIMES=0
      TRGH = DFLOAT(ITRGH)
      CALL CHANGE(2,28,TRGH)
      CALL CHANGE(2,31,TRGH)
      CALL CHANGE(2,56,TRGH)
      CALL CHANGE(2,59,TRGH)
      CALL CHANGE(2,84,TRGH)
      PLOTN = PLOTN + 1
      CALL TAE(FREMIN,FREMAX,NUMFRE,F0EST)
      F0EST = F0EST*DFLOAT(MODE)
      WRITE (*,111) F0EST
  111   FORMAT(' RESONANT FREQUENCY ESTIMATE FROM OPL ',F9.3)
*     IF (PLOTN.NE.1) FREMIN = RESFRE*(1.D0 - 0.5D0 / QUAL)
*  START THE COMPLEX EIGENFREQUENCY ALGORITHM WITH THE DRIVEN SYSTEM Q.
      IF ((QUAL.LT.200.D0).AND.(QUAL.GT.0.D0)) THEN
      DO 100 IFREQ=1,NUMFRE
      IF (NUMFRE.EQ.1) THEN
       FREQ = FREMIN
      ELSE
      FREQ = FREMIN + (FREMAX-FREMIN)*DFLOAT(IFREQ)/DFLOAT(NUMFRE-1)
      END IF
      FREQ=FREQ*DFLOAT(MODE)
      W = TWOPI * FREQ
      CALL TAE1(W,FOFW,FPLUS,PAMB)
      AMPLIT(IFREQ)=CDABS(P1(1))
  100  FREQU(IFREQ) =  FREQ
*  GET THE Q AND RESONANT FREQUENCY USING THE CONSTANT AMPLIT DRIVER
*  RESPONSE.
       CALL QUAFAC(AMPLIT,FREQU,QUAL,RESFRE)
       WRITE (29,1010) RESFRE,QUAL,TRGH-293.D0
       WRITE (27,*) TRGH-293.D0,1.D0/QUAL,MODE
      WRITE (28,*) TRGH-293.D0,RESFRE,MODE
      WRITE (*,1010) RESFRE,QUAL,TRGH-293.D0
 1010  FORMAT(' ROTE: RES FREQ=',F9.3,' Q=',F9.3,' DELTAT=',F9.3,' K')
      ELSE  ! LINEARLY INTERPOLATE TO GET A START FOR QUAL AND RESFRE.
*  1/QUAL AND RESFRE ARE ASSUMED TO BE LINEAR IN DELTA T.
      QUAL=1.D0/QOLD+(QOLD-QOLD2)*(TRGH-TOLD)/((TOLD2-TOLD)*QOLD2*QOLD)
      QUAL = 1.D0 / QUAL
      RESFRE= RESOLD + (RSOLD2-RESOLD)*(TRGH-TOLD)/(TOLD2-TOLD)
       END IF ! THIS ENDS THE INITIAL SEARCH FOR A START Q AND RESFRE.
*  NOW GET THE COMPLEX EIGENFREQUENCY FOR COMPARISON.
*  INITIAL GUESS FOR THE NEWTON'S TECHNIQUE OF ROOT DETERMINATION.
      IF ((MODE.EQ.2).AND.((QUAL.GT.100.D0).OR.(QUAL.LT.0.D0)))
     *    THEN  ! THE ROUTINE IS OK FOR THE HIGHER MODE..... GO AHEAD
      W = TWOPI * RESFRE * (1.D0 - (0.D0,0.5D0)/QUAL)
      WSTART = W
      IF (((MODE.EQ.2).AND.(PLOTN.NE.1)).OR.(MODE.EQ.1)) W = W * WCORR
      WRITE (*,*) DREAL(W)/TWOPI,-DREAL(W)/(2.D0*DIMAG(W))
  110  CALL TAE1(W,FOFW,FPLUS,PAMB)
      NTIMES=NTIMES+1
      WPEW = W * (1.D0 + EPSIL)
      WMEW = W * (1.D0 - EPSIL)
```

```
      CALL TAE1(WPEW,FOFWPE,DUMB,PAMB)
      CALL TAE1(WMEW,FOFWME,DUMB,PAMB)
      DFOFW = (FOFWPE - FOFWME) / (2.D0 * EPSIL)
      WNEW = W - 100.D0 * FOFW / DFOFW
      EPSIL = (WNEW - W)*2.D-4/(WNEW+W)
*     TEST = CDABS((WNEW-W)/(WNEW+W))
      TESTF = CDABS(FOFW/FPLUS)
*     IF ((TEST .GT. 1.D-4) .OR. (TESTF .GT. 1.D-4)) THEN
      IF (TESTF .GT. 1.D-5) THEN
       W = WNEW
       GOTO 110
      ELSE            ! COMPLEX EIGENFREQUENCY HAS BEEN FOUND.
       W = (W + WNEW) / 2.D0
       WCORR = W / WSTART
       WRITE (*,*) NTIMES
       WRITE (*,*) FOFW
      END IF          ! TEST.GT. OR TESTF.GT CONDITIONAL.
* GET THE Q AND RESONANT FREQUENCY.
      RESFRE = DREAL(W) / TWOPI
      QUAL = -DREAL(W)/(2.D0 * DIMAG(W))
      WRITE (39,1011) RESFRE,QUAL,TRGH-293.D0,PAMB
      WRITE (37,*) TRGH-293.D0,1.D0/QUAL,MODE
      WRITE (38,*) TRGH-293.D0,RESFRE,MODE
      WRITE (*,1011) RESFRE,QUAL,TRGH-293.D0,PAMB
 1011 FORMAT(' EIG: F0',F9.3,' Q',F9.3,' DT',F9.3,' K',' PAMB',F10.2)
* DETERMINE IF ONSET HAS BEEN ACHIEVED: IF SO, GET DT AND RESFRE, NEXTP
      IF (PLOTN .EQ. 1) THEN
        RESOLD = RESFRE
        QOLD  = QUAL
        TOLD  = TRGH
      ELSE
*       IF (QOLD*QUAL .LT. 0.D0) THEN
*         INTERPOLATE TO GET THE ONSET DELTA T.
*         TONSET = TOLD + (TRGH - TOLD)/(1.D0 - QOLD/QUAL)
*          WRITE (44,*) PAMB,TONSET-293.D0,MODE
*          WRITE (*,1117) PAMB,TONSET-293.D0,MODE
*1117  FORMAT(' AMBIENT PRES ',F10.2,' ONSET DELTAT',F9.3,' MODE',I3)
*          GOTO 17
*         ELSE       ! RESET OLD PARAMETERS TO NEW PARAMETERS.
          RSOLD2 = RESOLD
          QOLD2  = QOLD
          TOLD2  = TOLD
          RESOLD = RESFRE
          QOLD  = QUAL
          TOLD  = TRGH
*       END IF       ! ONSET CONDITIONAL.
      END IF          ! PLOTN .EQ. 1
      END IF          ! CONDITIONAL ON MODE.EQ.2 AND Q>100.
 10   CONTINUE        ! TEMPERATURE LOOP INCREMENT
      TNOLD2=TNOLD
      TNOLD=TONSET
 17   CONTINUE        ! PRESSURE LOOP INCREMENT
 18   CONTINUE        ! MODE LOOP INCREMENT
      END
```

Frontiers of Nonlinear Acoustics: Proceedings of 12th ISNA
edited by M.F. Hamilton and D.T. Blackstock
Elsevier Science Publishers Ltd, London, 1990

Development of Nonlinear Waves in a Thermoacoustic Prime Mover

A.A. Atchley, H.E. Bass and T.J. Hofler
Physics Department
Naval Postgraduate School
Monterey, CA 93943

Abstract

Following the onset of self oscillation in a thermoacoustic prime mover a periodic signal with an acoustic overpressure of 1-8 % of ambient pressure (3 atm of Helium) is observed. The waveform adopts a non-sinusoidal shape which is assumed to be the result of nonlinear propagation. There are, however, other possible sources of this nonlinearity which must be examined in the future. These include a varying cold end temperature when displaced amplitudes approach the depth of the heat exchangers and effects of the large amplitude acoustic signal on the assumed linear variation of temperature within the thermoacoustic stack.

Introduction

Thermoacoustic prime movers convert stored thermal energy into useful work in the form of sound. Referring to Figure 1, a typical prime mover configuration consists of a stack of plates, called the prime mover stack (or simply, the stack), which is in thermal contact with two heat exchangers. For the work reported here, one end of the prime mover stack was held at elevated temperatures while the other end was held at ambient (room) temperature. However, the important quantity is the temperature difference across the prime mover stack, not the absolute temperatures of either end. The prime mover stack and heat exchangers are housed within an acoustic resonator. The prime mover stack/heat exchanger/resonator assembly is called a (thermoacoustic) prime mover.

Thermal energy is stored in the prime mover by imposing a temperature difference across the stack, the two quantities being proportional. In order for the prime mover to produce net positive work, i.e. to produce audible sound, the amount of stored energy converted to sound must exceed the amount of acoustic energy dissipated by losses in the

prime mover. The dominant loss mechanism for the type of gases and frequencies of interest here are thermal and viscous losses at the resonator walls and the stack and heat exchanger surfaces. The prime mover is said to have reached "onset" when the temperature difference across the stack is sufficient for the prime mover to generate and sustain detectable levels of sound. The use of the word "detectable" is not meant to imply that onset is a subtle question of detection thresholds. When onset is reached, the observer (and everyone else in the room) knows it.

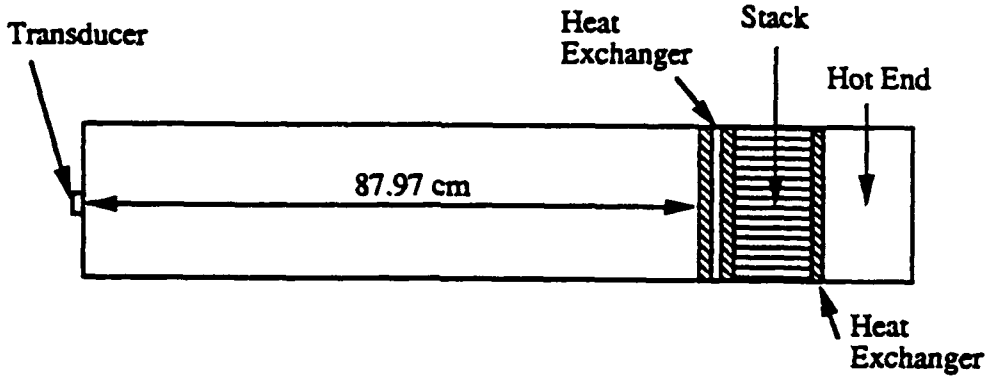

Figure 1. Prime Mover

Once onset of self oscillation is reached, the acoustic amplitude in the tube immediately assumes a large value, typically about 1% of the ambient pressure. The observed waveform is noticeably non-sinusoidal. As more energy is supplied to the hot end of the stack, the temperature of that end increases only slightly while the acoustic amplitude in the tube increases rapidly. Since we are interested in efficient conversion of heat into sound, this is a very favorable operating regime. Unfortunately, as the acoustic amplitude increases, an increasing fraction of the acoustic energy appears as higher harmonics - harmonic distortion increases. It is this increase in non-linear generation of harmonics that will be the subject of this paper.

Experimental System

The resonance tube is made from a 88.1 cm long,3.82 cm ID copper tube connected to an ambient heat exchanger, stainless steel prime mover stack, and nickel hot end. The hot end consists of a 5.00 cm long, 3.82 cm ID nickel tube and a heat exchanger. One end of the tube is capped and accommodates a type K thermocouple probe used to sense the hot heat exchanger temperature. The hot heat exchanger consisting of 25, 0.051 cm thick, 0.762

cm long nickel plates. The gap between each pair of adjacent plates is 0.102 cm.

The prime mover stack consists of 35, 0.25 cm thick, 3.42 cm long 304 stainless steel plates spaced by 0.079 cm and is housed within a thin walled stainless steel tube. A temperature gradient is established across this stack to supply the required heat flux.

The ambient heat exchanger is employed to maintain one end of the stack at a constant ambient temperature. The construction of this heat exchanger is very similar to the hot heat exchanger, except it has a length of 1.02 cm and contains 25 copper plates. The ambient heat exchanger actually consists of two such stacks separated by a 0.15 cm gap.

Control of the temperature gradient across the prime mover stack is achieved by an OMEGA a Model HBA 202040 heater and a Neslab Model RET-110 constant temperature bath. The heater is mounted to surround the nickel heater section. Electrical power is provided to the heater through a variac. Water is circulated by the constant temperature bath through a water jacket which surrounds the ambient heat exchanger, also circulated through flexible plastic tubing which is wrapped around the copper tube to maintain a uniform temperature. Three type E thermocouples were glued to the top, middle, and bottom the the long copper section of the prime mover to sense the temperature along that section.

The closed end of the copper tube accommodates an ENDEVCO Model 8510B-5 piezoresistive pressure transducer, housed within a back volume. A high impedance leak is provided between the resonator and the back volume to eliminate dc pressure difference with little effect on acoustic pressure differences.

Experimental Results

Figures 2 and 3 show the waveform and the spectrum of the sound generated by the prime mover above onset. The mean gas pressure is 307 kPa. The temperature difference across

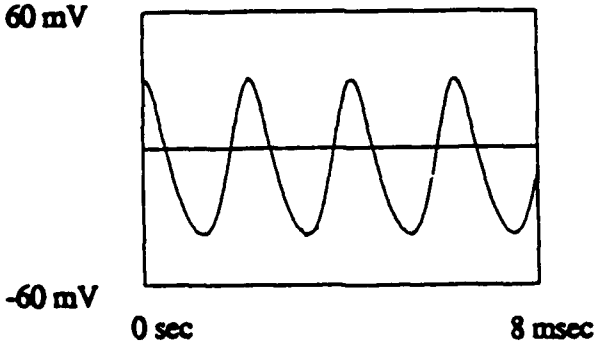

Figure 2. Waveform of the sound generated by the prime mover at a temperature difference of 325 °C.

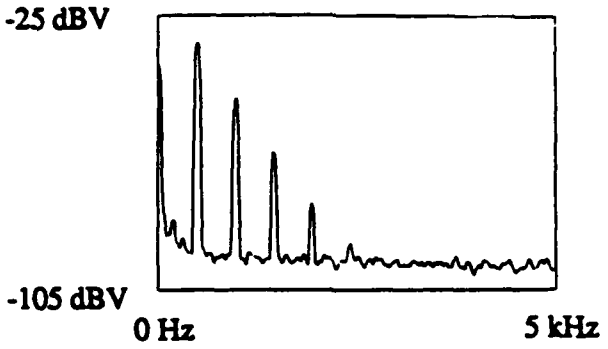

Figure 3. Spectrum of waveform shown in Figure 2.

the stack is 325 °C which is slightly above onset. The signal exhibits slight distortion, particularly in the positive cycle. Figure 3 shows that the difference in spectrum level between the first few modes is larger than 15 dB. Figures 4 and 5 show results for a temperature difference of 368 °C, the signal is distorted sharply in both positive and negative half-cycles. The difference between spectrum levels for the first few modes has decreased further to less than 6 dB and more energy has been spread to higher modes.

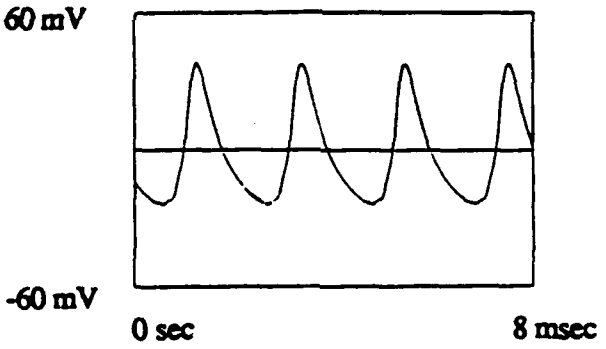

Figure 4. Waveform of the sound generated by the prime mover at a temperature difference of 368 °C.

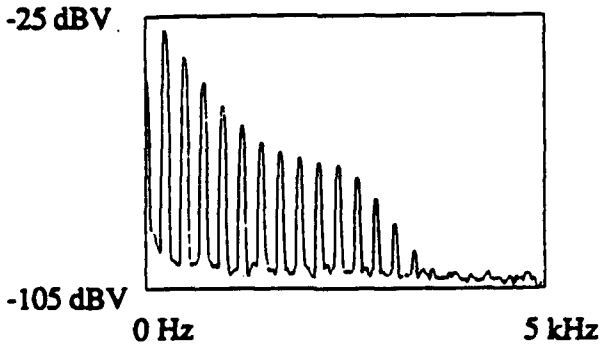

Figure 5. Spectrum of waveform shown in Figure 4.

The peak positive pressure amplitudes for temperature differences of 325, 368, and 433 °C amplitude are approximately 3.3, 13.5, and 24.2 kPa, respectively. These amplitudes correspond to approximately 1.1, 4.4 and 7.9% of mean gas pressure.

There can be little doubt that the signal at the higher frequencies is being generated by the fundamental. If we examine the frequency of these spectral peaks, they are integral multiples of the fundamental to within four significant digits and have no measurable line width.

Interpretation of Results

Prediction of harmonic generation (one method of describing the non-sinusoidal waveform) is not straight forward even with a good understanding of dissipation mechanisms in the stack. In a resonance tube, the frequency of overtones depends upon dispersion while harmonic generation results in exact multiples of the fundamental. This means that sound generated nonlinearly will be generated at a frequency different from a tube resonance. We will develop here only a qualitative treatment.

We apply a treatment of finite amplitude standing waves by Coppens and Sanders [1]. They have shown that the ratio of the amplitude of the second harmonic to that of the fundamental is given by

$$\frac{P_2}{P_1} = \frac{1}{2} P_1 \left(\frac{\beta}{\rho_0 c_0^2} \right) Q_2. \tag{1}$$

Similarly, the amplitude of the third harmonic to that of the fundamental is given by

$$\frac{P_3}{P_1} = P_1 \left(\frac{P_2}{P_1} \right) \frac{\beta}{\rho_0 c_0^2} Q_3. \tag{2}$$

In these equations $\beta = (\gamma+1)/2$, ρ_0 is the ambient density of the gas, c_0 is the infinitesimal amplitude sound speed, $Q_2 = (\sqrt{2}\,\omega/4\,\alpha\,c_0)\cos\theta_2$ and $Q_3 = (\sqrt{3}\,\omega/4\,\alpha\,c_0)\cos\theta_3$. α is the attenuation coefficient, which is related to the quality factor q as $\alpha = \omega/2qc_0$. For a system driven at its fundamental frequency [1], $\tan\theta_2 = 0.414$ and $\tan\theta_3 = 0.732$.

Above the onset of self oscillation, the q of the fundamental q_1 is infinite. Therefore q_1 must be estimated from the q's higher modes. The prime mover is dominated by wall losses and so $q_n \approx \omega_n^{1/2}$.

The peak amplitude of the fundamental in Figure 3 is 3.3 kPa. Assuming T = 293 k (which is approximately true for most of the prime mover) and an ambient pressure of 307 kPa, $\rho_0 = 0.54$ kg/m3, $\beta = 1.33$ and $c_0 = 1008$ m/s. The q of the third mode is 68.

Performing the calculations yields (P_2/P_1) = -20 dB and (P_3/P_1) = -32 dB. Referring to Figure 3 shows that the measured values are closer to -16 and -32 dB, respectively, in reasonable agreement with theory.

For the case shown in Figure 5 the calculations predict (P_2/P_1) = -7 dB and (P_3/P_1) = -8 dB while the measured values are -7.6 and -14.5 dB, respectively. At even higher fundamental amplitudes, the results are even less acceptable.

Although the results of this analysis are not extremely accurate, they do serve as a motivation to carry the treatment further. The reasons for the discrepancies are not clear.

Conclusions

At this point, we are not in a position to determine the relative contributions from non-linear propagation and non-linear generation to the observed waveform distortion. At the very minimum, such a determination will require an accurate model for velocity dispersion in the prime mover. This area is receiving attention now. Beyond that, the equations which give rise to acoustic gain have been linearized. A numerical solution of the coupled momentum and energy equation might identify significant non-linear terms in the coefficient of gain.

Acknowledgements

This work was supported in part by the Office of Naval Research.

References

1. A.B. Coppens and J.V. Sanders, Finite-amplitude standing waves in rigid-walled tubes, J. Acoust. Soc. Am. 43(3), 516-529 (1968).

Measurement and calculation of acoustic propagation constants in arrays of small air-filled rectangular tubes

Heui-Seol Roh, W. Patrick Arnott, and James M. Sabatier
National Center for Physical Acoustics, University of Mississippi, University, Mississippi 38677

Richard Raspet
Department of Physics and Astronomy, University of Mississippi, University, Mississippi 38677

(Received 18 July 1990; accepted for publication 20 January 1991)

An experimental and theoretical investigation of sound propagation in a porous sample composed of capillary tubes with rectangular cross sections is described in this paper. An experimental technique valid for low flow resistivity and high porosity porous samples was developed to measure the attenuation and phase velocity in the porous material. This technique uses transmission of a short pulse in a large tube through the porous sample and subsequent frequency domain analysis in the range 200–1300 Hz. Good agreement was obtained if an anomalous tortuosity factor of 1.1 is used in the theory. A scaling factor for relating cylindrical and square tube capillary theories, known as the dynamic shape factor, was investigated. Propagation constants computed from use of a near unity dynamic shape factor in the cylindrical pore theory agree favorably with calculations based on the square pore theory for the frequencies and pore radii used in the experiment.

PACS numbers: 43.20.Mv, 43.55.Ev, 43.28.Fp, 43.50.Vt

INTRODUCTION

The interaction of sound with porous media has many practical applications and a long history. Porous media are ideal sound absorbers for use in architectural acoustics and anechoic chambers. The porous nature of the earth's surface and ocean bottoms can greatly influence the propagation of sound in the air and oceans. An example of the diverse uses of sound propagation in porous media comes from our laboratory, where we recently used measurements and theory for sound propagation in the porous ground to determine physical parameters that are related to the agricultural suitability of the soils investigated.[1]

Several models[2-5] for porous media are based on the adaptation of the solution for sound propagation in cylindrical capillary tubes to pores of irregular geometries. The basic fluid field equations used in these models are a simplified version of the linearized Navier–Stokes equations[3] for a fluid. The approximation employed in this calculation is that the transverse fluid velocities are much smaller than the longitudinal fluid velocity. Zwikker and Kosten[5] were first to obtain the solution based on the simplified version of the fluid model equations and showed that these solutions agreed with Kirchhoff's exact solution[4] in the limit of high and low frequencies. Tijdeman[6] and Stinson[7] investigated the range of validity of the Zwikker and Kosten solution in comparison to the more rigorous Kirchhoff solution and determined that the condition for the approximation to hold was the condition on velocities listed above. Tijdeman refers to the Zwikker and Kosten theory as the "low reduced frequency approximation."

We have developed a porous media model for rectangular cross-section capillary tubes. The rectangular pore calculation is based on the low reduced frequency approximation. Specifically, the model allows one to compute propagation constants and characteristic impedances for porous media consisting of rectangular pores. The effects of a slight capillary tube curvature or tortuosity are accounted for in this model. For the single pore, a series solution is used for the particle velocity, pressure, density, and temperature. The extension of the single-pore theory to bulk media consisting of an array of pores is developed using standard techniques.[2,5] This is discussed in Sec. I. The single-pore solution for rectangular pores has been developed independently by Stinson.[7]

The rectangular pore model is compared to attenuation and phase velocity measurements. The ceramic porous samples used in the experiment consisted of nominally straight capillary tubes having square cross sections. These low flow resistivity, high porosity samples may be useful for low-frequency sound absorption. A more thorough description of the porous samples and experimental technique is given in Sec. II. Comparison of theory and experiment is discussed in Sec. III.

A general theory for arbitrary pore shape[8] was developed by introducing a scale factor known as the dynamic shape factor to scale between different pore geometries. The limiting cases for this scaling factor are circular pores and parallel slits. The limiting cases of rectangular pores are square pores and parallel slits, which give rectangular pore theory a wide range of applicability. The dynamic shape factor for square pores is frequency dependent, just as it is for parallel slits.[8] A discussion of the dynamic shape factor for square pores is given in Sec. IV.

I. PROPAGATION IN RECTANGULAR PORE MEDIA

Sound propagation in a single rectangular capillary tube is developed first. The acoustic field in the pore is specified to

 0001-4966/91/062617-08$00.80

first order in the acoustic variables. Boundary conditions at the pore wall are that the walls are rigid and thus the total particle velocity is taken as zero. Due to the high heat capacity and thermal conductivity of the pore wall, the temperature of the fluid in the pore at the boundary is taken to be the same as the pore wall. We do not assume any internal mean flow." The single-pore theory is then used to develop the theory for a porous material consisting of an array of rectangular capillary tubes possibly having a slight longitudinal curvature or tortuosity.

A. Acoustical disturbances in a single rectangular capillary tube

The coordinate system shown in Fig. 1 has the z axis parallel to the tube axis. The transverse dimension is spanned by an x-y coordinate system with the origin at the lower left corner of the rectangle. First-order acoustic variables are the real parts of

$$p(z,t) = p_0 + p_1(z)\exp(-i\omega t), \tag{1}$$

$$\mathbf{v}(x,y,z,t) = [v_x(x,y,z), v_y(x,y,z), v_z(x,y,z)] \times \exp(-i\omega t), \tag{2}$$

$$T(x,y,z,t) = T_0 + T_1(x,y,z)\exp(-i\omega t), \tag{3}$$

and

$$\rho(x,y,z,t) = \rho_0 + \rho_1(x,y,z)\exp(-i\omega t). \tag{4}$$

Subscript zero refers to ambient values; subscript 1 implies first order; and in Eq. (2) the x, y, and z components of particle velocity are v_x, v_y, and v_z, respectively. Equations (1), (3), and (4) are the acoustic pressure, temperature, and density. Acoustical disturbances within the pore are taken to satisfy the following relations:

$$-i\omega\rho_0 v_z(x,y,z) = -\frac{dp_1(z)}{dz} + \eta\left(\frac{\partial^2}{\partial x^2} + \frac{\partial^2}{\partial y^2}\right) v_z(x,y,z), \tag{5}$$

$$-i\omega\rho_1(x,y,z) + \rho_0\left(\frac{\partial v_x(x,y,z)}{\partial x} + \frac{\partial v_y(x,y,z)}{\partial y} + \frac{\partial v_z(x,y,z)}{\partial z}\right) = 0, \tag{6}$$

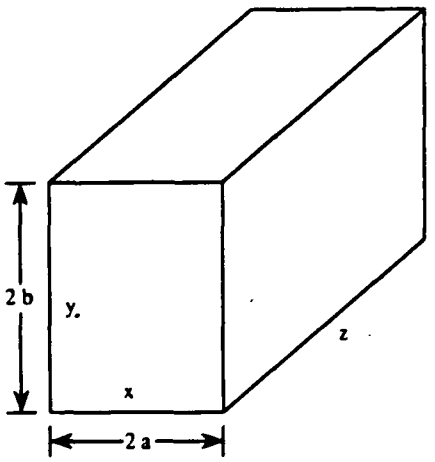

FIG. 1. Coordinate system and geometry for the single pore calculation

$$\rho_1(x,y,z) = -\rho_0\beta T_1(x,y,z) + (\gamma/c^2)p_1(z), \tag{7}$$

and

$$-i\omega\rho_0 c_p T_1(x,y,z) = -i\omega\beta T_0 p_1(z) + \kappa\left(\frac{\partial^2}{\partial x^2} + \frac{\partial^2}{\partial y^2}\right) T_1(x,y,z). \tag{8}$$

These relations are given in the frequency domain where $\partial/\partial t$ is replaced by $-i\omega$, where t is time and ω is angular frequency. Response functions and transport coefficients are c_p, the constant pressure heat capacity per unit mass; γ is the ratio of specific heats; c is the adiabatic sound speed; $\beta = -(\partial\rho/\partial T)_p/\rho_0$, is the thermal expansion coefficient; η is the viscosity; and κ is the thermal conductivity. In order, these equations express the z component of the equation of motion, continuity or mass conservation, equation of state for density, and heat transfer. Equations (5)–(8) are the same set of equations used by Zwikker and Kosten.[5] In using these approximate equations the assumption is that the transverse velocity components v_x and v_y are much less than the longitudinal velocity v_z. Further discussions of these approximations can be found in Appendix B of Ref. 6, Appendix A of Ref. 10, and Ref. 7.

The following notation will be used to facilitate comparison with Attenborough's results.[2,8] A dimensionless "shear-wave number" that is proportional to the ratio of the pore radius and the viscous boundary layer thickness is $\lambda = R(\rho_0\omega/\eta)^{1/2}$. Here R is a characteristic transverse dimension of the pore. For definiteness we take R to be twice the transverse pore area divided by the transverse pore perimeter. Thus R, which is twice the hydraulic radius,[11] is the tube radius for a cylindrical pore and the semiwidth for a square pore. "Wide tubes" with the same R are acoustically equivalent, i.e., they have the same propagation constants.[3] A dimensionless number proportional to the ratio of the pore radius to the thermal boundary layer thickness is $\lambda_t = R(\rho_0\omega c_p/\kappa)^{1/2}$ or $\lambda_t = \lambda N_{\mathrm{Pr}}^{1/2}$, where $N_{\mathrm{Pr}} = \eta c_p/\kappa$ is the Prandtl number.

To make rapid progress, denote the z component of the particle velocity v_z by

$$v_z(x,y,z) = \frac{F(x,y;\lambda)}{i\omega\rho_0}\frac{dp_1(z)}{dz}. \tag{9}$$

Similarly, denote the acoustic pore temperature by

$$T_1(x,y,z) = [(\gamma-1)/c^2\rho_0\beta]p_1(z)F(x,y;\lambda_t). \tag{10}$$

The thermodynamic relation $T_0\beta^2/c_p = (\gamma-1)/c^2$ can be used in Eq. (8) for T_1. The particle velocity and temperature, Eqs. (5) and (8), reduce to the simple forms

$$F(x,y;\lambda) + \frac{R^2}{i\lambda^2}\left(\frac{\partial^2}{\partial x^2} + \frac{\partial^2}{\partial y^2}\right) F(x,y;\lambda) = 1 \tag{11}$$

and

$$F(x,y;\lambda_t) + \frac{R^2}{i\lambda_t^2}\left(\frac{\partial^2}{\partial x^2} + \frac{\partial^2}{\partial y^2}\right) F(x,y;\lambda_t) = 1, \tag{12}$$

respectively, subject to the boundary condition $F = 0$ at the pore boundary. This is the particle velocity and excess temperature boundary condition. The solution for $F(x,y;\lambda)$ for rectangular pore boundaries is[12]

$$F(x,y;\lambda)=\frac{16}{\pi^2}\sum_{m,n\ \text{odd}}\frac{\sin(m\pi x/2a)\sin(n\pi y/2b)}{mnY_{m,n}(\lambda)}, \tag{13}$$

where

$$Y_{m,n}(\lambda)=1+(i\pi^2/\lambda^2)[(b^2m^2+a^2n^2)/(a+b)^2] \tag{14}$$

and twice the ratio of transverse pore area to perimeter is $R=2ab/(a+b)$. [Recall that $\lambda=R(\rho_0\omega/\eta)^{1/2}$.] In the sums, m and n are odd numbers ranging from $1-\infty$. For later use, the average $F(\lambda)=[1/(4ab)]\int F(x,y;\lambda)dx\,dy$ over the pore cross section is

$$F(\lambda)=\frac{64}{\pi^4}\sum_{m,n\ \text{odd}}\frac{1}{m^2n^2Y_{m,n}(\lambda)}. \tag{15}$$

The z component of the particle velocity is given by Eq. (9) with $F(x,y;\lambda)$ in Eq. (13) and the excess temperature is given by Eq. (10) with the replacement of λ in Eq. (13) by λ_T.

To derive a wave equation for the pressure, the fluid equations in Eqs. (5)–(8) are averaged over the pore cross section. Denote by $\rho_1(z)=[1/(4ab)]\int\rho_1(x,y,z)dx\,dy$ the average of the acoustic density in the pore and use similar notation for $v_z(z)$ and $T_1(z)$ for the transverse area average of $v_z(x,y,z)$ and $T_1(x,y,z)$. Use of Eqs. (9) and (10) for the z component of the particle velocity and temperature and the fluid equations (5)–(8) results in a set of averaged equations:

$$\frac{i\omega\rho_0}{F(\lambda)}v_z(z)=\frac{dp_1(z)}{dz}, \tag{16}$$

$$-i\omega\rho_1(z)+\rho_0\frac{dv_z(z)}{dz}=0, \tag{17}$$

and

$$\rho_1(z)=\{[(1-\gamma)F(\lambda_T)+\gamma]/c^2\}p_1(z). \tag{18}$$

The boundary conditions, $v_x(x,y,z)=0$ and $v_y(x,y,z)=0$ at the boundary, were used in obtaining Eq. (17) from the continuity equation (6). Also, Eq. (10) for $T_1(z)$ was used in the equation of state (7) to obtain Eq. (18). Following Attenborough[2] we define a complex density from Eq. (16) and complex compressibility from Eq. (18).

$$\tilde{\rho}=\rho_0/F(\lambda) \tag{19}$$

and

$$\tilde{C}=(1/\rho_0)(\rho_1/p_1)=[(1-\gamma)F(\lambda_T)+\gamma]/\rho_0c^2. \tag{20}$$

Eliminating ρ_1 from the continuity and state equations (17) and (18) and using Eqs. (19) and (20) we obtain

$$i\omega\tilde{\rho}v_z(z)-\frac{dp_1(z)}{dz}=0 \tag{21}$$

and

$$\frac{dv_z(z)}{dz}-i\omega\tilde{C}p_1(z)=0. \tag{22}$$

B. Extension to bulk media: Propagation constants and characteristic impedance

Consider a fluid half-space overlying a porous half-space saturated by the same fluid. The pores are taken to have a rectangular cross section and we let the capillary tube axis of each pore be at an angle θ with respect to the surface normal. The tortuosity $q=1/\cos\theta$ for such a porous sample.[2,5,8,11] The open volume divided by the total volume is the porosity Ω of the sample. The boundary conditions are continuity of volume velocity (from mass conservation) and the continuity of pressure (from Newton's third law) at the porous interface.[2,3,5,8] Since fluid only flows into the pores, the bulk particle velocity V_{zb} in the porous media is $V_{zb}=\Omega v_z/q$.[2,11] In order to account for propagation in a slanted pore (or other tortuous path), the differential dz in Eqs. (21) and (22) is replaced with $q\,dz$, where $q>1$ is the tortuosity.[2,5,8] Thus the bulk acoustical equations are

$$i\omega\tilde{\rho}q\frac{V_{zb}(z)}{\Omega}-\frac{dp_1(z)}{q\,dz}=0 \tag{23}$$

and

$$\frac{dV_{zb}(z)}{\Omega\,dz}-i\omega\tilde{C}p_1(z)=0. \tag{24}$$

Differentiating Eq. (23) by z and eliminating V_{zb} with Eq. (24) give an expression

$$\frac{d^2p_1(z)}{dz^2}+\omega^2\tilde{\rho}\tilde{C}q^2p_1(z)=0 \tag{25}$$

for the pressure in the porous media. Assuming $p_1\propto\exp(ikz)$ gives the dispersion relation

$$k^2=\omega^2q^2\tilde{\rho}\tilde{C}=(\omega^2/c^2)q^2\{[(1-\gamma)F(\lambda_t)+\gamma]/F(\lambda)\} \tag{26}$$

for the complex wave number k. From Eq. (23), the characteristic impedance is

$$Z=\frac{\tilde{\rho}\omega q^2}{\Omega k}=\frac{\rho_0}{F(\lambda)^{1/2}}\frac{q}{\Omega}\frac{c}{[(1-\gamma)F(\lambda_t)+\gamma]^{1/2}}. \tag{27}$$

The plane-wave pressure reflection coefficient r_p for a wave normally incident from the fluid half-space on the porous sample is

$$r_p=\frac{Z-\rho_0c}{Z+\rho_0c}=\frac{\{F(\lambda)[(1-\gamma)F(\lambda_t)+\gamma]\}^{1/2}-\Omega/q}{\{F(\lambda)[(1-\gamma)F(\lambda_t)+\gamma]\}^{1/2}+\Omega/q}. \tag{28}$$

This relation will be used in the next section. Principal results of this section are the propagation constant (26) and characteristic impedance (27), which for rectangular pore porous media are to be evaluated with the function $F(\lambda)$ given in Eq. (15).

II. MEASUREMENT OF THE PHASE VELOCITY AND ATTENUATION

A. Description of the porous media

A schematic drawing of the porous sample is shown in Fig. 2. Each subsection of the composite sample was of the nominal length 7.68 cm. Figure 2 indicates a composite sam-

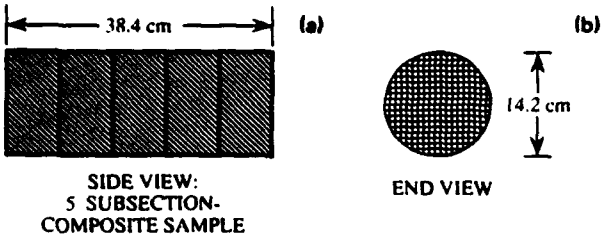

FIG. 2. (a) Side and (b) end view of a square pore porous sample. To form the total sample several pieces of the nominal length 7.68 cm were put together. It was not possible to align the squares from subsection to subsection.

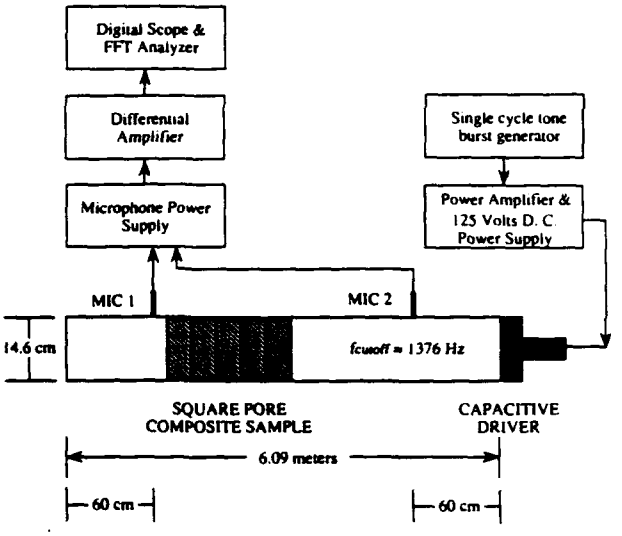

FIG. 3. Block diagram of the apparatus used to determine the phase velocity and attenuation of sound in low flow resistivity, high porosity samples.

ple made from five individual pieces. Individual pieces were taped together at the joint. A sheet of Teflon was wrapped around the composite to facilitate insertion of the sample into the plane-wave measurement tube and seal the sample–tube interface. Individual pieces were ceramics made by Corning.[13] The pores of each piece were nominally square in cross section and nominally straight in the longitudinal direction.

Three different square pore media were investigated. Table I lists characteristics of each. In Table I, porosity was estimated using $\Omega = (\text{number of pores/unit area}) \times (2a)^2$, where a is the square semiwidth. Flow resistivity was computed using (see Ref. 8) $\sigma = 8\eta q^2 s/a^2\Omega$, where s is a steady flow shape factor $s = 0.89$ for square pores[11] and a tortuosity $q = 1.1$ was estimated from fitting the theory and experiment for the propagation constants as discussed below. In comparison with other porous media,[8] the square pore samples have low flow resistivity and high porosity. The average semiwidths are listed in Table I for the 200- and 400-pores/in.^{2} material, for which the pore cross-sectional shape is well approximated as a square. However, due apparently to differences in the manufacturing process, the pores of the 300-pores/in.^{2} samples were not well approximated by a square shape. Two opposite corners of the otherwise square shape were rounded. The semiwidth of $a = 0.50$ mm listed in Table I for the 300-pores/in.^{2} samples was determined from the shortest diagonal length divided by $(2^{3/2})$. No explicit use was made of the calculated flow resistivity in the theory for the propagation constants.

B. Experimental apparatus

A block diagram for the experimental apparatus used to determine the attenuation and phase velocity of sound in porous media is shown in Fig. 3. A single cycle of a sine wave of duration 1.3 ms (for a center frequency of 750 Hz) was generated using a function generator. The signal was amplified and was added to a dc polarizing voltage of 125 V. The capacitive driver consisted of an aluminized mylar membrane stretched over a grooved backplate.[14] A Teflon ring around the perimeter of the driver was used to hold the mylar in place and seal the driver inside the tube. The tube was made of aluminum and had a length of 6.09 m, an inside diameter of 14.6 cm, and a wall thickness of 1.11 cm. Holes were made and threaded in the tube 60 cm from each end and the microphones were inserted to be flush with the inner tube wall. A minicomputer with a 12-bit analog-to-digital board was used to record and analyze the amplified microphone signals. The digitizing rate was 300 kHz. The function generator was used to trigger the minicomputer and 30 pulses were averaged in the time domain for each measurement. The purpose of microphone 2 was to give a reference time and space location for a pulse traveling in the empty tube, so that the ambient sound speed could be determined from the pulse arrival time at microphone 1.

A single microphone measurement method was used to determine the propagation constants in the square pore media. Figure 4(a) shows microphone 1 measurement of pulses with and without a sample present in the tube. As expected, the pulse measured with the sample present is delayed in time and attenuated on account of passage through the porous media. The Fourier transform of a typical pulse indicated that the pressure level was about 20 dB above the background for frequencies in the range 200–1300 Hz. The cutoff frequency[3] above which nonplanar modes can propagate in the tube is 1376 Hz.

TABLE I. Geometrical properties of the three porous samples used.

Pores/unit area (in.$^{-2}$)	Semiwidth a (mm)	Porosity Ω (%)	Flow resistivity σ (N m^{-4} s)
200	0.77	73	368
300	0.50	47	1356
400	0.57	81	606

C. Determination of attenuation and phase velocity by the transfer function method

Denote by $p_0(t)$ the incident pressure pulse at the right end of the sample and denote by $p_0(f)$ the Fourier transform of $p_0(t)$. The spectrum $p(f)$ after passage through a sample of length D_m is

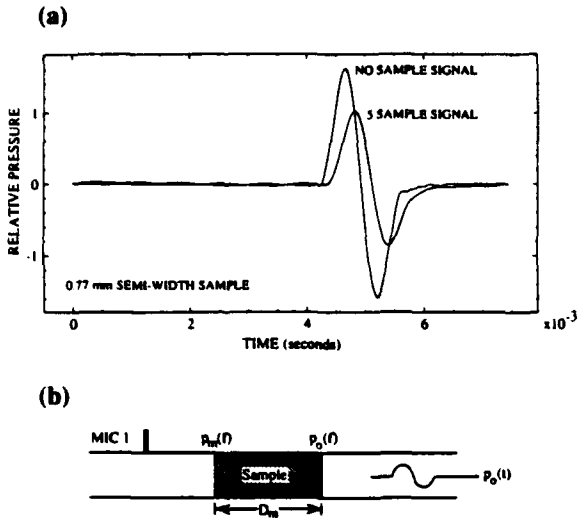

FIG. 4. (a) Sample waveforms for microphone 1 with and without the porous material in the tube. The porous media was constructed as shown in Fig. 2. (b) Expanded schematic view of the tube and porous sample in Fig. 3. The Fourier transform after the incident pulse passes through the sample is $p_m(f)$.

$$p_m(f) = p_0(f)\exp(ikDm)\frac{1-r_p^2}{1-r_p^2\exp(2ikD_m)}, \tag{29}$$

where r_p is the frequency dependent pressure reflection coefficient (28) and k is the complex wave number for the porous media (26). Since the tube has a large diameter we approximate the characteristic impedance of the tube by $\rho_0 c$, where c is the adiabatic sound speed in air. The $\exp(ikD_m)$ factor accounts for propagation through the sample, the $(1-r_p^2)$ factor is for transmission into and out of the sample, and the denominator accounts for the multiple reflection of waves within the sample.

In Eq. (29) the subscript m refers to the number of subsections used for a measurement. For example, $m=5$ in Figs. 2 and 3. We may form a transfer function $h_m(f)$ from the results of two experiments on different porous sample lengths. The Fourier transform of the time domain pulses recorded by microphone 1 in Fig. 4(b) for two different sample lengths gives, from use of Eq. (29), a transfer function

$$h_m(f) = p_m(f)/p_1(f) \approx \exp[i(k-k_0)(D_m - D_1)], \tag{30}$$

where $k_0 = \omega/c$ is the wave number for sound in air and k is given in Eq. (26). In Eq. (30) the single subsection spectrum $p_1(f)$ was used as a reference to divide out the frequency response of the capacitive driver and microphone, and the transmission coefficient $(1-r_p^2)$ in Eq. (29). The second part of Eq. (30) is an approximation because we have assumed $[(1-r_p^2\exp 2ikD_1)/(1-r_p^2\exp 2ikD_m)] \approx 1$. The reflection coefficient r_p in Eq. (28) is significantly less than 1 for two reasons. First, $|F(\lambda)| \approx 1$ for the frequency range of the present experiment as a consequence of the low flow resistivity of the square pore samples used. Second, for the square pore material the porosity Ω is large. Hence by Eq. (28) we expect $r_p^2 \approx 0$. Measurements of r_p with microphone 2 in Fig. 3 for a nominal frequency of 750 Hz gave $|r_p^2| \approx (0.03, 0.05, \text{and } 0.03)$ for the (200, 300, and 400)-pores/in.^{2} samples, respectively.

The phase velocity and attenuation constant are computed from $k = \omega/c_{ph} + i\alpha$,

$$c_{ph}(f) = 2\pi f/[(D_m - D_1)^{-1}\,\mathrm{Im}\ln(h_m) + k_0], \tag{31}$$

and

$$\alpha(f) = -[20(D_m - D_1)^{-1}/\ln(10)]\,\mathrm{Re}\ln(h_m), \tag{32}$$

where c_{ph} is the phase velocity; α is the attenuation in dB/cm; and $\mathrm{Re}\ln(h_m)$ and $\mathrm{Im}\ln(h_m)$ refer to the real and imaginary parts of $\ln(h_m)$, respectively.

Equations (30)–(32) were used to analyze the time domain pulses to obtain experimentally the phase velocity and attenuation for the square pore media. In all cases, we averaged over 30 time domain pulses before taking transforms. We also used five subsections, so that $m=5$ in Eqs. (30)–(32) and $(D_m - D_1) = 30.7$ cm nominally. Since a transfer function technique was used, it was not necessary to determine the pressure absolutely or the frequency response of the microphone. A central assumption that was verified experimentally was the repeatability of any pulse measurements since $p_5(t)$ and $p_1(t)$ were measured at different times. The experimental results for the three different pore sizes given in Table I are displayed in Fig. 5. The experimental technique described here is similar to a method used by Ding[15] to measure the reflection coefficient of absorbents.

An error analysis can be made by using an unapproximated transfer function for Eq. (30) in Eqs. (31) and (32). Let $\Delta = r_p^2[\exp(2ikD_m) - \exp(2ikD_1)]$. The fractional error in phase velocity that occurs due to the approximation in Eq. (30) is $\delta_c \approx \mathrm{Im}\,\Delta c_{ph}(f)/[2\pi f(D_m - D_1)]$. Similarly, for attenuation, $\delta_\alpha \approx 0.2\,\mathrm{Re}\,\Delta/[\alpha(f)\ln 10(D_m - D_1)]$, where $(D_m - D_1)$ is in meters. Use of representative numbers for the 200-in.$^{-2}$ material gives $\delta_c \approx 1\%$ and $\delta_\alpha \approx 7\%$. To improve on the error, D_m and D_1 should both be uniformly increased. The errors introduced by making the approximation in Eq. (30) are the greatest source of error.

III. DISCUSSION OF EXPERIMENTAL AND THEORETICAL ATTENUATION AND PHASE VELOCITY

The experimental and theoretical attenuation and phase velocity were determined from use of Eqs. (30)–(32) and (26), respectively, and $k = \omega/c_{ph} + i\alpha$. Figure 5(a) and (b) shows the experimental and theoretical attenuation constant and phase velocity. For the theory, the physical constants used were $\gamma = 1.4$, $N_p = 0.707$, $\rho_0 = 1.2$ kg/m^3, $\eta = 1.85\times10^{-5}$ kg/(m s), and the adiabatic sound speed c from the propagation time of a pulse between microphones 1 and 2 in Fig. 3 with no sample in the tube.

To obtain the acceptable agreement among theory and experiment indicated in Fig. 5(a) and (b), a tortuosity of $q = 1.1$ was used. Referring to Eq. (26) for the propagation constant k, note that the effect of tortuosity (which is $q \geqslant 1$)

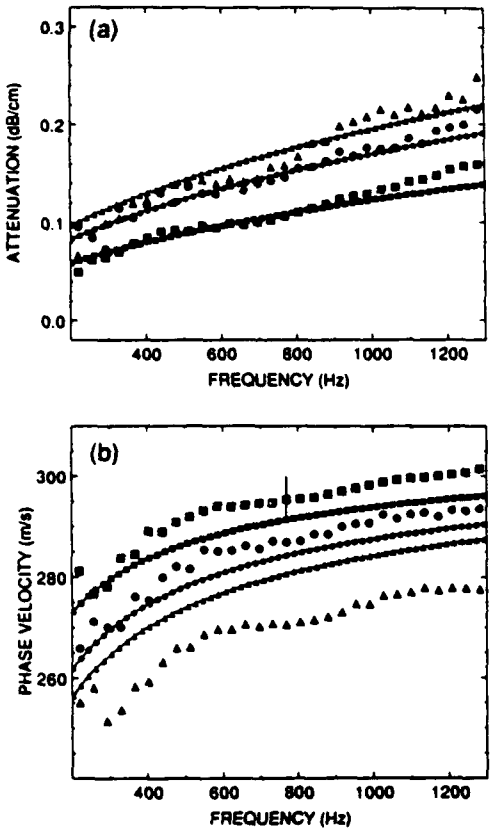

FIG. 5. (a) Experimental and theoretical attenuation and (b) phase velocity for the three square pore semiwidths given in Table I. The solid symbols are experimental points. The squares, circles, and triangles are the 200-, 400-, and 300-in.$^{-1}$ results. The error in (a) was estimated to be twice the size of the square symbols. A representative error bar is shown in (b).

is to increase the attenuation α and decrease the phase velocity, as one would intuitively expect. The calculated propagation constant for a tortuosity $q = 1$ results in an attenuation 10% lower than the measured value and a phase velocity 10% above the measured value. The discrepancy between experimental and theoretical phase velocity in Fig. 5(b) for the 300-pores/in.^{2} samples having pores of semiwidth 0.50 mm may be due to the irregular shape of the pore cross section, as described in Sec. II A.

Pores that have a tortuosity other than 1 have a radius which is not constant along the pore, a slight curvature or tilt with respect to the axis normal to the surface, or are in a material for which the rigid frame assumption is not valid.[5] In the ceramic square pore material used in the experiment, the pores were straight and the pore walls had a density and stiffness much greater than that of air. However, the semiwidth of the squares as determined with a measuring microscope at the sample surface varied by approximately 5% from the average value. This variation could result in a tortuosity other than 1 if the 5% radius variation also extended down a single pore. Another possibility for a tortuosity other than 1 is that the ceramic pore walls were also porous. Use of a measuring magnifying glass indicated that the pore walls were indeed porous, with an average pore diameter of about 75 μm and pores as large as 100 μm. Wall pores were spaced by about 150 μm. Apparently, the wall pores did not connect adjacent square pores. Intuitively, it seems that the effects of porous walls would be to increase the compressibility of the gas and hence decrease the phase velocity. The attenuation would also increase, which is what was observed experimentally. Champoux[16] reported a tortuosity of 1.2 for the 200- and 400-pores/in.^{2} samples using a nonacoustical technique.[17]

It was not possible to align the pores in neighboring subsections of the composite sample, as discussed in Sec. II A. To investigate the effects of misalignment, attenuation and phase velocity were measured for composite samples consisting of one to five subsections. In the single subsection measurement the reference for the transfer function in Eq. (30) was taken to be the empty tube signal. The discrepancy between these measurements was less than 3% and showed no systematic trends. Sample misalignment was probably not the cause of an apparent tortuosity greater than 1.

IV. DYNAMIC SHAPE FACTOR FOR SQUARE PORES

The hypothesis of Attenborough's[8] cylindrical capillary-tube-based porous media theory was that a circular pore of radius a/n, where n is known as the dynamic shape factor, could be made acoustically equivalent to another pore of characteristic radius a by proper choice of n. The condition for acoustical equivalence is taken to be

$$\mathrm{Im}\,\tilde{\rho}_c(\lambda/n) = \mathrm{Im}\,\tilde{\rho}_s(\lambda), \tag{33}$$

where we recall that $\lambda = a(\rho_0\omega/\eta)^{1/2}$ for a circular pore of radius a or a square pore of semiwidth a and subscripts c and s refer to circular and square pores, respectively. This condition occurs since the imaginary part of the complex density $\tilde{\rho}$ is very large for small λ and thus determines the behavior of the propagation constants and impedance for small λ.[8]

The complex density is given generally for rectangular pores in Eq. (19). For square pores of semiwidth a the function $F_s(\lambda)$ is

$$F_s(\lambda) = \frac{64}{\pi^4} \sum_{m,n\ \mathrm{odd}} \frac{1}{m^2n^2[1 + (i\pi^2/4\lambda^2)(m^2 + n^2)]} \tag{34}$$

from Eqs. (14) and (15) for the special case $a = b$. For cylindrical pores,[2]

$$F_c(\lambda/n) = 1 - [2/\sqrt{i}(\lambda/n)][J_1(\sqrt{i}\lambda/n)/J_0(\sqrt{i}\lambda/n)], \tag{35}$$

where the dynamic shape factor n has been inserted and the J's are Bessel functions. The range[8] of n is thought to be $0.5 < n < 1$. The dependence of n on the shear-wave number λ is shown in Fig. 6.

The shear-wave-number range in our experiments was $4.5 < \lambda < 18$. As indicated in Fig. 6, n is a frequency dependent parameter, which has been previously noted.[8] Choosing a representative value of $\lambda = 4.532$, the corresponding value of the dynamic shape factor is $n = 0.97$. Propagation constants are shown in Fig. 7 for square and circular pore theories, where the value $n = 0.97$ was used. Propagation constants for circular pores were computed from the use of Eq. (35) for $F(\lambda)$ in Eq. (26) for k. There is less than 1% differ-

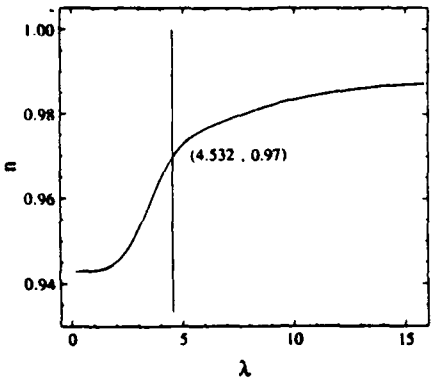

FIG. 6. Dynamic shape factor n to scale between the square and circular pores of semiwidth a and radius a/n, respectively.

ence between the propagation constants calculated with these theories.

V. CONCLUSION

We have developed a model for porous media consisting of rectangular pore capillary tubes. We accounted for viscous and thermal dissipation. A series solution was obtained for the transverse variation of the longitudinal velocity and the excess temperature. A measurement technique using frequency domain analysis of short pulses propagated through high porosity, low flow resistivity samples was developed for determining propagation constants. Propagation constants were measured for a ceramic porous media having straight capillary tube openings with square cross sections. Use of an anomalous tortuosity factor $q = 1.1$ resulted in favorable agreement among experimental and theoretical values of the propagation constants. It was argued that the nonunity tortuosity value was due to the finite porosity of the ceramic pore walls. A dynamic shape factor $n = 0.97$ was suggested as the radius scaling factor for square and circular pore theories for the frequency range (200–1300 Hz) and pore sizes (0.50–0.77-mm semiwidth square pores) of this investigation. Future work will involve an investigation of the anomalous tortuosity and propagation constant measurements on longer samples.

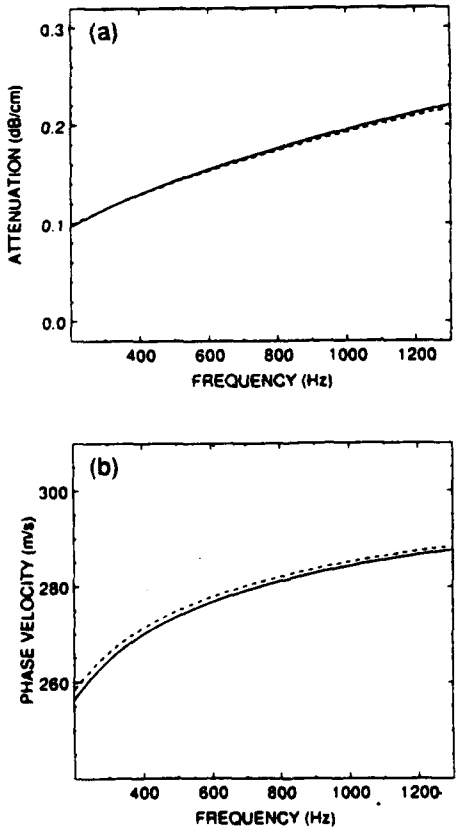

FIG. 7. (a) Attenuation and (b) phase velocity computed using a square pore (solid line) of semiwidth $a = 0.50$ mm and a circular pore (dashed line) of radius $a = 0.50$ mm/n, where $n = 0.97$ is a dynamic shape factor.

ACKNOWLEDGMENTS

We are grateful to Michael R. Stinson and Yvan Champoux for discussions and tortuosity measurements on some of the porous samples used in this investigation. Conversations with Keith Attenborough, Henry E. Bass, and Kevin L. Williams are also appreciated.

[1] J. M. Sabatier, H. Hess, W. P. Arnott, K. Attenborough, and M. Romkens, "*In situ* measurements of soil physical properties by acoustical techniques," Soil Sci. Soc. Am. J. **54**, 658–672 (1990).
[2] K. Attenborough, "Acoustical characteristics of porous materials," Phys. Rep. **82**, 179–227 (1982).
[3] A. D. Pierce, *Acoustics: An Introduction to Its Physical Principles and Applications* (Acoustical Society of America, New York, 1989), Chap. 10.
[4] J. W. S. Rayleigh, *The Theory of Sound* (Dover, New York, 1945), Vol. II.
[5] C. Zwikker and C. W. Kosten, *Sound Absorbing Materials* (Elsevier, Amsterdam, 1949), Chap. 2.
[6] H. Tijdeman, "On the propagation of sound waves in cylindrical tubes," J. Sound Vib. **39**, 1–33 (1975).
[7] M. Stinson, "The propagation of plane sound waves in narrow and wide circular tubes, and generalization to uniform tubes of arbitrary cross-sectional shape," J. Acoust. Soc. Am. **89**, 550–558 (1991).
[8] K. Attenborough, "Acoustical characteristics of rigid fibrous absorbents and granular materials," J. Acoust. Soc. Am. **73**, 785–799 (1983).
[9] A. Cummings and I. J. Chang, "Acoustic propagation in porous media with internal mean flow," J. Sound Vib. **114**, 565–581 (1987).
[10] G. W. Swift, "Thermoacoustic engines," J. Acoust. Soc. Am. **84**, 1145–1180 (1988).
[11] P. C. Carman, *Flow of Gases Through Porous Media* (Academic, New York, 1956).
[12] L. S. Han, "Hydrodynamic entrance lengths for incompressible laminar flow in rectangular ducts," J. Appl. Mech. **27**, 403–409 (1960). The author gives the solution for our Eq. (11) for a coordinate system at the center of a rectangle. He uses the differential equation for a different purpose than the present paper.
[13] The ceramics were manufactured by Corning Incorporated, Industrial Products Division, Corning, New York 14831.
[14] F. D. Shields, H. E. Bass, and L. N. Bolen, "Tube method of sound ab-

sorption measurement extended to frequencies far above cut off," J. Acoust. Soc. Am. 62, 346–353 (1977).
[15] Y. Ding, "A wave-tube impulse method for measuring sound-reflection coefficient of absorbents," Acustica 57, 188–190 (1985).
[16] Y. Champoux (private communication, 1990).
[17] Y. Champoux and M. R. Stinson, "Measurement of tortuosity of porous material and implications for acoustical modeling," J. Acoust. Soc. Am. Suppl. 1 87, S139 (1990).

General formulation of thermoacoustics for stacks having arbitrarily shaped pore cross sections[a)]

W. Pat Arnott, Henry E. Bass, and Richard Raspet
National Center for Physical Acoustics, Physical Acoustics Research Group, Department of Physics and Astronomy, University of Mississippi, University, Mississippi 38677

(Received 4 March 1991; revised 14 July 1991; accepted 2 August 1991)

Theoretical treatments of thermoacoustics have been reported for stacks with circular pore and parallel plate geometries. A general linear formulation is developed for gas-filled thermoacoustic elements such as heat exchangers, stacks, and tubes having pores of arbitrary cross-sectional geometry. For compactness in the following, F represents the functional form of the transverse variation of the longitudinal particle velocity. Generally, F is a function of frequency, pore geometry, the response functions and transport coefficients of the gas used, and the ambient value of the gas density. Expressions are developed for the acoustic temperature, density, particle velocity, pressure, heat flow, and work flow from knowledge of F. Heat and work flows are compared in the short stack approximation for stacks consisting of parallel plates, circular, square, and equilateral triangular pores. In this approximation, heat and work flows are found to be greatest for the parallel plate stack geometry. Pressure and specific acoustic impedance translation theorems are derived to simplify computation of the acoustical field quantities at all points within a thermoacoustic engine. Relations with capillary-pore-based porous media models are developed.

PACS numbers: 43.35.Ud, 43.28.Kt

INTRODUCTION

In a broad view, thermoacoustics can be regarded as the study of effects due to the interaction of heat and sound. A large and growing subbranch is concerned with thermoacoustics in fluid-filled (gas and liquid) resonators though observations of heat-driven oscillations in tubes date back to at least the late 18th century. A full, linear, theoretical investigation of these oscillations was performed first by Rott.[1] The reciprocal mode of operation, which uses a sound wave in a resonator to transport heat from cold to hot as in a refrigerator, has also been of recent interest. This thermoacoustic streaming has its analogy in acoustic streaming, which is the D.C. transport of momentum by an acoustic wave. Merkli and Thomann[2] found experimental verification for their theory of thermoacoustic streaming in a driven resonance tube. Rott and Merkli and Thomann were mainly interested in thermoacoustic effects in a single tube having a circular cross section. Rott and Zouzoulas[3] also investigated thermally driven acoustic oscillations for circular tubes with variable cross-sectional area.

Wheatley, Cox, Swift, Hofler, and others have developed the connection between the acoustical portion of thermoacoustics and a broader thermodynamics point of view. Swift[4] has reviewed much of this work, from fundamentals to state-of-the-art. Thermoacoustic elements such as heat exchangers and a stack, as shown in Fig. 1(a), are used to investigate prime movers and heat pumps. In the thermodynamic point of view heat exchangers and stacks are thought of as heat reservoirs and engines, respectively. This point of view enhances the understanding of thermoacoustics and is very helpful in evaluating practical devices.

An exposed view of a thermoacoustic element is shown in Fig. 1(b). Thermoacoustic elements consist of a parallel combination of many elementary capillary tubes or pores. In Fig. 1(b) the pores have square cross sections. The theory for a thermoacoustic heat engine is built up from knowledge

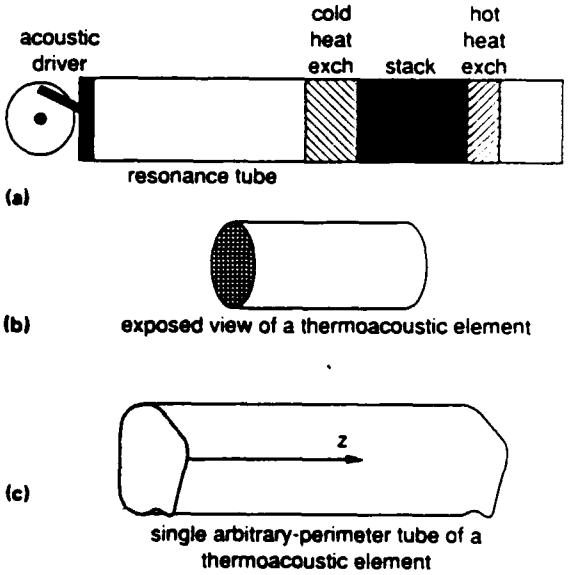

FIG. 1. (a) Generic arrangement used in thermoacoustic heat engines. Thermoacoustic elements are the heat exchangers, resonator sections, and stacks. (b) An exposed view of a thermoacoustic element consisting of a parallel combination of square capillary tubes. (c) A single arbitrary-perimeter capillary tube for use in a thermoacoustic element.

[a)] This work was presented, in part, at the 120th Meeting of the Acoustical Society of America [J. Acoust. Soc. Am. Suppl. 1 88, S96 (1990)].

 0001-4966/91/123228-10$00.80

of thermoacoustic effects in a single capillary tube. Both Rott[5] and Swift[4] considered thermoacoustic effects for acoustic oscillation between parallel plates.

The initial intent of this study was to investigate thermoacoustic effects in a stack having square pores as shown in Fig. 1(b). Inexpensive sources of square pore stack material are ceramic monolithic catalyst supports often used in automobile catalytic converters.[6] This ideal-geometry material was previously used to verify first-principles theory for sound propagation in porous media.[7] Since ceramic has a low thermal conductivity in comparison to most metals, it is attractive for use as a stack as parasitic heat loss due to thermal conduction reduces efficiency.

In this paper, thermoacoustics is investigated for stacks having arbitrary pore geometries (parallel plates, rectangular pores, equilateral-triangle pores, circular pores, etc.). In particular, our interest is in the following question: *What are the minimum necessary calculations to describe the acoustics of gas-filled thermoacoustic elements made of arbitrary-perimeter capillary tubes*? An example of an arbitrary-perimeter capillary tube is shown in Fig. 1(c). Rott[5] pursued this question to the point of computing the acoustical quantities for parallel plate and circular pore geometries. Here, the acoustic field quantities and the second-order energy flow are considered for arbitrary perimeter pores. Heat and work flows are compared in the short stack approximation for stacks having the aforementioned pore geometries to investigate the effects of pore geometry. In addition, connections are established between thermoacoustic theory and capillary-tube-based porous media theory. An analogous investigation has recently been performed for porous media by Stinson.[8]

Once the acoustical properties of the separate thermoacoustic elements have been determined, the elements must be connected in series inside of a resonator as shown in Fig. 1(a). Previously, numerical integration of the acoustical equations was used to compute field quantities in the stack since, in general, a temperature gradient exists from one end to the other.[1,4] The physical parameters of ambient density, viscosity, sound speed, thermal conductivity, etc., are temperature dependent and thus depend on location within the stack. Here, specific acoustic impedance and pressure translation theorems are developed to compute all acoustical field quantities and energy flow at each point in the resonance tube shown in Fig. 1(a). Translation theorems are relations between specific acoustic impedance or pressure at location z and the value of these quantities at a different location $z - d$. Using the translation theorem approach it is easy to analyze complicated systems, e.g., a resonator containing a refrigeration stack, a prime mover stack, and heat exchangers.

Section I A contains the basic fluid equations and assumptions. The force equation is considered in Sec. I B and the transverse temperature profile is given in Sec. I C. A differential equation is given for the the acoustic pressure in Sec. I D. Sections I A–I D apply to a single capillary tube of arbitrary perimeter. The specific acoustic impedance and pressure translation theorems are developed in Sec. I E for thermoacoustic elements. Expressions are given in Sec. I F for heat and work flows in terms of pressure and specific acoustic impedance. A numerical analysis technique for the present formulation is given in Sec. I G. An application of the theory is given in Sec. II where heat and work flows are computed in the short stack approximation for stacks having a variety of pore cross sections. Here, the emphasis is on investigating the effects pore geometry have on heat and work flows.

I. PROPAGATION IN THERMOACOUSTIC ELEMENTS

The name stack was originally descriptive of the parallel plate arrangement used for the thermoacoustic element which possibly has a temperature gradient down it. The pores in the parallel plate arrangement are described in their transverse direction as parallel plates and as straight tubes in their longitudinal direction [the z direction in Fig. 1(c)]. For arbitrary pore geometries, the stack or heat exchangers can be described as a section of a porous medium. In this section, the fluid field equations and assumptions necessary to treat the general case are established. An equation for the pressure in a single pore is established. Enroute, reference is made to the terminology used in acoustical modeling of porous media. With the specific acoustic impedance assumed known at the hot end of the stack, impedance and pressure translation theorems are derived for the stack. Heat and work flows are computed for arbitrary pore geometries and are expressed in terms of pressure and specific acoustic impedance.

A. Fluid field equations and assumptions

The transverse coordinates in a pore are taken to be x and y, and the longitudinal coordinate is z as shown in Fig. 1(c). The ambient temperature is taken to be a function of z in the stack. Assumed is that the pore walls are of sufficiently high heat capacity and thermal conductivity, in comparison to that of the gas, that the pore wall temperature is locally unaffected by temperature variations in the gas caused by an acoustic wave. Also assumed are that constant frequency pressure variations exist in the pore and that the pore walls are rigid and nonporous. The pore is taken to be infinitely long in the z direction. With these assumptions, the task is to derive the pore acoustic field to first order in the acoustic variables.

The fluid quantities in a pore approximated to first order are

$$P(z,t) = P_0 + P_1(z)\exp(-i\omega t), \tag{1}$$

$$\mathbf{v}(x,y,z,t) = [\mathbf{v}_r(x,y,z) + v_z(x,y,z)\hat{z}]\exp(-i\omega t), \tag{2}$$

$$T(x,y,z,t) = T_0(z) + T_1(x,y,z)\exp(-i\omega t), \tag{3}$$

$$s(x,y,z,t) = s_0(z) + s_1(x,y,z)\exp(-i\omega t), \tag{4}$$

$$\rho(x,y,z,t) = \rho_0(z) + \rho_1(x,y,z)\exp(-i\omega t). \tag{5}$$

In order, Eqs. (1)–(4) are the approximations to first order for pressure, particle velocity, temperature, entropy, and density. Acoustic waves of radian frequency ω are assumed. Where shown, subscript 0 indicates ambient values and subscript 1 the acoustic or first-order values. In Eq. (2),

$\mathbf{v}_r(x,y,z)$ and $v_z(x,y,z)$ are the transverse and longitudinal components of particle velocity. The ambient temperature $T_0(z)$ is assumed to depend on z. Note the definition to be used frequently below: $T_{0z} \equiv dT_0(z)/dz$. The ambient density in Eq. (5) also depends on position z. Because of the ambient temperature gradient physical parameters including density, viscosity η, thermal conductivity κ, adiabatic sound speed c, and the coefficient of thermal expansion $\beta = -(\partial\rho/\partial T)_p/\rho_0$ also depend on position.

The Navier–Stokes fluid field equations are given for example in Ref. 9. The Navier–Stokes equations can be simplified to model sound propagation in narrow tubes. Physically, the transverse variation (in the tube cross section) of particle velocity, temperature, etc., is much greater than the longitudinal variation (down the tube) due to the close proximity of walls where boundary conditions must be met. For constant frequency waves, the approximate set of fluid field equations to first order are

$$-i\omega\rho_0 v_z(x,y,z) = -\frac{dP_1(z)}{dz} + \eta\nabla_r^2 v_z(x,y,z), \tag{6}$$

$$-i\omega\rho_1(x,y,z) + \frac{\partial[\rho_0(z)v_z(x,y,z)]}{\partial z} + \rho_0(z)\nabla_r\cdot\mathbf{v}_r(x,y,z) = 0, \tag{7}$$

$$\rho_1(x,y,z) = -\rho_0(z)\beta T_1(x,y,z) + (\gamma/c^2)P_1(z), \tag{8}$$

$$s_1(x,y,z) = (c_p/T_0)T_1(x,y,z) - (\beta/\rho_0)P_1(z), \tag{9}$$

and

$$-i\omega\rho_0(z)c_p T_1(x,y,z) + \rho_0(z)c_p v_z(x,y,z)T_{0z} = -i\omega\beta T_0 P_1(z) + \kappa\nabla_r^2 T_1(x,y,z), \tag{10}$$

where the transverse gradient and Laplacian operators are defined by $\nabla_r = \partial/\partial x\,\hat{x} + \partial/\partial y\,\hat{y}$ and $\nabla_r^2 = (\partial^2/\partial x^2 + \partial^2/\partial y^2)$, c_p is the isobaric heat capacity per unit mass, and γ is the ratio of specific heats. In order, these equations approximately express the z component of the equation of motion, continuity or mass conservation, equations of state for density and entropy, and heat transfer. Except for the T_{0z} terms in Eq. (10), these are the equations for the low reduced-frequency approximation[10] given by Zwikker and Kosten[11] in their solution for the propagation of sound in circular pores. In the derivation of Eq. (10), the convective derivative for the entropy is evaluated using the equation of state Eq. (9) and the relation $\mathbf{v}\cdot\nabla s = v_z(x,y,z)ds_0(z)/dz = c_p \times v_z(x,y,z)\,T_{0z}/T_0$. Equation (10) expresses that the temperature at a fixed position changes due to motion of the ambient fluid, due to compression of the gas, and due to heat conduction. Further discussion of these equations and the validity of the approximations may be found in Refs. 4, 8, and 10.

Several variations in notation should be noted. First, the viscous and thermal boundary layer thicknesses are given by $\delta_\nu = (2\eta/\omega\rho_0)^{1/2}$ and $\delta_\kappa = (2\kappa/\omega\rho_0 c_p)^{1/2}$. Swift[4] writes most equations in terms of δ_ν and δ_κ. Tijdeman[10] and Attenborough[12] introduce a dimensionless "shear wave number" $\lambda = R(\rho_0\omega/\eta)^{1/2}$ or $\lambda = 2^{1/2}R/\delta_\nu$, where R is a characteristic transverse dimension of the pore. They also use the dimensionless thermal disturbance number $\lambda_T = R(\rho_0\omega c_p/\kappa)^{1/2}$ or $\lambda_T = 2^{1/2}R/\delta_\kappa$ for the ratio of the pore radius to the thermal boundary layer thickness. Use of the Prandtl number $N_{pr} = \eta c_p/\kappa$ gives the relation $\lambda_T = \lambda N_{pr}^{1/2}$. For definiteness, take R to be twice the ratio of the transverse pore area to the pore perimeter so for a circular or square pore, R is the pore radius. This value of R is twice the hydraulic radius of the pore. In this paper the λ and λ_T notation is used.

B. Transverse velocity profile in a pore

To obtain a solution to the equation of motion, Eq. (6), the z component of velocity is taken to be

$$v_z(x,y,z) = \frac{F(x,y;\lambda)}{i\omega\rho_0}\frac{dP_1(z)}{dz}. \tag{11}$$

From the equation of motion, Eq. (6), $F(x,y,\lambda)$ satisfies

$$F(x,y;\lambda) + (R^2/i\lambda^2)\nabla_r^2 F(x,y;\lambda) = 1, \tag{12}$$

subject to the boundary condition that $F(x,y;\lambda)$ is zero at the pore walls. This is the boundary condition on particle velocity at the pore wall. *As will become apparent in the following, this is the only differential equation which needs to be solved for determining the first-order acoustic quantities and second-order heat and work flows.*

In anticipation of later developments, averages over the pore cross section, defined for example by $v_z(z) = A^{-1}\int v_z(x,y,z)dx\,dy$, where A is the area of the pore cross section, are taken. Denote by $v_z(z)$ and $F(\lambda)$ the area average of $v_z(x,y,z)$ and $F(x,y;\lambda)$ over the cross section of the pore. The averaged equation of motion for the fluid can now be expressed simply as

$$v_z(z) = \frac{dP_1(z)/dz}{i\omega\rho_0(z)}F(\lambda). \tag{13}$$

Capillary-tube-based porous media modeling[11,12] introduces a complex density $\tilde{\rho}(z;\lambda)$ at this point which is defined as

$$\tilde{\rho}(z;\lambda) = \rho_0(z)/F(\lambda). \tag{14}$$

The complex density is the apparent dynamical density of the fluid in the pore.

C. Transverse temperature profile in a pore

The equation for excess temperature $T_1(x,y,z)$ in the pore fluid is given by Eq. (10). Algebraic rearrangement followed by use of the thermodynamic relation $T_0\beta^2/c_p = (\gamma-1)/c^2$ for the first term on the right and by use of Eq. (11) results in

$$T_1(x,y,z) + (R^2/i\lambda_T^2)\nabla_r^2 T_1(x,y,z) = \frac{\gamma-1}{c^2\rho_0\beta}P_1(z) - \frac{T_{0z}}{\rho_0\omega^2}F(x,y;\lambda)\frac{dP_1(z)}{dz}. \tag{15}$$

Assume $T_1(x,y,z)$ can be written in the form

$$T_1(x,y,z) = G_a(x,y;\lambda_T)[(\gamma-1)/c^2\rho_0\beta]P_1(z) - G_b(x,y;\lambda,\lambda_T)\frac{T_{0z}}{\rho_0\omega^2}\frac{dP_1(z)}{dz}. \tag{16}$$

The excess temperature changes due to compression and expansion of the gas and from the second term, displacement of gas which can have different ambient temperatures on account of the temperature gradient.

Effects on $T_1(x,y,z)$ of thermal conductivity and viscosity are accounted for in the dimensionless functions $G_a(x,y;\lambda_T)$ and $G_b(x,y;\lambda,\lambda_T)$. For an inviscid, nonthermally conducting gas $G_a = G_b = 1$. Use of Eq. (16) splits Eq. (15) into two equations corresponding to the two driving terms

$$G_a(x,y;\lambda_T) + (R^2/i\lambda_T^2)\nabla_\tau^2 G_a(x,y;\lambda_T) = 1, \tag{17}$$

$$G_b(x,y;\lambda,\lambda_T) + (R^2/i\lambda_T^2)\nabla_\tau^2 G_b(x,y;\lambda,\lambda_T) = F(x,y;\lambda). \tag{18}$$

The boundary condition is $T_1(x,y,z) = 0$ for x and y on the pore boundary; therefore, $G_a(x,y;\lambda_T) = 0 = G_b(x,y;\lambda,\lambda_T)$ on the boundary are the boundary conditions for these functions. Comparing Eq. (17) with Eq. (12), the solution for Eq. (17) follows immediately:

$$G_a(x,y;\lambda_T) = F(x,y;\lambda_T). \tag{19}$$

To obtain the solution for $G_b(x,y)$ in Eq. (18), the differential equation resulting from use of Eq. (19) in Eq. (17) along with the differential equation for $F(x,y;\lambda)$ in Eq. (12) can be used to show that

$$G_b(x,y;\lambda,\lambda_T) = [F(x,y;\lambda_T) - N_{pr}F(x,y;\lambda)]/(1 - N_{pr}). \tag{20}$$

The excess temperature is

$$T_1(x,y,z) = [(\gamma - 1)/c^2\rho_0\beta]F(x,y;\lambda_T)P_1(z) - \frac{T_{0z}}{\rho_0\omega^2}\frac{F(x,y;\lambda_T) - N_{pr}F(x,y;\lambda)}{1 - N_{pr}}\frac{dP_1(z)}{dz}. \tag{21}$$

The equation of state for the acoustic density fluctuation, Eq. (8), can be combined with the expression for the acoustic temperature, Eq. (21), to give

$$\rho_1(x,y,z) = (1/c^2)(\gamma - (\gamma - 1)F(x,y;\lambda_T))P_1(z) + \frac{\beta T_{0z}}{\omega^2}\frac{F(x,y;\lambda_T) - N_{pr}F(x,y;\lambda)}{1 - N_{pr}}\frac{dP_1(z)}{dz}. \tag{22}$$

The first term on the right of Eq. (22) can be used to define a complex compressibility.

When T_{0z} is zero, Eq. (22) can be used to define a complex compressibility which is useful in porous media theory. Denote by $\rho_1(z)$, $F(\lambda_T)$, and $F(\lambda)$ as the average of $\rho_1(x,y,z)$, $F(x,y;\lambda_T)$ and $F(x,y;\lambda)$ over the cross section of the pore. Following the capillary-tube approach of porous media modeling,[12] the complex compressibility is defined as

$$\tilde{C}(z;\lambda_T) = \frac{1}{\rho_0}\frac{\rho_1(z)}{P_1(z)}, \tag{23}$$

and from Eq. (22), with $T_{0z} = 0$, is given by

$$\tilde{C}(z;\lambda_T) = (1/\rho_0 c^2)[\gamma - (\gamma - 1)F(\lambda_T)]. \tag{24}$$

The cross-sectionally averaged density can then be expressed as

$$\rho_1(z) = \rho_0\tilde{C}(z;\lambda_T)P_1(z) + \frac{\beta T_{0z}}{\omega^2}\frac{F(\lambda_T) - N_{pr}F(\lambda)}{1 - N_{pr}}\frac{dP_1(z)}{dz}. \tag{25}$$

The motivation for averaging the density over the cross section of the pore becomes apparent in the next section.

D. Pressure equation in a pore

The continuity equation, Eq. (7), along with the equation of motion, Eq. (13), and the equation of state for the density, Eq. (25), can be combined to yield an equation for the pressure in a pore. When averaging the continuity equation over the pore area the integral $A^{-1}\int\nabla_\tau\cdot\mathbf{v}_\tau(x,y,z)dx\,dy$ is encountered. Use of the divergence theorem in the x,y plane gives $A^{-1}\int\nabla_\tau\cdot\mathbf{v}_\tau(x,y,z)dx\,dy = A^{-1}\int\mathbf{n}\cdot\mathbf{v}_\tau \times(x,y,z)dS = 0$ since $\mathbf{v}_\tau(x,y,z) = 0$ on the perimeter S having outward normal $\mathbf{n}$. Consequently, the cross-sectionally averaged continuity equation for the pore is

$$-i\omega\rho_1(z) + \frac{d}{dz}(\rho_0(z)v_z(z)) = -i\omega\rho_1(z) + \rho_0(z)\frac{d}{dz}v_z(z) - \beta\rho_0(z)T_{0z}v_z(z) = 0, \tag{26}$$

where $d\rho_0(z)/dz = -\beta(z)\,\rho_0(z)\,T_{0z}$ was used on the second form. The v_z and dv_z/dz terms can be evaluated using Eq. (13):

$$-i\omega\rho_1(z) + \frac{\rho_0(z)}{i\omega}\frac{d}{dz}\left(\frac{F(\lambda)}{\rho_0(z)}\frac{dP_1(z)}{dz}\right) - \frac{F(\lambda)}{i\omega}\beta T_{0z}\frac{dP_1}{dz} = 0. \tag{27}$$

Multiplying Eq. (27) by $i\omega/F(\lambda)$ and using Eq. (25) for $\rho_1(z)$ the equation for pressure is

$$\frac{\rho_0}{F(\lambda)}\frac{d}{dz}\left(\frac{F(\lambda)}{\rho_0}\frac{dP_1(z)}{dz}\right) + 2\alpha(\lambda,\lambda_T)\frac{dP_1(z)}{dz} + k(\lambda,\lambda_T)^2P_1(z) = 0, \tag{28}$$

where

$$\alpha(\lambda,\lambda_T) = \frac{\beta T_{0z}}{2}\left(\frac{F(\lambda_T)/F(\lambda) - 1}{1 - N_{pr}}\right), \tag{29}$$

and

$$k(\lambda,\lambda_T)^2 = \frac{\omega^2}{c^2}\frac{1}{F(\lambda)}[\gamma - (\gamma - 1)F(\lambda_T)]. \tag{30}$$

In the absence of a temperature gradient $T_{0z} = 0$ so $\alpha(\lambda,\lambda_T) = 0$. The complex wave number in the pore is then given by $\pm k$, which is the usual form found in porous media modeling.[7,12] The form of the equation for pressure is reminiscent of the time analog of a damped harmonic oscillator; however, here α and k are complex quantities.

E. Specific acoustic impedance and pressure translation theorems

It is appropriate to establish the terminology used in this section. The *specific acoustic impedance* of an acoustical me-

dium is equal to the ratio of the total acoustic pressure and *total particle velocity*. For example, in a fluid layer, the total acoustic pressure is a combination of a downgoing wave and an upgoing wave. The *acoustic impedance* is equal to the ratio of the total acoustic pressure and the *total volume velocity*. For porous media the appropriate boundary conditions at a surface are continuity of pressure, and continuity of volume velocity or equivalently continuity of acoustic impedance.[12] For adiabatic sound, the *characteristic or intrinsic impedance* is equal to $\rho_0 c$ where ρ_0 is the ambient density and c is the adiabatic sound speed.

To this point, propagation in a single pore of infinite length has been considered. Consider now a porous sample [e.g., Fig. 1(b)] consisting of a parallel combination of many identical single straight pores [e.g., Fig. 1(c)] of finite length and denote by N the number of pores per unit area in the cross section. Define by V_{zb} a bulk particle velocity averaged over unit cross section of porous sample, by A_{res} the area of the resonator at the face of the sample, and by A the area of a single pore in the sample. Volume velocity is $A_{res} V_{zb} = N A A_{res} v_z = \Omega A_{res} v_z$ where $\Omega = NA$ is the porosity of the sample. Thus, in the analysis of thermoacoustic elements with many pores, v_z is replaced with V_{zb}/Ω in all of the single pore equations. At boundaries, $P_1(z)$ and $V_{zb}(z)$ or equivalently $Z(z) = P(z)/V_{zb}(z)$ are continuous, where $Z(z)$ is the specific acoustic impedance.

Rayleigh developed an impedance translation theorem for homogeneous fluid layers.[13] The impedance translation theorem relates the specific acoustic impedance at one side of a layer to that at the other. In this manner, one may apply the theorem as many times as necessary to compute the specific acoustic impedance at any surface in the layered media. This translation theorem is applicable to heat exchangers and resonator sections, but is not applicable to the stack because the physical parameters such as density, sound speed, etc., depend on z in a continuous manner on account of the temperature gradient. Impedance and pressure translation theorems, which take into account the dependence of physical parameters on position, will be derived for the stack.

The relevant expressions are the average force equation for a bulk sample from Eq. (13) and $v_z(z) = V_{zb}(z)/\Omega$,

$$\frac{i\omega\rho_0}{\Omega} V_{zb}(z) = F(\lambda) \frac{dP_1(z)}{dz}, \tag{31}$$

the definition of specific acoustic impedance,

$$Z(z) = P_1(z)/V_{zb}(z), \tag{32}$$

and the expression for pressure, Eq. (28). Eliminating $P_1(z)$ and $V_{zb}(z)$ from these expressions using a procedure similar to that of Ref. 14 gives

$$\frac{dZ(z)}{dz} = ik(z)Z_{int}(z)\left(1 - \frac{Z(z)^2}{Z_{int}(z)^2}\right) + 2\alpha(z)Z(z), \tag{33}$$

where $\alpha(z)$ and $k(z)$ are given in Eqs. (29) and (30) and

$$Z_{int} = \rho_0\omega/[\Omega F(\lambda)k] \tag{34}$$

is analogous to the intrinsic or characteristic impedance of a porous medium.[12] The combination of Eqs. (31) and (32) gives

$$\frac{dP_1(z)}{dz} = ik(z)Z_{int}(z)\frac{P_1(z)}{Z(z)}. \tag{35}$$

The defined quantities k, α, and Z_{int} in Eqs. (33) and (35) depend on position because of the temperature gradient.

Expressions (33) and (35) are a set of coupled first-order differential equations which can be readily solved using numerical techniques. The well-known fourth-order Runge–Kutta algorithm is a recommended numerical method. Assume given values of $P_1(z)$ and $Z(z)$ at position z as shown schematically in Fig. 2. Then pressure and specific acoustic impedance are determined at $z - d$ from use of the algorithm $P_1(z-d) = \mathrm{RK}[P_1(z), Z(z)]$ and $Z(z-d) = \mathrm{RK}[Z(z)]$ where RK is symbolic notation for the Runge–Kutta algorithm. Thus this method of determining the pressure and impedance is similar to Rayleigh's impedance translation theorem.

For thermoacoustic elements not having temperature gradients (such as heat exchangers and sections of the resonator), Rayleigh's impedance translation theorem[13] can be written for porous media as

$$Z(z-d) = Z_{int}\frac{Z(z)\cos(kd) - iZ_{int}\sin(kd)}{Z_{int}\cos(kd) - iZ(z)\sin(kd)}. \tag{36}$$

The pressure translation theorem is

$$P_1(z-d) = P_1(z)\{\cos(kd) - i[Z_{int}/Z(z)]\sin(kd)\}. \tag{37}$$

In Eqs. (36) and (37), k is the complex wave number for heat exchangers or open sections of the tube and can be determined from the porous media expression, Eq. (30). Use of these translation theorems will be discussed in Sec. I G.

Knowledge of heat and work flow is central to thermoacoustics. In the next section, heat and work flows are evaluated for arbitrary pore perimeters and are expressed in terms of pressure and specific acoustic impedance.

F. Heat and work flow

The time averaged energy flow to second order (subscript 2) is[4]

$$\bar{H}_2(z) = \bar{Q}_2(z) + \bar{W}_2(z) - \bar{Q}_{loss}(z), \tag{38}$$

where time-averaged heat flow due to hydrodynamic transport is

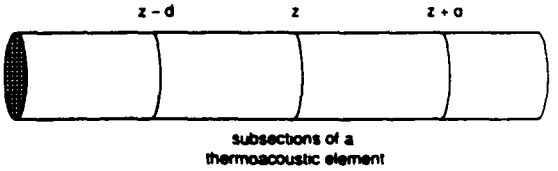

FIG. 2. Subsection of a thermoacoustic element, shown here having square pore capillary tubes. For the stack thermoacoustic element, an arbitrary number of subsections may be used in spanning the temperature difference at the ends of the stack.

$$\bar{\dot{Q}}_2(z) = \frac{\Omega\ A_{\rm res}}{2}\,{\rm Re}\,\frac{1}{A}\int_A [\rho_0 c_p v_z(x,y,z) T_1^*(x,y,z) - \beta T_0 v_z(x,y,z) P_1^*(z)]\,dx\,dy; \quad (39)$$

the heat flow due to conduction down a temperature gradient is

$$\bar{\dot{Q}}_{\rm loss}(z) = \Omega\ A_{\rm res}\kappa_{\rm gas} T_{0z} + (1-\Omega) A_{\rm res}\kappa_{\rm stack} T_{0z}; \quad (40)$$

and the time-averaged work flow (or power) is

$$\bar{\dot{W}}_2(z) = \frac{\Omega\ A_{\rm res}}{2}\,{\rm Re}\,\frac{1}{A}\int_A v_z(x,y,z) P_1^*(z)\,dx\,dy. \quad (41)$$

Here, $A_{\rm res}$ is the cross-sectional area of the resonance tube at point z, A is the cross-sectional area of a single pore, Ω is porosity, $\kappa_{\rm gas}$ and $\kappa_{\rm stack}$ are the thermal conductivity of the gas and stack, * indicates complex conjugation, and Re indicates the real part of the expression. The product $(\Omega A_{\rm res})$ is cross-sectional open area of the tube at position z.

To determine $\bar{\dot{Q}}_2(z)$ and $\bar{\dot{W}}_2(z)$ use is made of Eq. (21) for $T_1(x,y,z)$ and Eq. (11) for $v_z(x,y,z)$ in Eqs. (39) and (40). Resulting expressions are

$$\bar{\dot{Q}}_2(z) = \frac{\Omega A_{\rm res}}{2}\frac{\rho_0 c_p}{A}\,{\rm Im}\int_A \frac{F(x,y;\lambda)}{\omega\rho_0} P_{1z}(z) \times\left(\frac{\gamma-1}{c^2\rho_0\beta} F^*(x,y;\lambda_T) P_1^*(z) - \frac{T_{0z}}{\rho_0\omega^2}\frac{F^*(x,y;\lambda_T) - N_{\rm pr}F^*(x,y;\lambda)}{1-N_{\rm pr}} \times P_{1z}^*(z)\right)dx\,dy - \beta T_0\,\bar{\dot{W}}_2(z), \quad (42)$$

where $P_{1z}(z) = dP_1(z)/dz$ and

$$\bar{\dot{W}}_2(z) = \frac{\Omega\ A_{\rm res}}{2}\frac{1}{A}\,{\rm Im}\int_A \frac{F(x,y;\lambda)}{\omega\rho_0} P_{1z}(z) P_1^*(z)\,dx\,dy. \quad (43)$$

Recall the definitions $\lambda_T = N_{\rm pr}^{1/2}\lambda$ and

$$F(\lambda) = \frac{1}{A}\int_A F(x,y;\lambda)\,dx\,dy. \quad (44)$$

The following general integral result, which is proven at the end of this section,

$$I_1 \equiv \frac{1}{A}\int_A F(x,y;\lambda) F^*(x,y;\lambda_T)\,dx\,dy = [F(\lambda)N_{\rm pr} + F^*(\lambda_T)]/(N_{\rm pr}+1), \quad (45)$$

and the integral that may be evaluated using Eq. (45)

$$I_2 \equiv \frac{1}{A}\int_A F(x,y;\lambda) F^*(x,y;\lambda)\,dx\,dy = \lim_{N_{\rm pr}\to 1} I_1 = {\rm Re}\,F(\lambda), \quad (46)$$

are necessary to evaluate Eqs. (42) and (43). By making use of these integrals and the thermodynamic relation $\gamma - 1 = \beta^2 T_0 c^2/c_p$, heat and work flows are

$$\bar{\dot{Q}}_2(z) = \frac{\Omega A_{\rm res}}{2}\beta T_0\left[{\rm Im}\left(\frac{P_{1z}(z)P_1^*(z)}{\rho_0\omega} \times\frac{F^*(\lambda_T) - F(\lambda)}{1+N_{\rm pr}}\right) - \frac{T_{0z}}{\beta T_0}\frac{c_p}{\rho_0\omega^3}|P_{1z}(z)|^2 \times\frac{{\rm Im}[F^*(\lambda_T) + N_{\rm pr}F(\lambda)]}{1-N_{\rm pr}^2}\right], \quad (47)$$

and

$$\bar{\dot{W}}_2(z) = \frac{\Omega\ A_{\rm res}}{2}\,{\rm Im}\left(\frac{P_{1z}(z)P_1^*(z)}{\rho_0\omega}F(\lambda)\right). \quad (48)$$

Equations (47) and (48) are general expressions for heat and work flows with the functional form of $F(\lambda)$ dependent on the particular pore geometry. It can be shown that Eqs. (38), (47), and (48) are the same as Swift's[4] equation (A30) for the special case of parallel plate geometries and assuming the $\epsilon_s = 0$ (appropriate for gas thermodynamics) in Swift's theory. To aid in comparing results, note that $F^*(\lambda) = 1 - f_\nu$ and $F^*(\lambda_T) = 1 - f_\kappa$ where f_ν and f_κ are used in Swift's notation.

Since impedance and pressure translation theorems have been derived for arbitrary locations within the resonator, and specifically for the stack element, it is useful to express heat and work flows in terms of the specific acoustic impedance $Z(z)$ and pressure $P_1(z)$. From the definition of specific acoustic impedance, $Z(z) = P_1(z)/[\Omega v_z(z)]$, and Eq. (13) for $v_z(z)$,

$$\frac{dP_1(z)}{dz} = P_{1z}(z) = \frac{i\omega\rho_0 P_1(z)}{\Omega F(\lambda) Z(z)}. \quad (49)$$

Heat and work flows are

$$\bar{\dot{Q}}_2(z) = \frac{A_{\rm res}}{2}\frac{\beta T_0}{1+N_{\rm pr}}\frac{|P_1(z)|^2}{|Z(z)|^2} \times\left\{{\rm Re}\left[Z(z)^*\left(\frac{F^*(\lambda_T)}{F(\lambda)} + N_{\rm pr}\right)\right] - \frac{T_{0z}}{\beta T_0}\frac{\rho_0 c_p}{\Omega\omega}\frac{1}{|F(\lambda)|^2} \times\frac{{\rm Im}[F^*(\lambda_T) + N_{\rm pr}F(\lambda)]}{1-N_{\rm pr}}\right\} - \beta T_0\,\bar{\dot{W}}_2(z), \quad (50)$$

and

$$\bar{\dot{W}}_2(z) = (A_{\rm res}/2)[|P_1(z)|^2/|Z(z)|^2]\,{\rm Re}\,Z(z). \quad (51)$$

In Eqs. (50) and (51), $P_1(z)$ and $Z(z)$ are global variables in that they depend on the detailed arrangement of all elements of the thermoacoustic engine, and $F(\lambda)$ and $F(\lambda_T)$ depend on the local properties of the gas and stack geometry.

The remainder of this section is devoted to proof of Eq. (45). From Eq. (12), Eq. (45) can be written as

$$I_1 = \frac{1}{A}\int_A F(x,y;\lambda)\left(1 + \frac{R^2}{i\lambda_T^2}\nabla_r^2 F^*(x,y;\lambda_T)\right)dx\,dy. \quad (52)$$

Use of the vector identity for the divergence of the product of a scalar and a vector and the definition of $F(\lambda)$ give

$$I_1 = F(\lambda) + \frac{1}{A}\frac{R^2}{i\lambda_T^2} \times \int_A \nabla_r \cdot [F(x,y;\lambda)\nabla_r F^*(x,y;\lambda_T)]\,dx\,dy - \frac{1}{A}\frac{R^2}{i\lambda_T^2}\int_A \nabla_r F(x,y;\lambda) \cdot \nabla_r F^*(x,y;\lambda_T)\,dx\,dy, \quad (53)$$

where the gradient operator in the x,y plane is ∇_r. The divergence theorem in the x,y plane can be applied to the second integral in Eq. (53):

$$\int_A \nabla_r \cdot [F(x,y;\lambda)\nabla_r F^*(x,y;\lambda_T)]\,dx\,dy = \int_S \mathbf{n} \cdot [F(x,y;\lambda)\nabla_r F^*(x,y;\lambda_T)]\,dS = 0, \quad (54)$$

where dS is an element of perimeter on the pore of arbitrary shape, and $\mathbf{n}$ is the outward normal at the pore wall. The integral in Eq. (54) is zero by the boundary condition $F(x,y;\lambda) = 0$ for x and y on S. Thus

$$I_1 = F(\lambda) - \frac{1}{A}\frac{R^2}{i\lambda_T^2}\int_A \nabla_r F(x,y;\lambda) \cdot \nabla_r F^*(x,y;\lambda_T)\,dx\,dy. \quad (55)$$

Now, Eq. (12) for $F(x,y;\lambda)$ could have been used in Eq. (45), rather than for $F^*(x,y;\lambda_T)$ as was done to obtain Eq. (55). Had this been done, Eq. (55) would be

$$I_1 = F^*(\lambda_T) + \frac{1}{A}\frac{R^2}{i\lambda^2}\int_A \nabla_r F(x,y;\lambda) \cdot \nabla_r F^*(x,y;\lambda_T)\,dx\,dy. \quad (56)$$

Eliminating the common integral between Eqs. (55) and (56) gives Eq. (45).

G. Numerical evaluation of an engine's performance

The first and simplest situation considered is the frequency response of a nondriven tube below the onset of oscillation. An example based on Fig. 1(a) will suffice to demonstrate the procedure for computing the frequency response using the impedance translation theorem. The acoustic driver is considered to deliver constant amplitude acoustic oscillations of radian frequency ω of insufficient amplitude to acoustically stimulate the transport of heat from cold to hot. An ideal microphone located near the driver is used to determine the frequency response $P_1(z = 0,\omega)$.

Assume a steady-state equilibrium in which a temperature gradient exists across the stack as a result of heat input at the hot exchanger and heat removal at the cold exchanger. The open tube sections of the resonator are taken to be at the same temperature as the nearest heat exchanger. The ambient temperature of the stack will not, in general, vary linearly from the cold to hot end due to the temperature dependence of the stack and gas thermal conductivity. The ambient temperature is assumed known at all points.

To determine the frequency response, one starts with a known value of specific acoustic impedance at the rigid end of the tube in Fig. 1(a). Specific acoustic impedance here can be evaluated using the expression for the boundary layer impedance of a rigid wall.[13] Use of Eq. (36) determines Z first at the hot-heat exchanger, open-tube interface, and then at the stack-hot-heat exchanger interface. The value of Z at this interface is the starting value for the Runge–Kutta algorithm solution of Eqs. (33). Then, use of Eq. (36) determines Z first at the cold-heat exchanger, open-tube interface, and finally at the position of the acoustic driver. For known acoustic driver response (e.g., constant displacement, etc.), the pressure can be determined absolutely at the driver location using the driver response and the calculated expression for specific acoustic impedance. It should be noted that all variables in Eqs. (33) and (36) are to be evaluated at the local position of the thermoacoustic element or subsection. The translation theorem approach for computing acoustical quantities is a superior way of performing calculations for resonators containing many thermoacoustic elements.

The second example considered is evaluation of a thermoacoustic refrigerator. Though the typical configuration[4] used for a refrigerator has the acoustic driver at the hot (ambient) exchanger, the arrangement shown in Fig. 1(a) will suffice for the present discussion. The driver is assumed to deliver sufficient acoustic power to the tube that heat is thermoacoustically transported from the cold to the ambient heat exchanger. Experimental and theoretical evidence[15] indicates that the ambient temperature distribution in the stack is, in general, different from that which would occur for a simple temperature gradient with no acoustic transport of heat. Indeed the second term of $\overline{Q}_2(z)$ in Eq. (50) has a temperature gradient multiplied by a factor depending on the pressure and impedance that acts as a dynamical coefficient of thermal conductivity.

Steady-state equilibrium of the refrigerator is achieved when the ambient temperature throughout the system is constant. No net heat is absorbed into the walls of the stack (i.e., heat engine) so $\overline{H}_2(z)$ is a constant in the stack.[4,15] Quantities assumed known are the pressure and specific acoustic impedance at the right end of the tube, the hot-heat exchanger temperature, and the steady-state constant value of $\overline{H}_2$ in the stack. The unknown quantities of interest are the cold-heat exchanger temperature, the power delivered by the acoustic driver, and the net heat flow from the cold-heat exchanger. One may compute the Carnot coefficient of performance (COP) from the hot- and cold-heat exchanger temperatures.[4] This COP may be compared to the coefficient of performance computed from the ratio of the net heat flow from the cold exchanger and the power delivered by the driver.[4]

Specific acoustic impedance and pressure at the stack-hot-heat exchanger interface can be determined from use of translation theorems in Eqs. (36) and (37). Then, with $\overline{H}_2$ a known constant, Eq. (38) along with Eqs. (40), (50), and (51) are used to solve for $T_{0z}(z)$, the ambient temperature gradient in the stack. Runge–Kutta integration of the coupled set of three first-order equations, $T_{0z}(z)$, $P_1(z)$ from

Eq. (35), and $Z(z)$ from Eq. (33), is used to determine the ambient temperature distribution $T_0(z)$ in the stack and thus the cold-heat exchanger temperature. Translation theorems can then be used to compute the pressure and impedance elsewhere in the tube. Equation (51) is used to compute the power delivered by the driver. By energy conservation, the difference in $\dot{H}_2$ between the cold heat exchanger–stack interface and the open-tube–cold heat exchanger interface is the amount of heat flowing out of the cold heat exchanger. This method of analyzing thermoacoustic refrigerators was first described in Ref. 15.

II. HEAT AND WORK FLOWS IN THE SHORT STACK APPROXIMATION FOR VARIOUS STACK GEOMETRIES

Heat and work flows are compared for stacks having different pore geometries. In addition to the square pore stack shown in Fig. 1(b), parallel plate, circular, and equilateral triangular capillary tubes will be considered.

The short stack approximation was used by Swift[4] to get an interpretable analytical expression for energy flow. Figure 3 shows the arrangement for the short stack approximation. The stack is assumed to be short enough that the empty tube standing wave is unaffected. The temperature difference between opposite ends of the stack is assumed to be much less than the average temperature at the stack center so that the thermophysical quantities are approximately constant and are evaluated at the average temperature. Stack porosity is Ω.

Pressure and specific acoustic impedance at z are, from Eqs. (36) and (37),

$$Z(z) = i\rho_0 c \cot[k_0(L-z)], \tag{57}$$

and

$$P_1(z) = P_1(L)\cos[k_0(L-z)] \approx i\rho_0 c V_0 \cos[k_0(L-z)]/\sin(k_0 L), \tag{58}$$

where the wave number in the empty tube is k_0. Use of Eqs. (57) and (58) in the heat flow equation, Eq. (50), gives

$$\overline{\dot{Q}}_2(z) = \frac{A_{\rm res}}{2}\frac{P_1(L)^2}{\rho_0 c}\frac{\beta T_0}{1+N_{\rm pr}} \times \frac{\sin[2k_0(L-z)]}{2}\,\mathrm{Im}\left(\frac{F^*(\lambda_T)}{F(\lambda)}\right) \times\left(1-\Gamma\frac{\mathrm{Im}[F(\lambda_T)+N_{\rm pr}F^*(\lambda)]}{\mathrm{Im}[F(\lambda_T)F(\lambda)](1-N_{\rm pr})}\right), \tag{59}$$

where

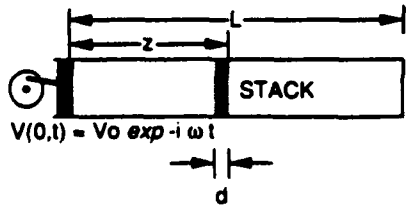

FIG. 3. Arrangement for the short stack approximation.

$$\Gamma = \frac{T_{0z}}{T_0}\frac{\beta T_0 c\tan[k_0(L-z)]}{\omega\Omega(\gamma-1)} = T_{0z}\frac{c_p\tan[k_0(L-z)]}{\omega\Omega\beta T_0 c}. \tag{60}$$

In the inviscid approximation for which $N_{\rm pr}=0$ and $F(\lambda)=1$,

$$\overline{\dot{Q}}_2(z) = \frac{A_{\rm res}}{2}\frac{P_1(L)^2}{\rho_0 c}\beta T_0\frac{\sin[2k_0(L-z)]}{2} \times \mathrm{Im}F^*(\lambda_T)(1-\Gamma). \tag{61}$$

Physically, the term $\mathrm{Im}\,F^*(\lambda_T)$ is a measure of the dynamical thermal interaction between the gas and solid. Recall that $\lambda_T = R(\rho_0\omega c_p/\kappa)^{1/2}$, where R is twice the ratio of capillary pore area to pore perimeter. The function $F(x,y;\lambda_T)$ is a solution to the partial differential equation, Eq. (12), for a particular pore geometry and $F(\lambda_T)$ is the average of this quantity over the pore cross section. According to Eq. (61), stacks made of pores for which $\mathrm{Im}\,F^*(\lambda_T)$ is a large value will result in the greatest heat flow.

Work flow is given generally by Eq. (51). No work is done in the region to the right of the stack in Fig. 3, which can be verified readily by using the impedance of Eq. (57) in Eq. (51). In this region, pressure and velocity have standing wave phasing. To compute the work done in the stack, use is made of the impedance translation theorem to get the impedance at the left side of the stack. In the short stack approximation, $k_0 d \approx \omega d/c \ll 1$; hence, $Z(z-d)$ can be approximated from a simple finite difference approximation of Eq. (33),

$$Z(z-d) = Z(z)\left(1-2\alpha d-\frac{i\rho_0\omega d}{F(\lambda)\Omega Z(z)} + \frac{idZ(z)k^2F(\lambda)\Omega}{\rho_0\omega}\right). \tag{62}$$

After some manipulation, work flow to first order in $k_0 d$ is

$$\overline{\dot{W}}_2(z) = \frac{A_{\rm res}\Omega}{2}P_1(L)^2\frac{T_0\beta^2\omega d}{\rho_0 c_p} \times \mathrm{Im}\,F^*(\lambda_T)\cos^2[k_0(L-z)] \times\left(1-\Gamma\frac{\mathrm{Im}[F(\lambda_T)/F(\lambda)]}{\mathrm{Im}\,F(\lambda_T)(1-N_{\rm pr})}\right) + \overline{\dot{W}}_{2\rm visc}(z), \tag{63}$$

where work due to viscosity is

$$\overline{\dot{W}}_{2\rm visc}(z) = \frac{A_{\rm res}\Omega}{2}\frac{P_1(L)^2}{\rho_0 c^2}\omega d\sin^2[k_0(L-z)] \times\{\mathrm{Im}\,F^*(\lambda)/[F(\lambda)F^*(\lambda)]\}. \tag{64}$$

Work flow in the inviscid approximation is

$$\overline{\dot{W}}_2(z) = (A_{\rm res}\Omega/2)P_1(L)^2(T_0\beta^2\omega d/\rho_0 c_p) \times \mathrm{Im}\,F^*(\lambda_T)\cos^2[k_0(L-z)](1-\Gamma). \tag{65}$$

Equations (63) and (65) are the acoustic power absorbed by

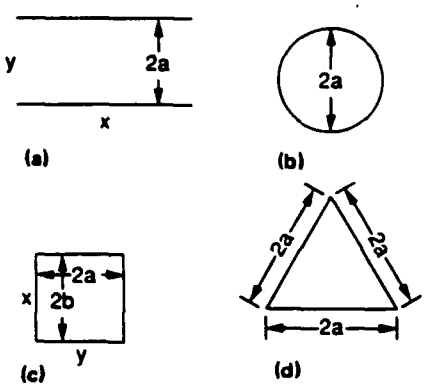

FIG. 4. (a) Parallel plate, (b) circular, (c) rectangular, and (d) equilateral triangular capillary tube geometries considered for the short stack approximation. For example, (c) corresponds to the stack shown in Fig. 1(b).

the stack, with and without gas viscosity, and when these quantities are negative, it indicates that acoustic power is being produced by the stack. Stacks made of pores for which Im $F^*(\lambda_T)$ is a large value will result in the greatest work flow.

Work and heat flows are to be compared for the various pore geometries shown in Fig. 4(a)–(d). In the inviscid short stack approximation, pores with a large value of Im $F(\lambda)^*$ will have the greatest heat and work flows as indicated by Eqs. (61) and (65). According to Fig. 5, which shows the real and imaginary parts of $F(\lambda)$ for the various pore geometries, the parallel plate geometry has the largest value of Im $F(\lambda)^*$. The value occurs for $\lambda_c \approx 3.2$, which allows one to compute the optimal operating frequency from the relation $\lambda_c = (\rho_0 \omega c_p/\kappa)^{1/2} R$. In other words, you can get about 10% more heat and work flows in thermoacoustics by choosing to make your stack from parallel plates rather than the other pore geometries. The functional form of $F(\lambda)$ for the various pore geometries is given below.

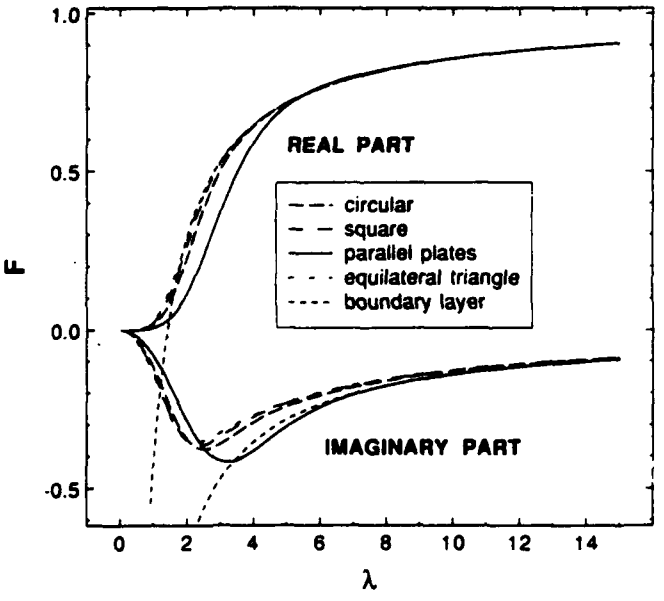

FIG. 5. Real and imaginary part of the $F(\lambda)$ for parallel plates, circular pores, square pores, and equilateral triangle pores. Heat and work flows are proportional to the imaginary part of $[F(\lambda)]$ in the short stack approximation thus indicating the parallel plate stack is the best choice for optimal thermoacoustic engines. Also shown is the boundary layer approximation of $F(\lambda)$ for all pore geometries, valid in the limit $\lambda \to \infty$.

Swift[4] and Rott[5] have worked out the parallel plate geometry stack. Parallel plates have also been of interest in porous media.[12,16] Denote by $2a$ the separation distance between plates. To be consistent with the definition of the characteristic pore radius R as being equal to twice the transverse pore area divided by the pore perimeter, take $R = 2a$. The y axis is centered at the midpoint between plates with the z axis extending in the longitudinal direction. The function $F(y;\lambda)$ that satisfies the differential equation for the transverse dependence of the equation of motion, Eq. (12), is

$$F(y;\lambda) = 1 - \frac{\cosh(\sqrt{-i}\lambda/2\, y/a)}{\cosh(\sqrt{-i}\lambda/2)}. \tag{66}$$

The average of $F(y;\lambda)$ over the pore is defined as $F(\lambda) = 1/(2a)\int F(y;\lambda)\, dy$ and is

$$F(\lambda) = 1 - (2/\lambda\sqrt{-i})\tanh(\sqrt{-i}\lambda/2). \tag{67}$$

Rott has worked out the cylindrical pore[1] geometry stack. One type of porous media theory is based upon propagation in a single cylindrical capillary tube.[11,12,16] Denote by a the radius of the cylindrical pore. The characteristic pore radius for cylindrical pores is $R = a$. The radial coordinate of a cylindrical coordinate system centered at the middle of the circular pore is r. The function $F(r;\lambda)$ which satisfies the differential equation for the transverse dependence of the equation of motion, Eq. (12), is

$$F(r;\lambda) = 1 - J_0(\sqrt{i}\lambda r/a)/J_0(\sqrt{i}\lambda). \tag{68}$$

The average of $F(r;\lambda)$ over the pore is defined as $F(\lambda) = 2/a^2 \int F(r;\lambda) r\, dr$ and is

$$F(\lambda) = 1 - (2/\sqrt{i}\lambda)\left[J_1(\sqrt{i}\lambda)/J_0(\sqrt{i}\lambda)\right]. \tag{69}$$

Previous work has emphasized thermoacoustic stacks consisting of parallel plate pores and cylindrical pores. The basic equations are given here for stacks consisting of rectangular pores. Denote by $2a$ and $2b$ the length along the x and y axes of the rectangular pore cross section. Take the coordinate system origin to be at the lower left corner of the rectangular pore. It is convenient to define a function $Y_{mn}(\lambda)$ as

$$Y_{mn}(\lambda) = 1 + (i\pi^2/\lambda^2)[(b^2m^2 + a^2n^2)/(a+b)^2]. \tag{70}$$

The characteristic transverse dimension equal to twice the pore area divided by the pore perimeter is

$$R = 2ab/(a+b). \tag{71}$$

A series solution for the function $F(x,y;\lambda)$ which satisfies the differential equation for the transverse dependence of the equation of motion, Eq. (12), is[7,8]

$$F(x,y;\lambda) = \frac{16}{\pi^2} \sum_{m\ n\ \text{odd}} \frac{\sin(m\pi x/2a)\sin(n\pi y/2b)}{m\ n Y_{mn}(\lambda)}. \tag{72}$$

In all sums given in this section, m and n extend over positive odd integers. For a rectangular pore the average is defined by $F(\lambda) = 1/(4ab)\int F(x,y;\lambda)\,dx\,dy$, where the integral extends over the entire cross section of the pore. Then,

$$F(\lambda) = \frac{64}{\pi^4} \sum_{mn\ \text{odd}} \frac{1}{m^2 n^2 Y_{mn}(\lambda)}. \tag{73}$$

The function $F(x,y;\lambda)$ in Eq. (17) was obtained from a solution by Han[17] for the same differential equation as Eq. (12).

Equilateral triangular pores have been recently investigated by Stinson.[18] The pore geometry is shown in Fig. 4(d). The characteristic dimension is $R = a/3^{1/2}$ and

$$F(\lambda) = 1 - \frac{2}{\sqrt{-i}\lambda} \coth\left(\frac{3\lambda\sqrt{-i}}{2}\right) + \frac{4i}{3\lambda^2}. \tag{74}$$

In the boundary layer approximation appropriate for all pore geometries in the limit $\lambda \to \infty$,

$$F(\lambda) = 1 - (\sqrt{2}/\lambda)(1+i) = 1 - (\delta/R)(1+i), \tag{75}$$

where δ is the viscous or thermal boundary layer thickness and R is twice the pore area divided by the pore perimeter. Equation (75) can easily be derived from the large λ limit of Eqs. (67), (69), or (74). Physically, $2\delta/R$ is the area of the boundary layer divided by the pore cross-sectional area. Therefore, it is expected and noteworthy that pores with the same λ have the same complex wave number in the wide-tube limit; i.e., $\lambda \to \infty$.[13] Figure 5 gives a graphical illustration as to when the boundary layer approximation is useful for a particular pore geometry. It also illustrates why it was necessary for Rott[5] to improve upon the boundary-layer theory of thermoacoustics.

III. CONCLUSION

Linear thermoacoustics for gas-filled stacks has been reduced to calculation of a single function F. The function $F(x,y;\lambda)$ gives the transverse variation of the longitudinal particle velocity $v_z(x,y,z)$. It satisfies the partial differential equation, Eq. (12), and the boundary condition $F(x,y;\lambda) = 0$ for x and y on the pore perimeter. The average of $F(x,y;\lambda)$ over the pore cross section is $F(\lambda)$. The parameter λ is proportional to the ratio of the pore hydraulic radius and the viscous boundary layer thickness that would be appropriate for a flat pore boundary. Similarly, λ_T is proportional to the ratio of pore hydraulic radius and the thermal boundary layer thickness. The form of $F(\lambda)$ depends on pore geometry. All first-order acoustical field quantities (Sec. I A–D) and the second order energy flux (Sec. I F) can be evaluated using this function.

The general framework was used in Sec. II to investigate the optimal choice of capillary tube geometry for stacks. Heat and work flows evaluated in the inviscid, short stack approximation, are approximately 10% greater for the parallel plate stack geometry than for the circular, square, and equilateral-triangle pore geometries.

Impedance and pressure translation theorems were developed in Sec. I E for determining these quantities at all points in the resonator shown in Fig. 1(a). With this approach, analysis of complicated arrangements of thermoacoustic elements can be evaluated readily and in a unified manner. Work and heat flows were expressed in terms of specific acoustic impedance and pressure to take advantage of these theorems.

Finally, the function $F(\lambda)$ is also the key element of capillary-pore based porous media models.[12,15] Factors are used in these models to scale properties of random media to circular pores. Thus the scaling factors and methodology of porous media modeling can be readily adapted to be useful in thermoacoustics. After all, thermoacoustic elements are nothing more than sections of porous media, with the added richness of ambient temperature gradients.

ACKNOWLEDGMENTS

This work was supported by the Office of Naval Research. We are grateful to Mike Stinson for the triangular pore solution. We acknowledge insightful conversations with Greg Swift, Anthony Atchley, and Tom Hofler.

[1] N. Rott, "Thermoacoustics," Adv. Appl. Mech. 20, 135–175 (1980).
[2] P. Merkli and H. Thomann, "Thermoacoustic effects in a resonance tube," J. Fluid Mech. 70, 161–177 (1975).
[3] N. Rott and G. Zouzoulas, "Thermally driven acoustic oscillations. Part IV. Tubes with variable cross-section," Z. Angew. Math. Phys. 27, 197–224 (1976).
[4] G. W. Swift, "Thermoacoustic engines," J. Acoust. Soc. Am. 84, 1145–1180 (1988).
[5] N. Rott, "Damped and thermally driven acoustic oscillation in wide and narrow tubes," Z. Angew. Math. Phys. 20, 230–243 (1969).
[6] The ceramics are manufactured by, among others, Corning Incorporated, Industrial Products Division, Corning, NY 14831. For a discussion of their properties, see J. J. Burton and R. L. Garten, *Advanced Materials in Catalysis* (Academic, New York, 1977), Chap. 10.
[7] H. S. Roh, W. P. Arnott, J. M. Sabatier, and R. Raspet, "Measurement and calculation of acoustic propagation constants in arrays of small air-filled rectangular tubes," J. Acoust. Soc. Am 89, 2617–2624 (1991); W. P. Arnott, J. M. Sabatier, and R. Raspet, "Sound propagation in capillary-tube-type porous media with small pores in the capillary walls," J. Acoust. Soc. Am. 90, 3299–3306.
[8] M. R. Stinson, "The propagation of plane sound waves in narrow and wide circular tubes, and generalization to uniform tubes of arbitrary cross-sectional shape," J. Acoust. Soc. Am. 89, 550–558 (1991).
[9] A. L. Fetter and J. D. Walecka, *Theoretical Mechanics of Particles and Continua* (McGraw-Hill, New York, 1980).
[10] H. Tijdeman, "On the propagation of sound waves in cylindrical tubes," J. Sound Vib. 39, 1–33 (1975).
[11] C. Zwikker and C. Kosten, *Sound Absorbing Materials* (Elsevier, Amsterdam, 1949).
[12] K. Attenborough, "Acoustical characteristics of porous materials," Phys. Rep. 82, 179–227 (1982).
[13] A. D. Pierce, *Acoustics: An Introduction to Its Physical Principles and Applications* (American Institute of Physics, New York, 1989).
[14] L. M. Brekhovskikh, *Waves in Layered Media* (Academic, New York, 1980), p. 211.
[15] J. Wheatley, T. Hofler, G. W. Swift, and A. Migliori, "An intrinsically irreversible thermoacoustic heat engine," J. Acoust. Soc. Am. 74, 153–170 (1983).
[16] M. A. Biot, "Theory of propagation of elastic waves in a fluid-saturated porous solid," J. Acoust. Soc. Am. 28, 168–191 (1956).
[17] L. S. Han, "Hydrodynamic entrance lengths for incompressible laminar flow in rectangular ducts," J. Appl. Mech. 27, 403–409 (1960).
[18] M. R. Stinson and Y. Champoux, "Assignment of shape factors for porous materials having simple pore geometries," J. Acoust. Soc. Am. Suppl. 1 88, S121 (1990).

Sound propagation in capillary-tube-type porous media with small pores in the capillary walls

W. Patrick Arnott, James M. Sabatier, and Richard Raspet
National Center for Physical Acoustics, and the Department of Physics and Astronomy, University of Mississippi, University, Mississippi 38677

(Received 18 February 1991; revised 24 July 1991; accepted 7 August 1991)

Sound propagation in gas-filled capillary-tube-type porous media was investigated. The capillary tubes were taken to be nominally straight with very small pores in the walls of the capillary tubes. The complex wave number and the characteristic impedance of such media were evaluated. Application to ceramic samples having capillary pores with square cross sections and porous walls is developed as an explanation for the anomalous tortuosity factor previously inferred for this material. Specific acoustic impedance (SAI) measurements were performed for rigid-backed square pore ceramic media having finite wall porosity. It is shown that phase velocity is decreased, attenuation is increased, and characteristic impedance is decreased by finite wall porosity. SAI measurements were also performed after the wall pores were filled with water. These measurements agree favorably with the porous wall and nonporous wall theories, respectively. This work provides a model for the acoustical properties of gas-filled monolithic catalyst supports of which the square pore ceramic media is an example.

PACS numbers: 43.28.Fp, 43.50.Vt, 43.20.Mv

INTRODUCTION

Theory[1,2] and experiments[1] were recently reported for sound propagation in porous media consisting of straight capillary tubes having square cross sections. The experimental work was aimed at testing the efficacy of first-principle models for predicting the acoustical properties of porous media with well-defined geometries. The measured complex wave number[1] was approximately 10% larger than the values predicted from theory assuming nonporous walls. However, the ceramic porous sample used actually has walls that are porous, as indicated schematically in Fig. 1(a) and (b). A qualitative explanation for the discrepancy was that the finite porosity of the ceramic square pore wall should increase the bulk compressibility of air in the porous media and hence increase the complex wave number. This decreases the phase velocity and increases the attenuation, as was observed in the measurements. Effects of wall pores on propagation in porous media were also qualitatively discussed earlier.[3]

In this paper, the effects of finite wall porosity are included in the theory for sound propagation in a porous media consisting of nominally straight capillary tubes with much smaller pores in the capillary tube walls. The theory is cast in a sufficiently general form that it is useful for capillary tubes having geometries other than squares. Specific acoustic impedance (SAI) measurements of a rigid-backed ceramic sample and a previous measurement of the complex wave number[1] compare favorably with the porous-wall porous media theory. Wall pores were filled with water and the SAI measurements were repeated. These measurements agree favorably with nonporous wall theory. The theory shows that the complex wave number is *increased* and the characteristic impedance is *decreased* on account of finite wall porosity.

Finite wall impedance concepts have been used in related work. For a sufficiently wide tube, absorption of the plane wave mode can be accounted for using the expression for boundary layer impedance as a boundary condition at the tube wall.[4] Similarly, sound absorption in ducts with absorbing liners at the duct wall can be modeled using the liner impedance as a boundary condition.[5] These concepts also find use in bore hole measurements in geophysics.[6]

The ceramics used in this investigation are an example of a monolithic catalyst support.[7] Several manufacturers use these ceramics in automobile catalytic converters. Physical properties, such as the ability to hold coatings and low thermal conductivity, can be obtained by adjusting the ceramic wall porosity.[7] A combustible material that burns out during the final sintering is added to the raw ceramic mixture to increase the porosity for some applications.[7] The theory developed here provides a model for the low-frequency acoustical properties of gas-filled monolithic catalyst supports. These ceramics may be useful as low-frequency sound absorbers. They may also be useful in thermoacoustic heat engines due to their low thermal conductivity, regular geometry, wide spread availability, and low cost.

I. PROPAGATION IN POROUS WALL POROUS MEDIA

A. Assumptions

In ideal acoustics an often used approximation is that sound wave propagation is adiabatic and that the fluid is inviscid. At boundaries it is sufficient to assume continuity

[a] This work was presented at the 120th Meeting of the Acoustical Society of America [J. Acoust. Soc. Am. Suppl. 1 88, S143 (1990)].

 0001-4966/91/123299-08$00.80

of pressure and the normal component of particle velocity. Ideal acoustics boundary conditions are not sufficient to describe sound propagation in porous media for which the solid and fluid volumes are intermingled and are on the same order. Account must be taken of momentum and energy transport phenomena, viscosity and thermal conductivity, which occur as a result of velocity and temperature gradients. In viscous fluids it is usually a good assumption that the total particle velocity is zero at a rigid stationary boundary. For boundaries such as solid–gas interfaces compression and expansion of gas can result in transport of heat to and from the solid for parcels of gas sufficiently close to the walls. At boundaries gas and solid temperatures are assumed to be the same since in solids the heat capacity is usually much greater than that of the gas. Any local heating of the solid due to the gas is diffused throughout the solid since it is generally a much better heat conductor than the gas.

Dimensionless numbers indicate different regimes of disturbances in porous media. Denote by ρ_0, c_p, η, and κ the gas properties of ambient density, constant pressure heat capacity per unit mass, viscosity, and thermal conductivity. A measure of the relative magnitude of viscous and thermal diffusion in the gas is given by the Prandtl number, $N_{\mathrm{Pr}} = \eta c_p/\kappa$. Gas viscous and thermal penetration depths for oscillations of radian frequency ω are $\delta_\eta = (2\eta/\rho_0\omega)^{1/2}$ and $\delta_\kappa = (2\kappa/\rho_0\omega c_p)^{1/2} = \delta_\eta/N_{\mathrm{Pr}}^{1/2}$, respectively. Denote by R a characteristic transverse pore dimension, e.g., the pore radius for circular pores. A dimensionless shear wave number can be defined as $\lambda = 2^{1/2}R/\delta_\eta = R(\rho_0\omega/\eta)^{1/2}$. Similarly defined for thermal diffusion is a thermal disturbance number $\lambda_T = 2^{1/2}R/\delta_\kappa = R(\rho_0\omega c_p/\kappa)^{1/2} = \lambda N_{\mathrm{Pr}}^{1/2}$. For $\lambda \ll 1$, the magnitude of particle velocity in a pore is much less than that predicted by (inviscid) ideal acoustics and has nearly a quadratic dependence on the transverse coordinates as does dc flow through a capillary tube (Poiseuille flow). For $\lambda \gg 1$, the magnitude of particle velocity closely matches that predicted by ideal acoustics except in a thin boundary layer of thickness δ_η in which particle velocity changes rapidly to zero at the pore wall. For $\lambda_T \ll 1$ the gas temperature is the same as the wall temperature and density changes in the gas occur isothermally rather than adiabatically. For $\lambda_T \gg 1$ density changes are adiabatic except in the thin boundary layer δ_κ surrounding the pore wall over which density changes go from adiabatic to isothermal. A good measure of the characteristic transverse pore dimension is R = twice the transverse pore area/pore perimeter. For example, the characteristic dimension is $R = a$ for circular pores of radius a and for square pores of semiwidth a. This definition of R is twice the hydraulic radius.

Figure 1(a) and (b) represent the model for porous wall porous media. Darkened regions in these figures are the gas-filled portions of the media and the surrounding matrix is taken to be rigid. Plane waves are taken to be propagating in the z direction. Two types of pores are to be distinguished. The main pores are shown to be square in cross section, though this is not necessary for the theory developed below. The walls of the main pores have pores or holes of much smaller radii in them, and the wall pores are of average length d_w, as shown in Fig. 1(a). Main pores are not connected by wall pores, as indicated in Fig. 1(b). Transverse dimensions in the main pore are given by coordinates (x,y), as indicated in Fig. 1(a).

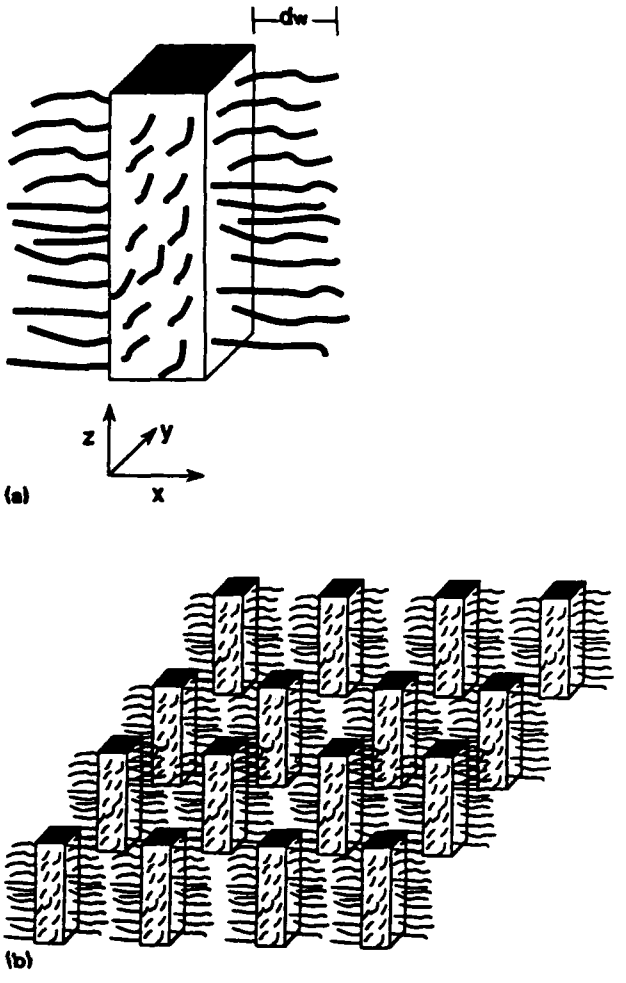

FIG. 1. (a) Single main pore with wall pores of length d_w. (b) Arrangement of main pores in the porous sample model. Wall pores are not taken to connect adjacent main pores. Air filled regions in (a) and (b) are dark.

The central assumptions are now given concerning oscillatory motion and condensation of gas in the wall pores. At the frequencies considered, particle velocity in the wall pores is much less than it would be for ideal acoustics as a result of gas viscosity and the small radii of wall pores. Condensation of gas in the wall pores is taken to occur isothermally at the same temperature as the solid matrix of the porous media. In terms of the dimensionless parameters, these assumptions are $\lambda_w < 1$ and $\lambda_{Tw} < 1$, where subscript w refers to wall pores.

The central assumption concerning pressure in the main pore is that it is only a function of the longitudinal coordinate z, not the transverse coordinates.[8] One justification of this assumption is that frequencies considered are much less than the cutoff frequency for radial modes in the main pore. This is the standard assumption for the pressure in nonporous wall porous media theory.[9] A second argument for this assumption is that the wall impedance is much greater than the characteristic impedance in the main pore and the pore diameter is much less than the acoustic wavelength.

The useful range of the porous-wall theory can be stated most generally in terms of the dimensionless numbers relating pore radius and the frequency-dependent viscous penetration depth. This model should be useful for porous media with main pores such that $\lambda > 1$ and wall pores such that $\lambda_w < 1$. These criteria were not derived from more general theory but appear to be consistent with the assumptions made above. In the experiments discussed below $4 < \lambda < 18$ and λ_w was estimated to be in the range $0 < \lambda_w < 1.2$. The frequencies considered were in the range 75–1300 Hz. Wall pore diameters ranged up to $\approx 100\ \mu$m, and the main pore width was 1.54 mm. Further discussion is given in Sec. III.

B. Analysis for porous wall porous media

Consequences of the assumptions given above on the linear acoustic equations in porous wall porous media are now developed. An $\exp(-i\omega t)$ sign convention will be used for constant frequency oscillations. In the frequency domain, linear acoustic quantities in a single main pore are transverse and longitudinal components of particle velocity, $\mathbf{v}(x,y,z) = \mathbf{v}_\tau(x,y,z) + v_z(x,y,z)\hat{z}$, pressure, $p(z)$, density, $\rho(x,y,z)$, and temperature, $T(x,y,z)$. Ambient quantities are density, ρ_0, temperature, T_0, and pressure, p_0. The transverse velocity has been computed for circular pores and nonporous walls by Tijdeman.[10]

A general result is established first. In the geometry of a single main pore in Fig. 1(a), the continuity equation is

$$-i\omega\rho(x,y,z) + \rho_0 \frac{\partial v_z(x,y,z)}{\partial z} + \rho_0 \nabla_\tau \cdot \mathbf{v}_\tau(x,y,z) = 0, \tag{1}$$

where $\nabla_\tau = \partial/\partial x\hat{x} + \partial/\partial y\hat{y}$ is the transverse gradient operator. Averaging Eq. (1) over the cross section of an arbitrarily shaped main pore, as shown in Fig. 2,

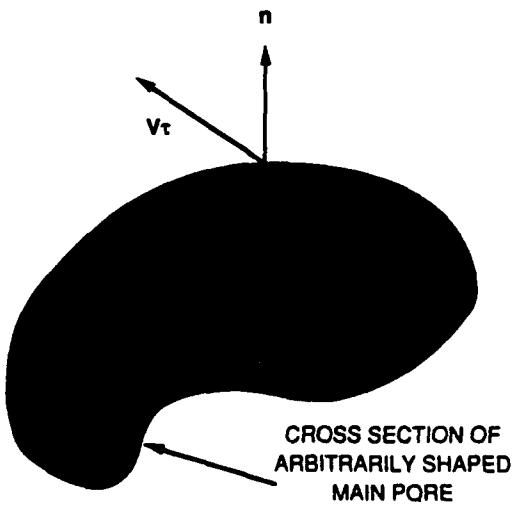

FIG. 2. Arbitrarily shaped cross section of a general main pore having perimeter S and area A. The outward normal is $\mathbf{n}(x,y,z)$ and $\mathbf{v}_\tau(x,y,z)$ is the tangential component of particle velocity. For main pores having square cross sections, as in Fig. 1(a), the cross section would be a square. Wall pores (not shown) are assumed to skirt the main pore.

$$-i\omega\rho(z) + \rho_0 \frac{dv_z(z)}{dz} + \frac{\rho_0}{A}\int_A \nabla_\tau \cdot \mathbf{v}_\tau(x,y,z)\,dx\,dy = 0, \tag{2}$$

where $\rho(z) = A^{-1}\int\rho(x,y,z)dx\,dy$ and $v_z(z) = A^{-1}\int v_z(x,y,z)dx\,dy$ are the cross-sectionally averaged acoustic density and z component of particle velocity for a main pore of cross-sectional area A, e.g., the square area in Fig. 1(a). Application to Eq. (2) of the divergence theorem in the (x,y) plane gives

$$-i\omega\rho(z) + \rho_0 \frac{dv_z(z)}{dz} + \frac{\rho_0}{A}\int_S \mathbf{n}(x,y)\cdot\mathbf{v}_\tau(x,y,z)\,dS = 0, \tag{3}$$

with S being the perimeter of a main pore having outward unit normal $\mathbf{n}$ and dS an element of perimeter. In the standard approach to capillary-tube-based porous models, the main pore wall is both rigid and nonporous and the boundary condition $\mathbf{v}_\tau = 0$ at the pore wall significantly simplifies the pore-averaged continuity equation to $-i\omega\rho(z) + \rho_0\, dv_z(z)/dz = 0$.

According to Eq. (3) average gas density in the main pore changes in time due to compression of the gas and as a result of mass flux $\rho_0\mathbf{n}(x,y)\cdot\mathbf{v}_\tau(x,y,z)$ into the pore wall. A reasonable assumption is that the porous wall radius of curvature in a transverse plane is much greater than typical wall pore diameters. Under this assumption the porous wall can be taken locally to be a flat surface having a specific acoustic impedance Z_w. In this averaged sense continuity of the normal component of $\mathbf{v}_\tau$ (Fig. 2 shows the normal) at the main-pore porous-wall boundary is taken to be

$$\mathbf{n}(x,y)\cdot\mathbf{v}_\tau(x,y,z) = p(z)/Z_w. \tag{4}$$

Here $p(z)/Z_w$ is the *longitudinal particle velocity* in the *wall pores* evaluated at the interface of the main pore and entrance to the wall pores. As discussed above, $p(z)$ is taken to be constant in a given cross section of a main pore. Use of the boundary condition, Eq. (4), in the continuity equation, Eq. (3), gives

$$-i\omega\rho(z) + \rho_0 \frac{dv_z(z)}{dz} + \frac{\rho_0 p(z)}{Z_w}\frac{S}{A} = 0, \tag{5}$$

where S is the perimeter of the arbitrarily shaped main pore, e.g., the square in Fig. 1(a).

Other relations among the acoustic quantities are provided by momentum, state, and heat flow equations. The z component of the momentum equation in a single main pore is[1]

$$-i\omega\rho_0 v_z(x,y,z) = -\frac{dp(z)}{dz} + \eta\nabla_\tau^2 v_z(x,y,z). \tag{6}$$

The boundary condition for Eq. (6) is $v_z(x,y,z) = 0$ for x and y on the nominal location of the main pore boundary. This boundary condition assumes that the *transverse particle velocity* in the *wall pores* is zero since wall pore diameters are much less than the viscous penetration depth. The solution of Eq. (6), when averaged over the cross section of the main pore, as was done above for the continuity equation, is written symbolically as[1]

$$i\omega\rho_0 v_z(z) = F(\lambda)\frac{dp(z)}{dz}, \tag{7}$$

where $F(\lambda)$ is a complex pore-geometry-dependent function that defines a complex density $\rho_0/F(\lambda)$ for gas in the main pore. Recall that $\lambda = R(\rho_0\omega/\eta)^{1/2}$, where $R = 2A/S$. For main pores having rectangular cross sections of semiwidths a and b, $R = 2ab/(a+b)$,

$$Y_{mn}(\lambda) = 1 + (i\pi^2/\lambda^2)[(b^2m^2 + a^2n^2)/(a+b)^2], \tag{8}$$

and the function $F(\lambda)$ is[1,2]

$$F(\lambda) = \frac{64}{\pi^4}\sum_{m,n\ \text{odd}}\frac{1}{m^2n^2Y_{mn}(\lambda)}. \tag{9}$$

The odd integers m and n in Eq. (9) range from 1 to ∞. Note that λ and hence $F(\lambda)$ is a function of a/b for rectangular pores.

Density changes in the wall pores are taken to occur isothermally, as discussed above. Excess temperature goes to zero at the nominal location of the main pore boundary, which is the usual boundary condition. The heat equation and equation of state can be combined to obtain an expression for the excess density in the main pore.[1] Averaging the excess density over the pore cross section gives[1]

$$\rho(z) = \{[\gamma - (\gamma-1)F(\lambda_T)]/c^2\}p(z), \tag{10}$$

where c is the adiabatic sound speed, γ is the ratio of specific heats, and $F(\lambda_T)$ is given by Eq. (9) for rectangular pores and argument $\lambda_T = N_{Pr}^{1/2}\lambda$. For wide main pores such that $\lambda_T \to \infty$, $F(\lambda_T)\to 1$ so that compressions are adiabatic and $\rho(z) = p(z)/c^2$. For narrow main pores such that $\lambda_T \to 0$, $F(\lambda_T)\to 0$ so that compressions are isothermal and $\rho(z) = p(z)/(c^2/\gamma)$. Use of Eq. (10) in the averaged continuity equation, Eq. (5), gives

$$-i\omega\left(\frac{\gamma-(\gamma-1)F(\lambda_T)}{c^2} + \frac{2i\rho_0}{R\omega Z_w}\right)p(z) + \rho_0\frac{dv_z(z)}{dz} = 0, \tag{11}$$

where $R = 2A/S$ was used.

The model is shown in Fig. 1(b) for a bulk porous media consisting of N main pores per unit area, each having cross-sectional area A. *The area A and porosity $\Omega = NA$ are to be measured, assuming that no wall pores are present.* For completeness, allow each main pore to also have a tortuosity q. In the present context, q allows for the possibility of a gentle longitudinal curvature of each main pore, or a tilt angle θ of the main pore axis for which $q = 1/\cos\theta$. Bulk acoustical equations for porous media are obtained by using $V_{zb}(z) = \Omega v_z(z)/q$ and by replacing dz with $q\,dz$.[1] Here $V_{zb}(z)$ is a bulk particle velocity averaged over unit cross section of porous sample. Resulting bulk equations are from Eq. (7),

$$i\omega\rho_0\frac{q}{\Omega}V_{zb}(z) = F(\lambda)\frac{dp(z)}{q\,dz}, \tag{12}$$

and from Eq. (11),

$$-i\omega\left(\frac{\gamma-(\gamma-1)F(\lambda_T)}{c^2} + \frac{2i\rho_0}{R\omega Z_w}\right)p(z) + \rho_0\frac{q}{\Omega}\frac{dV_{zb}(z)}{q\,dz} = 0. \tag{13}$$

Multiplying Eq. (13) by $(i\omega)$, taking d/qdz of Eq. (12), and eliminating $V_{zb}(z)$ from the resulting equations gives an equation for pressure waves of constant frequency,

$$\frac{d^2p(z)}{dz^2} + \frac{\omega^2}{(c/q)^2}\frac{\gamma-(\gamma-1)F(\lambda_T)}{F(\lambda)} \times\left(1 + \frac{c}{\gamma-(\gamma-1)F(\lambda_T)}\frac{2i}{\omega R\zeta_w}\right)p(z) = 0, \tag{14}$$

where $\zeta_w = Z_w/\rho_0 c$ is the normalized wall specific acoustic impedance.

The complex wave number and characteristic impedance of porous wall porous media are obtained from Eq. (14) and Eq. (12). Assuming $p \propto \exp(ikz)$, Eq. (14) yields a dispersion relation for the complex wave number k,

$$k = \pm k_{np}\xi, \tag{15}$$

where

$$k_{np} = [\omega/(c/q)]\sqrt{[\gamma-(\gamma-1)F(\lambda_T)]/F(\lambda)}, \tag{16}$$

is the propagation constant for *nonporous* main-pore walls and

$$\xi \approx 1 + c/[\gamma-(\gamma-1)F(\lambda_T)](i/\omega R\zeta_w), \tag{17}$$

where a binomial expansion for the square root was applied because $\zeta_w \gg 1$. From Eq. (12) the normalized characteristic impedance $\zeta = Z/\rho_0 c$ of the material is

$$\zeta = \zeta_{np}\xi^{-1}, \tag{18}$$

where

$$\zeta_{np} = \frac{1}{F(\lambda)^{1/2}}\frac{q}{\Omega}\frac{1}{\sqrt{\gamma-(\gamma-1)F(\lambda_T)}}, \tag{19}$$

is the impedance for *nonporous* main-pore walls[1] and

$$\xi^{-1} \approx 1 - c/[\gamma-(\gamma-1)F(\lambda_T)](i/\omega R\zeta_w). \tag{20}$$

Recall that ζ_w is the normalized wall specific acoustic impedance.

The model illustrated in Fig. 1(a) and (b) assumes wall pores are of length d_w and terminate in the pore wall. A reasonable model for wall impedance is a rigid-backed layer model with $\zeta_w = i\zeta_{cw}\cot(k_w d_w) \approx i\zeta_{cw}/(k_w d_w)$, where the cotangent approximation applies when $k_w d_w \ll 1$, k_w is the propagation constant for the wall pores, and ζ_{cw} is the normalized characteristic impedance of the wall. An impedance model for sufficiently low frequency and wall pores with geometries such that $\lambda_w < 1$ has $k_w = q_w\omega(8i\gamma)^{1/2}/(c\lambda_w)$ and $\zeta_{cw} = q_w(8i/\gamma)^{1/2}/(\Omega_w\lambda_w)$, where q_w and Ω_w are the tortuosity of wall pores and the porosity of the wall.[11] Wall porosity Ω_w is defined as the open volume in the walls divided by the total volume of the walls. Combining these expressions gives a wall-pore normalized specific acoustic impedance that is independent of λ_w,

$$\zeta_w \approx ic/\omega\gamma\Omega_w d_w. \tag{21}$$

Use of Eq. (21) in Eq. (17) gives

$$\xi \approx 1 + \frac{\gamma}{\gamma - (\gamma - 1)F(\lambda_T)} \frac{\Omega_w d_w}{R}$$

$$= 1 + \frac{\gamma}{\gamma - (\gamma - 1)F(\lambda_T)} \frac{\Omega_T - \Omega}{2\Omega}, \quad (22)$$

where in the second form, the total porosity Ω_T is the total open volume (wall-pore volume plus main pore volume) divided the total sample volume. Equation (22) was obtained using the relation

$$\Omega_T = \Omega(1 + 2\Omega_w d_w/R). \quad (23)$$

The total porosity Ω_T can be obtained from Eq. (23) by measuring Ω and R, and by optimizing agreement between theory and experiment to obtain Ω_w and d_w. This is discussed further in Sec. III.

For main pores large enough that $\lambda_T \gg 1$ so that $F(\lambda_T) = 1$, $\xi > 1$ is a real quantity. Consequences of $\xi > 1$ are seen in Eq. (15) and the definition $k = \omega/c_{ph} + i\alpha$, where c_{ph} is the phase velocity and α is the attenuation constant. Attenuation is increased by $\xi > 1$ and phase velocity decreased, and by Eq. (18) the characteristic impedance is decreased. The factor $\gamma/[\gamma - (\gamma - 1)F(\lambda_T)]$ may be attributed to the difference in compressibility of gas in the main pore and much smaller wall pores. Acoustical methods for determining the ratio $(\Omega_T - \Omega)/\Omega$ occurring in Eq. (22) may be of interest in nondestructive evaluation of materials.

The normalized specific acoustic impedance ζ_{rb} of a rigid-backed square pore sample is

$$\zeta_{rb} = i\zeta \cot(kL), \quad (24)$$

where L is its length. Calculations of ζ_{rb} will be compared with measurements in Sec. III. It is noteworthy that this measurement is sensitive to both the characteristic impedance ζ and the complex wave number k of the material when absorption over length $2L$ is not severe.

II. SPECIFIC ACOUSTIC IMPEDANCE MEASUREMENTS

The ceramic porous material has straight tubes with square cross sections, as shown schematically in Fig. 3. The side of the ceramic facing the impedance tube was flush mounted into an aluminum disk of thickness 1.27 cm. Another solid aluminum disk of the same thickness had a hole of depth 0.32 cm and diameter of 14.6 cm machined into it so that the ceramic could be attached. The ceramic and aluminum pieces were attached using epoxy. The solid aluminum disk acts as a rigid termination for the sample. An O ring was machined into the open disk to form a seal with the impedance tube. Threaded rod not shown in Fig. 3 was bolted between the aluminum pieces to add structural support. The outer ceramic surface was sealed against leaks by covering it with polyurethane.

Specific acoustic impedance (SAI) measurements were made on a square pore ceramic sample having a nominal cell density of $C = 200$ pores/in.^{2}, average square pore semiwidth a of 0.768 mm $\pm$ 0.01 mm, and length L of 49.5 cm. Porosity associated with main pores using $\Omega = C(2a)^2 = 73\%$. This value of porosity was computed assuming nonporous walls, as dictated by the theory in Sec. I. Wall thickness was $\approx$0.27 mm. The value $a = 0.77$ mm was used in the calculations. The uncertainty in a was computed from the standard error of 25 measurements.

After SAI measurements were made on the dry, porous wall sample, the ceramic was flooded with water. Strong molecular attraction between water molecules and the ceramic held water in the small volumes of the wall pores. However, water in the main pores was easily removed by shaking the sample. Thus a three phase (water, ceramic, and air) sample was produced. Because of the huge impedance mismatch though, the combination of wall-pore water and ceramic sample wall are considered a rigid matrix. This combination gave us an ideal porous sample consisting of straight, square-pore capillaries *with nonporous walls*. SAI measurements were also made on this three-phase sample.

Figure 4 shows a representative optical microscope photograph from several that were taken of the pore walls.

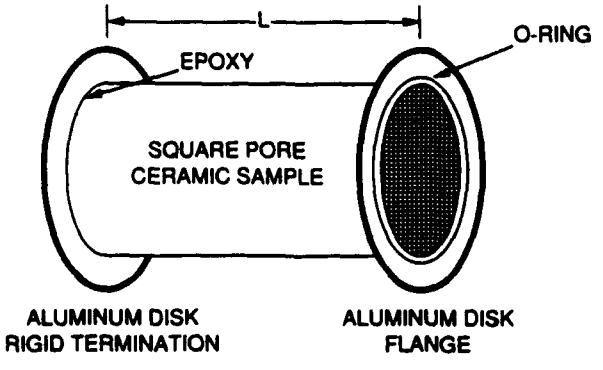

FIG. 3. Arrangement of ceramic sample and aluminum support disks. Threaded rod standoffs were used between the aluminum disks to add structural support. Impedance measurements were made with the ceramic sample attached to the impedance tube in Fig. 5.

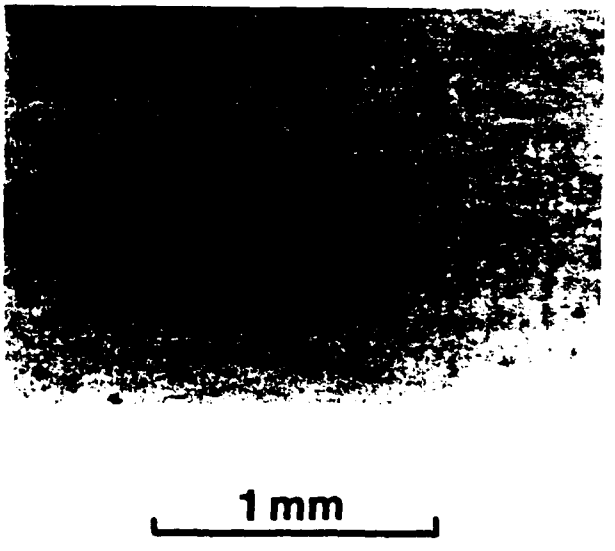

FIG. 4. Representative optical microscope photograph of the porous ceramic wall.

Clearly the ceramic sample has finite wall porosity. The larger pore diameters were estimated to be 100 μm. The interior wall pore volume is roughly spherically shaped, though the walls are not smooth. Wall pores with small diameters in Fig. 4 often open to larger diameter cavities in the ceramic walls. Wall porosity was estimated to be $\Omega_w = 49\%$ by maximizing agreement between the experimental impedance measurement and the theoretical expression, which is a function of Ω_w. An estimate of $d_w = 100\,\mu$m, the depth of wall pores, as shown schematically in Fig. 1(a), was made using a profileometer. The estimated values of Ω_w and d_w will be used in Sec. III to compute the total sample porosity from use of Eq. (23). It appeared that wall pores do not connect by air adjacent main pores.

An impedance tube shown schematically in Fig. 5 was used to measure the specific acoustic impedance of a rigid-backed ceramic sample shown schematically in Fig. 3. Impedance tube design criteria and theory of operation are described elsewhere.[12,13] A dynamic signal analyzer was used in a swept sine mode to drive a power amplifier that was connected to the Altec driver. Denote by H_{1i} the transfer function between microphones M1 and M2 in Fig. 5. The analyzer was also used to measure H_{1i}. The frequency range of interest was 75–1300 Hz, and the cutoff frequency for radial modes in the tube was approximately 1375 Hz. The analyzer was interfaced with a minicomputer to download H_{1i} for the impedance calculation. A transfer function H'_{1i} is measured and the measurement is repeated with the microphones reversed, obtaining H''_{1i}. Since the transfer function used in the calculation is $H_{1i} = (H'_{1i}/H''_{1i})^{1/2}$ the frequency response of each microphone cancels so that one need not be overly concerned with the microphone frequency response or calibration.

III. DISCUSSION OF EXPERIMENTAL AND CALCULATED COMPLEX WAVE NUMBER AND SPECIFIC ACOUSTIC IMPEDANCE

The complex wave number for $C = 200$ pores/in.^{2} ceramic samples was previously measured using a time domain technique. Experimental results are shown in Fig. 6(a) and (b) for phase velocity and attenuation constant. Also shown are theoretical results for porous-wall porous media theory [Eqs. (15) and (22)] and nonporous-wall theory [Eq. (16)]. Porous-wall theory results agree much more favorably with experimental points than the nonporous-wall theory. Porous-wall theory underestimates the attenuation constant though, particularly at higher frequencies. In previous work it was noted that use of an anomalous tortuosity $q = 1.1$ [in the nonporous-wall theory Eq. (16)] was necessary to obtain satisfactory agreement among theoretical and measured values of the complex wave number. This value of tortuosity is anomalous since porous media consisting of straight, rigid, nonporous capillary tubes, which was the model being used, has $q = 1$. The slightly frequency-dependent complex factor computed from Eq. (22) is $\xi \simeq 1.1$. This theoretical justification for multiplying the complex wave number by a nonunity factor ξ, even though the capillary tubes are straight, is a main result of this paper.

Measured and calculated specific acoustic impedance are shown in Fig. 7, with the real part in Fig. 7(a) and the imaginary part in Fig. 7(b). The theoretical expression for a

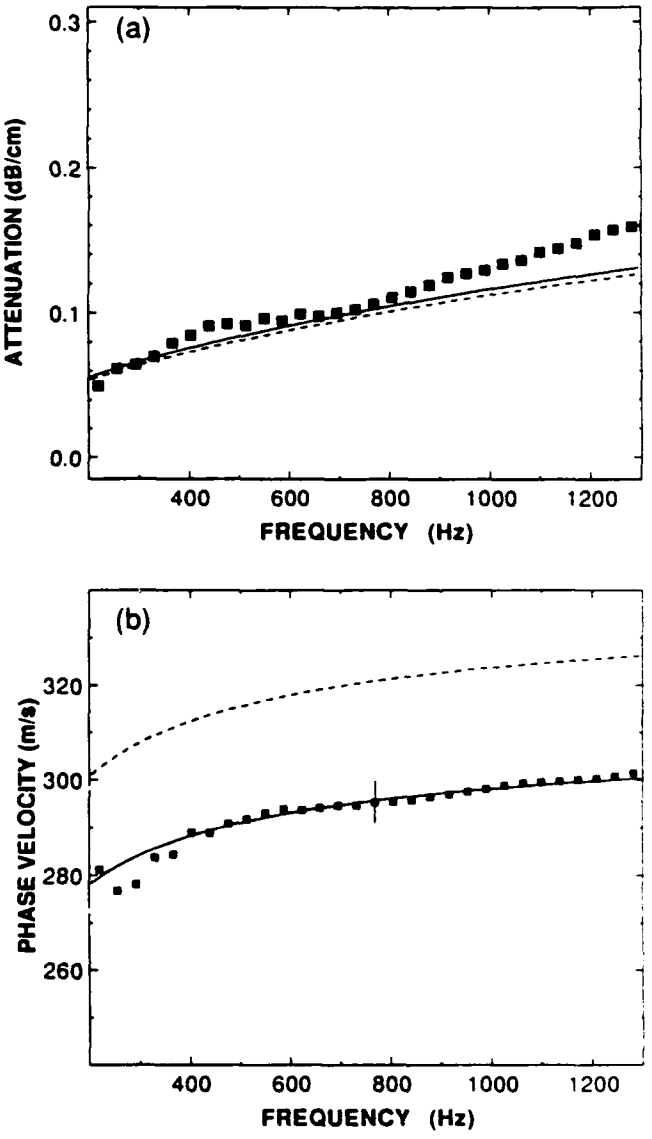

FIG. 6. (a) Attenuation constant and (b) phase velocity measurements and theory. The solid symbols are experimental results for ceramic square pore samples. Error bars were estimated to be twice the symbol size in (a) and a representative error bar is shown in (b). Solid lines and broken lines are porous-wall and nonporous-wall porous-media theory.

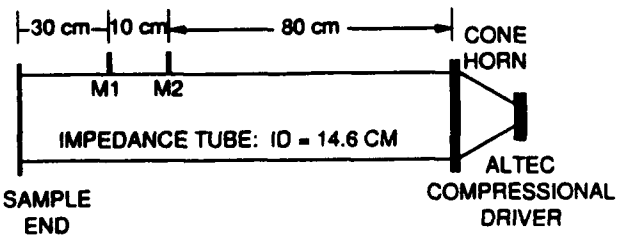

FIG. 5. Impedance tube geometry.

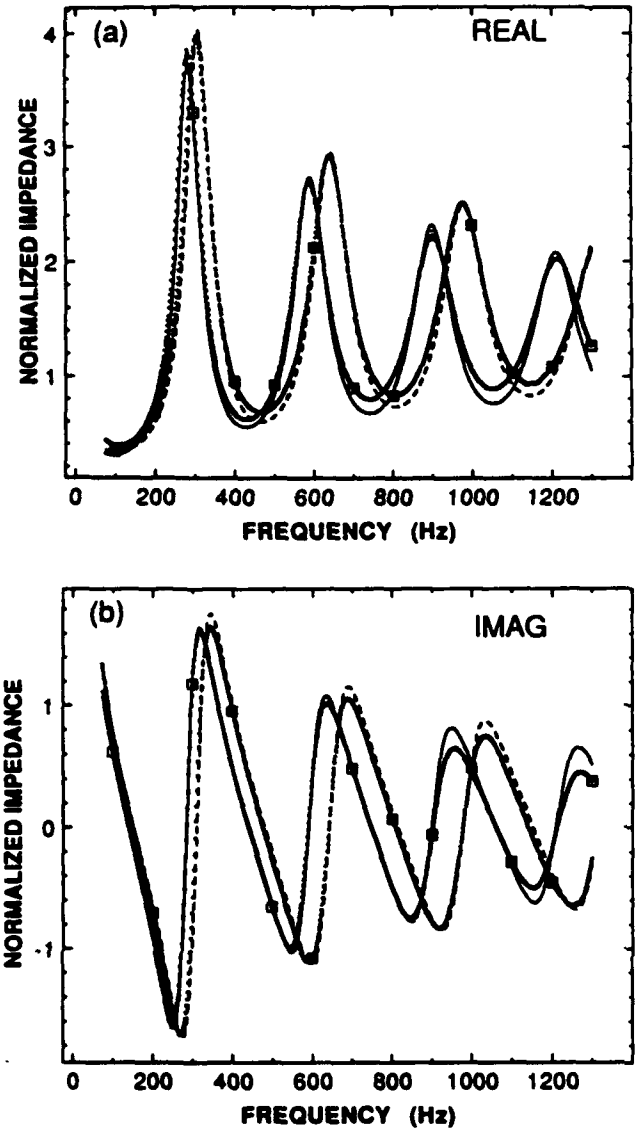

FIG. 7. (a) Real and (b) imaginary specific acoustic impedance measurements and theory. Experimental measurements are given by small squares, which nearly form a continuous curve. Measurements with the wall pores filled with water are marked with large, solid squares. These measurements agree favorably with the nonporous-wall theory given by the dashed lines. Measurements and theory for porous walls are marked with open squares and solid lines, respectively.

rigid-backed sample is given by Eq. (24). Impedance was normalized by the characteristic impedance of air. Constructive and destructive interference of downgoing and upgoing waves in the ceramic sample results in the obvious structure on the impedance curves. Nonporous-wall theory was computed from the use of Eq. (19), and porous-wall theory from Eq. (18) and Eq. (22). With the wall pores filled with water, SAI measurements agree favorably with nonporous-wall theory. When the wall pores are open SAI measurements agree favorably with porous wall theory. The location of peaks and minima agree favorably; however, the computed impedance is less than the measured impedance near minima of the real part. Part of this discrepancy may be attributed to boundary layer absorption on the rigid termination of the ceramic sample: This is not accounted for in Eq. (24). Porous-wall theory gives an impedance greater than the measured impedance for higher frequencies. This is consistent with phase velocity and attenuation measurements shown in Fig. 6, since the frequency of impedance maxima and minima is governed primarily by the phase velocity and the impedance magnitude is governed by the attenuation constant. The assumptions made in Sec. I A for developing the porous-wall porous-media theory are less valid for higher frequencies, since $\lambda_w \approx 1.2$.

Wall porosity Ω_w was used as an adjustable parameter in Eq. (22) to obtain the theoretical wall porosity SAI curves in Fig. 7(a) and (b). Champoux and Stinson measured,[14] using an air-based system,[15] the total porosity Ω_T of a ceramic sample of the same type used in our measurements. Use of Eq. (23) gives $\Omega_T = 0.82$, which is in acceptable agreement with the value $\Omega_T = 0.87 \pm 0.05$ determined by Champoux and Stinson.

In previous work, we referred to the effects of finite wall porosity as an "anomalous tortuosity factor." This notion is incorrect, for by Eq. (19), the characteristic impedance is proportional to tortuosity q. Thus characteristic impedance should increase if finite wall porosity simply caused the tortuosity to increase. Finite wall porosity increases the bulk compressibility of gas in the pores. Since the complex wave number (characteristic impedance) are proportional (inversely proportional) to the square root of compressibility, they increase (decrease) on account of finite wall porosity, as shown quantitatively in Eq. (15) [Eq. (18)].

IV. CONCLUSION

A theory has been developed for propagation in capillary-tube-type porous media in which the capillary tubes have small pores in the walls. The wall pores were modeled as a thin-layered impedance at the main pore wall. The wall impedance was taken to be reactive with the reactance due to small wall pores. Phase velocity is decreased, attenuation is increased, and characteristic impedance is decreased on account of finite wall porosity. Specific acoustic impedance measurements on a ceramic sample having both porous and nonporous walls agree favorably with the calculated values for these two cases. This model may be useful for sound propagation in soils having large cracks and for evaluating the walls of tubes that are susceptible to damage by pitting. This work offers an explanation for the anomalous tortuosity factor, which was used previously[1] for the square pore ceramic samples.

ACKNOWLEDGMENTS

We are grateful to Heui-Seol Roh and Henry E. Bass for their comments and suggestions, to Yvan Champoux and Michael R. Stinson for porosity measurements of our ceramic samples and to Brett Bolen for assistance with impedance tube measurements. Portions of this work were funded by the United States Department of Agriculture, the Office of Naval Research, and the U.S. Army Construction Engineering Research Laboratory.

[1] H. S. Roh, W. P. Arnott, J. M. Sabatier, and R. Raspet, "Measurement and calculation of acoustic propagation constants in arrays of small air-filled rectangular tubes," J. Acoust. Soc. Am. **89**, 2617–2624 (1991).
[2] M. Stinson, "The propagation of plane sound waves in narrow and wide circular tubes, and generalization to uniform tubes of arbitrary cross-sectional shape," J. Acoust. Soc. Am. **89**, 550–558 (1991).
[3] C. Zwikker and C. W. Kosten, *Sound Absorbing Materials* (Elsevier, Amsterdam, 1949), pp. 21 and 125.
[4] A. D. Pierce, Acoustics: *An Introduction to Its Physical Principles and Applications* (Acoustical Society of America, New York, 1989), pp. 532–534.
[5] P. M. Morse, *Vibration and Sound* (American Institute of Physics, New York, 1976), p. 371.
[6] J. E. White, *Underground Sound: Application of Seismic Waves* (Elsevier, New York, 1983), pp. 151–154.
[7] J. J. Burton and R. L. Garten, *Advanced Materials in Catalysis* (Academic Press, New York, 1977), Chap. 10.
[8] Equation (31.4), p. 371 of Ref. 5 shows that the principal mode in ducts with absorbing liners is not a perfect plane wave because the pressure amplitude depends on the transverse coordinates [x,y coordinates in Fig. 1(a)]. The transverse variation can be shown to be negligible in the limit of large wall impedance and small ratio of pore diameter to acoustic wavelength.
[9] See Figs. 2 and 3 in Ref. 2.
[10] H. Tijdeman, "On the propagation of sound waves in cylindrical tubes," J. Sound Vib. **39**, 1–33 (1975).
[11] This model is discussed in Ref. 4, p. 537. Use has been made of the definition of $\lambda_w = (\rho_0\omega/\eta)^{1/2}a_w$, where a_w is the wall pore radius assumed to be circular here. The normalized specific acoustic impedance ζ_w is that of a narrow short tube of length d_w for isothermal sound speed $c/\gamma^{1/2}$. Also see L. L. Beranek, *Acoustics* (American Instutute of Physics, New York, 1986), pp. 34–35.
[12] A. F. Seybert and D. F. Ross, "Experimental determination of acoustic properties using a two-microphone random-excitation technique," J. Acoust. Soc. Am. **61**, 1362–1370 (1977).
[13] J. Y. Chung and D. A. Blaser, "Transfer function method of measuring in-duct acoustic properties. I. Theory," J. Acoust. Soc. Am. **68**, 907–913 (1980).
[14] Y. Champoux (private communication, 1991).
[15] Y. Champoux, M. R. Stinson, and G. A. Daigle, "Air-based system for the measurement of porosity," J. Acoust. Soc. Am. **89**, 910–916 (1991).

Study of a thermoacoustic prime mover below onset of self-oscillation

Anthony A. Atchley, Henry E. Bass,[a] Thomas J. Hofler, and Hsiao-Tseng Lin[b]
Physics Department, Naval Postgraduate School, Monterey, California 93943

(Received 19 April 1991; accepted for publication 26 September 1991)

The frequency response of a thermoacoustic prime mover has been measured as a function of the mean gas pressure and temperature gradient across the prime mover stack. The quality factor Q and resonance frequency can be determined from the response. As the temperature gradient is increased, the Q increases, indicating a decrease in attenuation across the stack. At sufficiently large temperature differences (~ 300 K), the resonator goes into self-oscillation, indicating negative attenuation. Measurements are reported for helium and argon at pressures ranging from 170–500 kPa and temperature gradients ranging from zero to that required for onset of self-oscillation. The results are explained in terms of a counterpropagating, plane-wave analysis, based on techniques commonly used in porous media investigations. In general, the predictions of the analysis are in good agreement with experiment. The predictions of Q and the change in resonance frequency with mean gas pressure are within approximately 5% and 0.4% of measured values for the no temperature gradient cases. In the cases where temperature gradients are present, the agreement is quite good for the two highest mean pressures reported (370 and 500 kPa). There are some noticeable discrepancies at the lowest pressure (170 kPa). The reasons for these discrepancies are unknown.

PACS numbers: 43.25.Vt, 43.35.Ud

INTRODUCTION

Swift[1] and others[2,3] have developed theories that can be used to predict the onset of self-oscillation and the quality factor Q of a thermoacoustic prime mover. Their models are based on a thermodynamic approach that considers energy transfer and dissipation on the exposed surfaces. This treatment agrees with experimental results and includes all the applicable physics. It does have one disadvantage. As formulated, it is not simple to transfer extensive research of the acoustic properties of porous materials to performance predictions of thermoacoustic devices. One goal of this article is to develop such a formalism, which will be especially attractive when considering the use of alternate geometries in the prime mover stack.

In the following, we apply the standard treatment of acoustic waves in porous media and propagation in a tube with multiple boundaries to predictions of prime mover performance. Except for one equation for heat flow in the presence of a temperature gradient, all equations and their description can be found in standard acoustics textbooks.[4] As one might expect, all the needed expressions without a temperature gradient can be found in the works of Lord Rayleigh.[5]

I. EXPERIMENTAL APPARATUS AND PROCEDURE

We measured the frequency response of a thermoacoustic prime mover as a function of the mean gas pressure and temperature gradient across the prime mover stack. The quality factor Q and resonance frequency can be determined from the response. The temperature gradients ranged from zero to that required for the onset of self-oscillation. To gain confidence in the measurement technique, we first measured the response of two simpler resonator configurations: an empty, rigidly terminated tube, and the empty tube plus the ambient heat exchanger. These configurations, and that of the prime mover, are discussed in Sec. I A. Temperature control and measurement are discussed in Sec. I B, followed by a discussion of the data acquisition procedure in Sec. I C.

A. Resonator configurations

The three different resonator configurations are the empty, rigidly terminated resonant tube; the empty tube plus the ambient heat exchanger; and the prime mover. The empty resonator is made from two 3.82-cm-i.d. (inner diameter) copper tubes, separated by a 2.18-cm-long brass section having a slightly larger inner diameter. This brass section is called the ambient heat exchanger container. The lengths of the two sections of copper tube are 11.43 and 87.95 cm. One end of each section is fitted with a flange that allows them to be soldered to the ambient heat exchanger container. A 0.64-cm-thick copper cap is fixed to the other end of each section, forming a closed, rigid termination. The cap on the longer section houses a 1.9-cm-diam electret driver and a 0.59-cm-diam electret microphone. The driver and microphone are flush mounted and sealed in the end cap with epoxy. Even with the driver and microphone mounted in the end cap, our measurements show that it still behaves as a rigid termi-

[a] Permanent address: Department of Physics, University of Mississippi, University, MS 38677.
[b] Permanent address: Chung-Cheng Inst. of Technology, Taoyuan 33509, Taiwan, R.O.C.

 0001-4966/92/020734-10$00.80

nation. The total length of the resonator, including the heat exchanger container, is 101.56 cm (internal dimensions). The resonator is connected to a gas handling system, through a fill tube in the ambient heat exchanger container. This connection allows for evacuation of the resonator before pressurization with gas (helium or argon) and a system vent. A dial pressure gauge and an Omega model PX304-150AV pressure transducer are connected to the fill line to sense the mean pressure inside the tube. The driver input signal is provided by an HP 3325A function generator and amplified by a Techron model 7520 power amplifier. The microphone output signal is amplified by a preamplifier with a gain of 100.

The second configuration differs from the first only in that the ambient heat exchanger is mounted in the ambient heat exchanger container. The ambient heat exchanger consists of two stacks of parallel plates. Each stack is composed of twenty five 0.045-cm-thick, 1.02-cm-long copper plates. The gap between each plate is 0.104 cm. The two stacks are mounted in a 3.82-cm-i.d. copper tube such that there is a 0.15-cm gap between them. (This double stack heat exchanger is not necessary for these measurements; a single stack would suffice. However, the double stack will be needed in a future phase of this research.)

The third configuration, the prime mover, differs from the second by replacing the shorter section of copper tube used in the first two configurations with a different section This section consists of a nickel heater section, a nickel hot heat exchanger, and a stainless steel prime mover stack. The heater section consists of a 5.08-cm-o.d., 3.82-cm-i.d., 5.50-cm-long nickel tube. The 0.63-cm wall thickness along with the use of nickel with its high thermal conductivity is intended to insure that the temperature along the heater section is uniform. One end of the tube is rigidly capped and drilled to accommodate a thermocouple probe, used to sense the hot heat exchanger temperature. The hot heat exchanger is mounted at the other end of the heater section. This heat exchanger consists of twenty-five 0.045-cm-thick, 0.762-cm-long nickel plates. The gap between each plate is 0.104 cm. The distance from the closed end of the heater section to the beginning of the hot heat exchanger is 5.50 cm. The prime mover stack consists of thirty-five 0.028-cm-thick 304 stainless steel plates, 3.50 cm long and spaced by 0.077 cm. This stack is housed within a thin walled (0.05 cm thick) stainless steel tube. One end of this stainless steel tube is welded to the nickel tube such that the hot heat exchanger and prime mover stack are in contact. The other end of the stainless steel tube is fitted with a flange so that the entire section can be soldered to the ambient heat exchanger container. Summarizing the prime mover configuration, it consists of a 5.50-cm-long nickel tube, a 0.762-cm-long hot heat exchanger, a 3.50-cm-long prime mover stack, a 2.18-cm-long double stack ambient heat exchanger, and an 87.95-cm-long copper tube. The total length of the prime mover is 99.9 cm. The configuration is shown in Fig. 1.

B. Temperature control and measurement

The nature of the experiment requires that a temperature difference be established across the prime mover stack

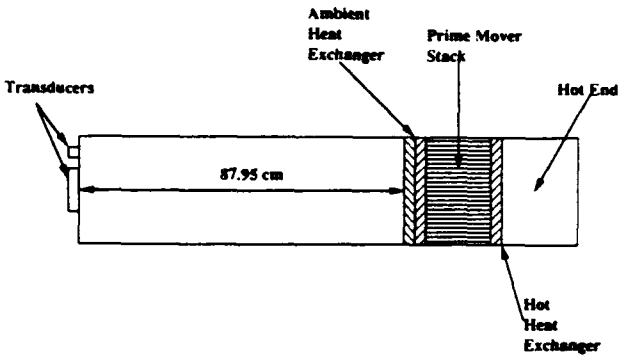

FIG. 1. Diagram of the prime mover configuration.

and maintained precisely (within 1 K). It is also necessary to eliminate temperature gradients elsewhere in the resonator. Temperature control of the prime mover is achieved as follows. An Omega Engineering model HBA 202040 nozzle heater is clamped to the nickel heater section. Electrical power is supplied to the heater through a variable ac transformer. The hot end is surrounded by insulation to reduce heat loss to the room and to help maintain a uniform temperature distribution along it. The ambient heat exchanger is maintained at near room temperature by circulating water through a jacket that surrounds it. The temperature of the water is maintained with a Neslab model RET-110 circulating temperature bath. After the water leaves the jacket it circulates through flexible plastic tubing that is wrapped around the majority of the length of the longer section of copper tube. This section of tube is also surrounded by styrofoam insulation to help maintain a uniform temperature distribution along its length.

The temperature of the prime mover is monitored by four thermocouples. A type K thermocouple is in contact with the center of the hot heat exchanger to sense the temperature of the hot end. Three type E thermocouples are glued to the top, middle, and bottom of the cold end to sense the temperature along that section. The reference temperature for the whole system is found by using a 4-wire resistance measurement of a thermistor mounted on an aluminum isothermal block. For the first two resonator configurations, the hot end is replaced by the shorter section of copper tube and the type K thermocouple is not used.

C. Data acquisition

The quality factor of the various resonator configurations is determined by measuring the steady-state frequency response. This measurement is accomplished by driving the resonator at frequencies near resonance and measuring the steady-state amplitude of the microphone output signal with a Stanford Research model SR-530 lock-in amplifier. The Q is determined by performing a least-squares fit of the data to the ideal response. Data acquisition is performed by a Standard 286 personal computer. Referring to Fig. 2, the computer communicates with the lock-in amplifier, the HP 3457A digital multimeter, and the HP 3325A function gen-

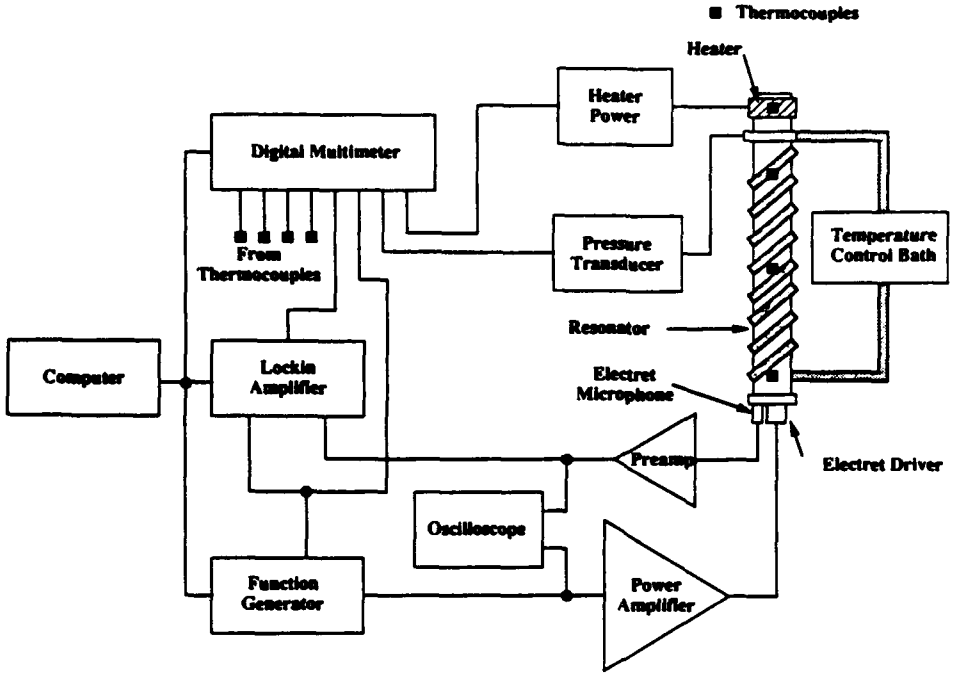

FIG. 2. Schematic diagram of the instrumentation used in the experiment.

erator through a GPIB interface. Through the execution of the controlling program, a source signal is supplied by the function generator to the electret driver. The output voltage from the microphone is amplified by a preamplifier and sent to the lock-in. The output of the lock-in, as well as all other data signals of interest, are fed to an HP 3457A multimeter. The output of the multimeter is recorded by the computer.

Before data acquisition is started, the resonator is evacuated and filled with helium or argon to the desired pressure. When data acquisition begins, the program records the mean gas pressure within the resonator. Next, the approximate resonance frequency and the half-power bandwidth are entered into the computer, which then determines the start and stop frequencies and the frequency increment. The program sets the driving frequency and measures temperatures, frequency, and the output of the lock-in. The program then increments the frequency and repeats the process. The time required to measure the frequency response is approximately 5 min.

The temperature along the entire length of the resonator is held uniform during the measurements on the first two configurations. For the prime mover configuration, the temperature of the hot end is set by adjusting the electrical power supplied to the heater. After the hot end has reached thermal equilibrium, data acquisition is initiated.

II. RESULTS AND ANALYSIS

The Q of the resonator was determined by fitting the steady-state frequency response to a standard resonance equation:

$$A(\omega) = A_{\max}/\left[1 + (\omega^2/\omega_0^2)Q^2(1 - \omega_0^2/\omega^2)^2\right]^{1/2}, \qquad (1)$$

where ω is the angular frequency of the drive and ω_0 is the resonance angular frequency.[6]

To model the experiment, a closed tube with counterpropagating plane waves is assumed as shown in Fig. 3. In each region, the acoustic pressure of the incident and reflected waves is expressed as $p_i^{(n)} = P_i^{(n)} e^{i(\omega t - kx)}$ and $p_r^{(n)} = P_r^{(n)} e^{i(\omega t + kx)}$, respectively. Continuity of pressure and volume velocity is assumed at each interface. Continuity of volume velocity is written in the form $(P_i^{(1)} - P_r^{(1)})/z_1 = (P_i^{(2)} - P_r^{(2)})/z_2$, where z is called the impedance of the region and defined in Appendix A. At the driving end ($x = 0$), $u(0,t) = i\omega l e^{i\omega t}$, where l is the effective driver displacement (assumed to be independent of load). The total complex acoustic pressure at the driving end P_{total} is $P_i^{(1)} + P_r^{(1)}$. The amplitude of the sound at the driving end, where the response is measured, is the absolute value of P_{total}. The expression for P_{total} is derived in Appendix A. As the frequency assumed for the calculation is incremented, P_{total} goes through a maximum, giving the resonance frequency f_0; f was changed in steps of 0.5 Hz. We computed values of A for frequencies spanning resonance and then performed a least-squares fit to Eq. (1) using Q as the adjustable parameter.

To calculate P_{total}, all that need be specified are the propagation constants in each region and the boundary conditions. The case of no temperature gradient is analyzed in

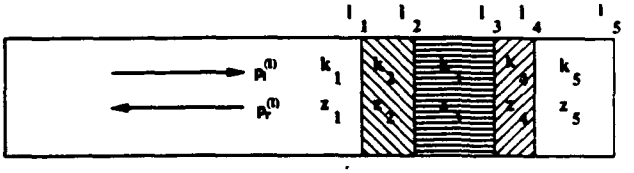

FIG. 3. Diagram showing the subdivision of the prime mover used for the counterpropagating plane-wave analysis. For analysis, the driver is assumed to be at the left.

TABLE I. Measured and predicted values of the resonance frequency and Q of the empty resonator for argon and helium gas at various pressures; Δf is the total change in resonance frequency with pressure.

Pressure (kPa)	f_0 (measured)	f_0 (predicted)	% error	Q (measured)	Q (predicted)	% error
			Argon			
170	155.6	156.0	+0.3	79	81	+2.5
238	155.8	156.5	+0.4	91	95	+4.4
307	156.0	156.5	+0.3	102	110	+7.8
376	156.1	156.5	+0.3	116	123	+6.0
	$\Delta f = 0.5$	$\Delta f = 0.5$	av = +0.3			av = +5.1
			Helium			
170	489.0	487.5	+0.3	48	50	+4.2
238	490.2	488.0	+0.4	57	59	+3.5
307	490.6	488.5	+0.4	64	67	+4.7
376	490.5	489.0	+0.3	70	74	+5.7
	$\Delta f = 1.6$	$\Delta f = 1.5$	av = +0.35			av = +4.5

Sec. II A below. Except in regions where plates are present, the propagation constants are computed from Shield's work.[7] In the regions where plates are present, the propagation constants are computed from the theory of sound propagation through porous media.[8,9] Pertinent results from porous media theory are discussed in Appendix B. Those unfamiliar with this type of analysis are advised to read Appendix B before proceeding. The case where temperature gradients are present is analyzed in Sec. II B.

A. Analysis of data taken with no temperature gradient

In the empty resonator case, we set $k_2, z_2, k_3, z_3, k_4, z_4, k_5, z_5$ equal to k_1, z_1, where k_1 is computed from Shield's work[7] as $k_1 = \omega/c_1 - i\alpha_1$. The impedance z_1 is computed as $z_1 = \omega\rho_0/k_1$. The length of the empty resonator is 1.0156 m. The measured and predicted Q's and resonance frequencies are shown in Table I for the resonator filled with argon and helium at various pressures.

For the resonator plus the ambient heat exchanger, $l_1 = 87.95$ cm; $l_2 = 90.13$ cm. The heat exchanger consists of parallel plates with a gap of 1.04 mm. The measured porosity is 0.667. Attenborough's theory[8] is used to compute z_2 and k_2; k_3 and k_5 and z_3 and z_5 are set equal to k_1 and z_1, respectively. The total resonator length is 1.0156 m. Results are shown in Table II. Again, experimental and theoretical results are in close agreement. Note that the sign of the error in Q has changed for helium compared to that in Table I, suggesting that more attenuation is predicted than actually observed.

Finally, for the case of the prime mover with no temperature gradient, $l_3 = 93.635$ cm and $l_4 = 94.397$. The full resonator length is 99.9 cm. The stack consists of parallel plates with a gap of 0.77 mm. The measured porosity is 0.76. It is clear that as the wave propagates from pores of one geometry to pores of a different geometry, the flow velocity will be changed. As an extereme example, offset parallel slits could completely block the flow. It is not so clear how one should include this effect. As a first approximation we have chosen to introduce as the porosity at the heat exchanger/stack interface, the fraction of area not blocked by either set of plates (0.53). A more accurate representation might follow the approach in Ref. 10. In any case, using 0.53 instead of 0.76 makes a difference of at most 10% in computed Q. Using 0.53 as the porosity of the stack, Attenborough's theo-

TABLE II. Measured and predicted values of the resonance frequency and Q of the resonator with the ambient heat exchanger for argon and helium gas at various pressures; Δf is the total change in resonance frequency with pressure.

Pressure (kPa)	f_0 (measured)	f_0 (predicted)	% error	Q (measured)	Q (predicted)	% error
			Argon			
170	156.4	156.5	+0.1	60	59	−1.7
238	156.5	157.0	+0.3	72	71	−1.4
307	156.4	157.0	+0.4	81	82	+1.2
376	156.7	157.0	+0.2	89	91	+2.2
500	157.1	157.0	−0.1	102	103	+1.0
	$\Delta f = 0.7$	$\Delta f = 0.5$	av = +0.2			av = +0.3
			Helium			
170	490.3	488.5	−0.4	36	35	−2.8
238	491.4	489.5	−0.4	43	42	−2.3
307	492.0	490.0	−0.4	49	49	0
376	493.1	490.5	−0.5	55	54	−1.8
	$\Delta f = 2.8$	$\Delta f = 2.0$	av = −0.4			av = −1.7

TABLE III. Measured and predicted values of the resonance frequency and Q of the prime mover with no temperature gradient for argon and helium gas at various pressures; Δf is the total change in resonance frequency with pressure.

Pressure (kPa)	f_0 (measured)	f_0 (predicted)	% error	Q (measured)	Q (predicted)	% error
			Argon			
170	161.6	162.0	+0.2	40	38	−5
238	161.8	162.0	+0.1	47	47	0
307	162.1	162.0	+0.0	54	53	−2
376	162.1	162.5	+0.2	58	59	+2
500	162.3	162.5	+0.1	68	70	+3
	$\Delta f = 0.7$	$\Delta f = 0.5$	av = +0.15			av = +2
			Helium			
170	505.2	504.5	−0.1	23	20	−13
238	507.2	505.5	−0.3	28	26	−7
307	508.5	506.0	−0.5	32	30	−6
376	509.4	507.0	−0.5	36	34	−6
500	510.5	507.5	−0.6	42	40	−5
	$\Delta f = 5.3$	$\Delta f = 3.0$	av = −0.4			av = −7

ry is again used to compute k_3 and z_3. Results are shown in Table III.

B. Analysis of data for a prime mover below onset

The expressions for the propagation constant and impedance derived in Appendix B must be altered when temperature gradients are present. To find these new expressions, we take the same approach as in Appendix B. The only difference being that we use a theoretical approach presented by Rott[3] and Swift[1] to solve for the acoustic velocity and temperature distribution across a slit in the presence of a temperature gradient. Using these results, we find expressions for the complex density and complex compressibility and finally k and z. Once we have k and z, we can find P_{total}.

The complex density is the same as that derived for the no temperature gradient case and derived in Appendix B. The result is

$$\rho_c = \rho_f \left(1 - \frac{\tanh[(1+i)a/\delta_\nu]}{(1+i)a/\delta_\nu}\right)^{-1}. \tag{2}$$

Swift writes for the appropriate heat balance equation

$$\rho_f c_p \left(i\omega\theta + u_1 \frac{dT_m}{dx}\right) - i\omega T_m \beta p = \lambda_h \frac{\partial^2 \theta}{\partial y^2}, \tag{3}$$

where ρ_f is the density of the gas, c_p the isobaric specific heat capacity (per unit mass), θ the variation in temperature due to the acoustic wave, u_1 the acoustic velocity in the direction of propagation, dT_m/dx the temperature gradient across the stack, T_m the mean temperature, β the coefficient of volume expansion, p the acoustic pressure, and λ_h the coefficient of thermal conduction. Again from Swift,

$$u_1 = \frac{i}{\omega\rho_f}\frac{dp}{dx}\left(1 - \frac{\cosh[(1+i)y/\delta_\nu]}{\cosh[(1+i)a/\delta_\nu]}\right). \tag{4}$$

Substituting this expression for u_1 into Eq. (3) gives

$$\rho_f c_p \left[i\omega\theta + \frac{i}{\omega\rho_f}\frac{dp}{dx}\left(1 - \frac{\cosh[(1+i)y/\delta_\nu]}{\cosh[(1+i)a/\delta_\nu]}\right)\frac{dT_m}{dx}\right] - i\omega T_m \beta p = \lambda_h \frac{\partial^2\theta}{\partial y^2}, \tag{5}$$

where $\delta_\nu = (2\nu/\omega)^{1/2}$, ν is the kinematic viscosity, and a is the semiwidth of the slit. Swift identifies a solution

$$\theta = \frac{T_m\beta}{\rho_f c_p}p - \frac{1}{\rho_f\omega^2}\left(1 - \frac{\sigma\cosh[(1+i)y/\delta_\nu]}{(\sigma-1)\cosh[(1+i)a/\delta_\nu]}\right) \times \frac{dp}{dx}\frac{dT_m}{dx} - \left[\frac{T_m\beta}{\rho_f c_p}p + \frac{(dp/dx)(dT_m/dx)}{(\sigma-1)\rho_f\omega^2} \times\left(1 + \frac{\epsilon_s f_\nu}{f_k}\right)\right]\frac{\cosh[(1+i)y/\delta_k]}{(1+\epsilon_s)\cosh[(1+i)a/\delta_k]}, \tag{6}$$

where $\sigma = \nu/\kappa_f$ is the Prandtl number, and the other new terms are defined in Table IV. As explained in Appendix B, the condensation of the gas in the slit can be expressed as

$$s = p/p_m - \theta/T_m. \tag{7}$$

Substituting Eq. (6) into Eq. (7), factoring out $p/\gamma p_m$, setting $T_m\beta = 1$, and recognizing that $p_m/\rho_f c_p T_m = (\gamma-1)/\gamma$ for an ideal gas give

$$s = \frac{p}{\gamma p_m}\left\{1 + \frac{c^2}{\omega^2}\left(1 - \frac{\sigma}{\sigma-1}\frac{\cosh[(1+i)y/\delta_\nu]}{\cosh[(1+i)a/\delta_\nu]}\right) \times \frac{\partial p/\partial x}{p}\frac{\partial T_m/\partial x}{T_m}\right.$$

TABLE IV. Symbols used in Eq. (6).

$$f_\nu = \frac{\tanh[(1+i)a/\delta_\nu]}{(1+i)a/\delta_\nu} \qquad f_k = \frac{\tanh[(1+i)a/\delta_k]}{(1+i)a/\delta_k}$$

$$\epsilon_s = \sqrt{\frac{\lambda_h\rho_f c_p}{\lambda_s\rho_s c_s}}\frac{\tanh[(1+i)a/\delta_s]}{\tanh[(1+i)b/\delta_s]}$$

$\delta_\nu = \sqrt{2\nu/\omega}$ — $\delta_k = \sqrt{2\kappa_f/\omega}$

$\delta_s = \sqrt{2\kappa_s/\omega}$ — $\kappa_f = \lambda_h/\rho_f c_p$

$\kappa_s = \lambda_s/\rho_s c_s$ — λ_h = thermal conductivity of the fluid

λ_s = solid thermal conductivity — ρ_s = solid density

c_s = solid specific heat/unit mass — b = half-width of solid

$$+\left[(\gamma-1)+\frac{c^2}{\omega^2}\left(\frac{1+\epsilon f_\nu/f_\kappa}{(\sigma-1)}\frac{\partial p/\partial x}{p}\frac{\partial T_m/\partial x}{T_m}\right)\right]$$
$$\times\frac{1}{1+\epsilon_S}\frac{\cosh[(1+i)y/\delta_\kappa]}{\cosh[(1+i)a/\delta_\kappa]}\Bigg\}. \quad (8)$$

Integrating the condensation across the slit gives

$$\bar{s}=\frac{p}{\gamma p_m}\left[1+\frac{(\gamma-1)f_\kappa}{1+\epsilon_S}+\frac{c^2}{\omega^2}\left(1-\frac{\sigma}{\sigma-1}f_\nu+\frac{f_\kappa+\epsilon f_\nu}{(\sigma-1)(1+\epsilon_s)}\right)\frac{\partial p/\partial x}{p}\frac{\partial T_m/\partial x}{T_m}\right]. \quad (9)$$

We use Zwikker and Kosten's[9] definition of complex compressibility [$C(\omega)=\bar{s}/\bar{p}=\bar{s}/p$] to get

$$C(\omega)=\frac{1}{\gamma p_m}\left[1+\frac{(\gamma-1)f_\kappa}{1+\epsilon_S}+\frac{c^2}{\omega^2}\left(1-\frac{\sigma}{\sigma-1}f_\nu+\frac{f_\kappa+\epsilon f_\nu}{(\sigma-1)(1+\epsilon_s)}\right)\frac{\partial p/\partial x}{p}\frac{\partial T_m/\partial x}{T_m}\right]. \quad (10)$$

For plane traveling waves, $\partial p/\partial x=ik(T_m)p$ and Eq. (10) becomes

$$C(\omega)=\frac{1}{\gamma p_m}\left[1+\frac{(\gamma-1)f_\kappa}{1+\epsilon_S}+ik\frac{c^2}{\omega^2}\left(1-\frac{\sigma}{\sigma-1}f_\nu+\frac{f_\kappa+\epsilon f_\nu}{(\sigma-1)(1+\epsilon_s)}\right)\frac{\partial T_m/\partial x}{T_m}\right]. \quad (11)$$

Finally, referring to Appendix B, we can compute k and z according to

$$k^2=\omega^2C(\omega)\rho_c. \quad (12)$$

The introduction of the complex density ρ_c results in a simple form for the wave equation and allows one to retain the form of Eq. (12). It should be noted, however, that in the process of deriving a wave equation from (B4), we ignored the x dependence of ρ_c, which results in the absence of the terms noted in footnote 11. This is the same level of approximation as using the values of the transport properties at the mean temperature in the stack. The impedance can now be written as

$$z=(k/\omega)/\Omega C(\omega). \quad (13)$$

Note that $C(\omega)$, k, and z depend on the direction of propagation.

The presence of a temperature gradient establishes a difference in propagation constants beyond a simple change in direction. In region 3,

$$p_i^{(3)}=P_i^{(3)}e^{i(\omega t-k_3x)}. \quad (14)$$

The reflected wave is

$$p_r^{(3)}=P_r^{(3)}e^{i(\omega t+k_3'x)}. \quad (15)$$

The only remaining task is to get an expression for P_{total}. The impedance z only enters in these calculations on application of the boundary conditions. At $x=l_3$, $z_3=z_3'=z$ calculated at $T_m=T_{\text{cold}}$. At $x=l_4$, $z_4=z_4'=z$ calculated at $T_m=T_{\text{hot}}$. To include this asymmetry, we must rewrite the boundary conditions at $x=l_3$ as

$$P_i^{(3)}e^{-ik_3l_3}+P_r^{(3)}e^{ik_3'l_3}=P_i^{(4)}e^{-ik_4l_3}+P_r^{(4)}e^{ik_4l_3} \quad (16)$$

and

$$\frac{1}{z_3}P_i^{(3)}e^{-ik_3l_3}-\frac{1}{z_3}P_r^{(3)}e^{ik_3'l_3}=\frac{1}{z_4}(P_i^{(4)}e^{-ik_4l_3}-P_r^{(4)}e^{ik_4l_3}), \quad (17)$$

or rewriting,

$$P_i^{(3)}\left[e^{-ik_3l_3}-B(z_4/z_3)e^{-ik_3l_3}\right]=-P_r^{(3)}\left[e^{ik_3'l_3}+B(z_4/z_3)e^{ik_3'l_3}\right] \quad (18)$$

and

$$P_r^{(3)}=(e^{-ik_3l_3}/e^{ik_3'l_3})([B-1]/[B+1]), \quad (19)$$

where B is defined in Appendix A. Working toward the driving end, we must apply a similar treatment at $x=l_2$,

$$P_i^{(2)}e^{-ik_2l_2}+P_r^{(2)}e^{ik_2l_2}=P_i^{(3)}e^{-ik_3l_2}+P_r^{(3)}e^{ik_3'l_2} \quad (20)$$

and

$$\frac{1}{z_2}(P_i^{(2)}e^{-ik_2l_2}-P_r^{(2)}e^{ik_2l_2})=\frac{1}{z_3'}P_i^{(3)}e^{-ik_3l_2}-\frac{1}{z_3'}P_r^{(3)}e^{ik_3'l_2} \quad (21)$$

or

$$P_i^{(2)}e^{-ik_2l_2}-P_r^{(2)}e^{ik_2l_2}=P_i^{(3)}\left(e^{-ik_3l_2}+e^{-ik_3l_3-ik_3'l_3}\frac{[B-1]}{[B+1]}e^{ik_3'l_2}\right) \quad (22)$$

or

$$P_i^{(2)}e^{-ik_2l_2}-P_r^{(2)}e^{ik_2l_2}=P_i^{(3)}z_2\left(\frac{1}{z_3'}e^{-ik_3l_2}-\frac{1}{z_3'}e^{-ik_3l_3-ik_3'l_3}\times\frac{[B-1]}{[B+1]}e^{ik_3'l_2}\right). \quad (23)$$

Dividing and setting the ratio on the right-hand side equal to C,

$$P_i^{(2)}e^{-ik_2l_2}+P_r^{(2)}e^{ik_2l_2}=CP_i^{(2)}e^{-ik_2l_2}-CP_r^{(2)}e^{ik_2l_2} \quad (24)$$

or

$$P_i^{(2)}e^{-ik_2l_2}[1-C]=-P_r^{(2)}e^{ik_2l_2}[1+C] \quad (25)$$

or

$$P_r^{(2)}=([C-1]/[C+1])e^{-2ik_2l_2}/P_i^{(2)}. \quad (26)$$

The pattern for no temperature gradient derived in Appendix A is now reestablished and P_{total} has the same form as in Appendix A.

Consistent with the discussion below Eq. (12), the speed of sound, viscosity, etc., within the stack are computed at the average temperature of the stack. The results of the calculations are shown in Figs. 4–6, along with the experimental data. These figures are graphs of $1/Q$, which is proportional to the net attenuation in the resonator, versus temperature difference, ranging from zero to that required for

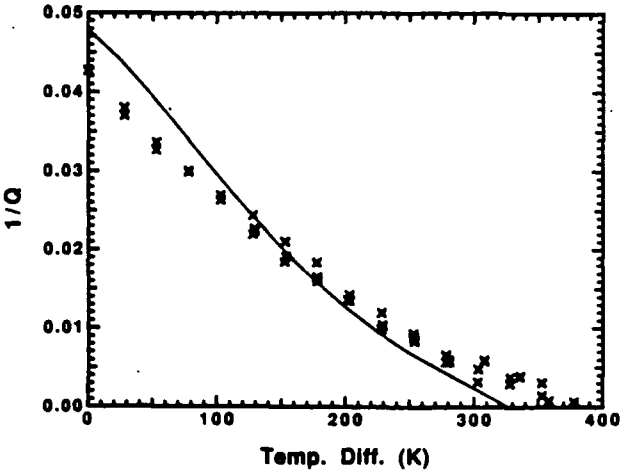

FIG. 4. Graph of $1/Q$ versus the temperature difference across the prime mover stack. The symbols represent the data, while the line represents the results of the calculations. The prime mover is filled with helium at a mean pressure of 170 kPa.

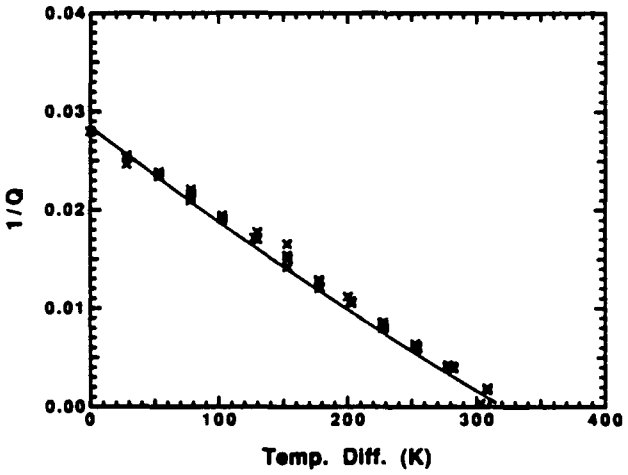

FIG. 5. Graph of $1/Q$ versus the temperature difference across the prime mover stack. The symbols represent the data, while the line represents the results of the calculations. The prime mover is filled with helium at a mean pressure of 376 kPa.

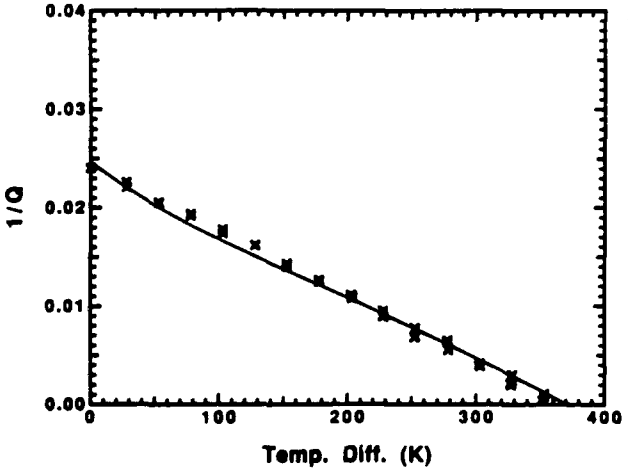

FIG. 6. Graph of $1/Q$ versus the temperature difference across the prime mover stack. The symbols represent the data, while the line represents the results of the calculations. The prime mover is filled with helium at a mean pressure of 500 kPa.

onset of self oscillation. The figures correspond to mean gas pressures of 170, 376, and 500 kPa, respectively. The individual symbols represent the measurements and the lines show the results of the calculations. The agreement between the theory and experiment at the two higher pressures is very good. There are some noticeable differences at the lowest pressure. The theory overpredicts the attenuation at low temperature differences and underpredicts the onset temperature ($1/Q = 0$).

Measurements were also made for the second and third longitudinal modes of the resonator at a mean gas pressure of 170 kPa. The data and calculations are shown in Fig. 7. The $\times$'s and solid lines correspond to the second mode, while the open squares and dashed lines correspond to the third. It was not possible to make measurements near onset for these modes, because the onset temperatures exceed that of the fundamental. The agreement is good. The tendency to overpredict the attenuation at zero gradient decreases, especially for the third mode. No conclusions can be drawn concerning the ability to predict the onset temperature.

III. SUMMARY AND DISCUSSION

The frequency response of a thermoacoustic prime mover has been measured as a function of the mean gas pressure and temperature gradient across the prime mover stack. The frequency response of two simpler resonator configurations was also measured in the absence of an applied gradient. The quality factor Q and resonance frequency were determined from the response. Rather than using a standing wave analysis such as that given by Swift,[1] we have analyzed the results in terms of counterpropagating plane waves, an approach used in studies of the acoustic properties of porous materials. The motivation behind this analysis is to develop the ability to transfer extensive research of porous materials to performance predictions of thermoacoustic devices. This type of analysis will be especially useful when considering the use of alternative geometries in the prime mover stack.

In general, the predictions of the counterpropagating plane-wave analysis are in good agreement with experiment. The predictions of Q and the change in resonance frequency with mean gas pressure are within approximately 5% and 0.4% of measured values for the no temperature gradient cases. In the cases where temperature gradients are present, the agreement is quite good for the two highest mean pressures reported (370 and 500 kPa). There are some noticeable discrepancies at the lowest pressure (170 kPa). Future work should attempt to incorporate the temperature dependence of the thermodynamic properties within the stack.

Surprisingly, some of the worst agreement is for small temperature gradients. The reason for this discrepancy is unknown. There is a tendency to underpredict the onset temperature at the lower pressure and slightly overpredict it at higher pressures. We have not presented data or predictions for the resonance frequency as a function of temperature gradient. However, the predictions agree with measured values to within a few Hz, a discrepancy of approximately 1%.

Even taking into consideration these discrepancies, our analysis provides a good overall prediction of the perfor-

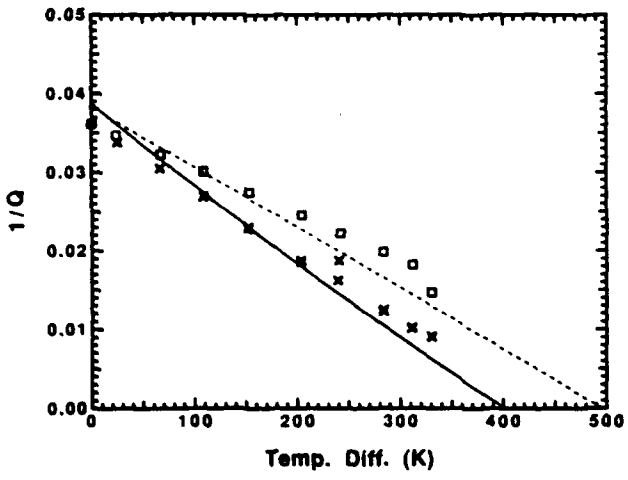

FIG. 7. Graph of $1/Q$ versus the temperature difference across the prime mover stack for the second and third longitudinal modes. The $\times$'s and solid line correspond to the second mode, while the open squares and dashed line correspond to the third. The prime mover is filled with helium at a mean pressure of 170 kPa.

mance of the prime mover below onset. However, the true test is predicting the performance above onset. There are several significant differences between prime movers above and below onset. Most obvious is that the acoustic amplitudes above onset are quite large. Ratios of acoustic pressure amplitude to mean gas pressure of 1%–10% are common. Yet, our analysis is based on linear acoustics. Beyond the theoretical complications added by introducing nonlinear effects, there are a number of experimental complications. For instance, the acoustic displacement amplitudes approach the length of the heat exchangers. Also, because of the large transport of heat, there is no assurance that the temperature gradient along the prime mover stack will be uniform.

The next logical step in this research is to investigate prime movers above onset, but still in the linear acoustics regime. This study requires the use of some type of known additional attenuation to limit the amplitudes. Also, the counterpropagating plane-wave analysis should be compared to Swift's analysis.[1]

ACKNOWLEDGMENTS

The authors are indebted to Keith Attenborough and James Sabatier for many discussions concerning the analysis. This work was supported by the Office of Naval Research and the Naval Postgraduate School Research Program.

APPENDIX A: DERIVATION OF P_{total}

The derivation of P_{total} in the absence of a temperature gradient is presented in this appendix. The combination of elements in the thermoacoustic prime mover creates a series of boundaries, each with a characteristic impedance. The total acoustic field inside the resonant tube will be evaluated by considering the field as a superposition of traveling waves moving in each direction through this series of boundaries and porous elements.

The incident and reflected waves in the five regions can be expressed as

$$p_i^{(1)} = p_i^{(1)} e^{i(\omega t - k_1 x)} \qquad p_r^{(1)} = p_r^{(1)} e^{i(\omega t + k_1 x)}$$
$$\vdots \qquad\qquad \vdots$$
$$p_i^{(5)} = p_i^{(5)} e^{i(\omega t - k_5 x)} \qquad p_r^{(5)} = p_r^{(5)} e^{i(\omega t + k_5 x)}$$

First consider the rigid end at $x = l_5$. For a rigid boundary, $u = 0$. Newton's law gives $\rho_0 \partial u/\partial t = -\nabla p$. Assuming time harmonic plane waves, $\partial u/\partial t = i\omega u$ so $i\omega\rho_0 u = -\nabla p$. Hence, the boundary condition $u = 0$ requires that $\nabla p = 0$ at $x = l_5$ or

$$\left[\nabla(P_i^{(5)} e^{i(\omega t - k_5 x)} + P_r^{(5)} e^{i(\omega t + k_5 x)})\right]_{x = l_5} = 0 \quad \text{(A1)}$$

or

$$P_r^{(5)} = e^{-2ik_5 l_5} P_i^{(5)}. \quad \text{(A2)}$$

Next, consider the boundary at $x = l_4$. Continuity of pressure gives

$$P_i^{(4)} e^{i(\omega t - k_4 l_4)} + P_r^{(4)} e^{i(\omega t + k_4 l_4)} = P_i^{(5)} e^{i(\omega t - k_5 l_4)} + P_r^{(5)} e^{i(\omega t + k_5 l_4)}, \quad \text{(A3)}$$

or, using Eq. (A2),

$$P_i^{(4)} e^{-ik_4 l_4} + P_r^{(4)} e^{ik_4 l_4} = P_i^{(5)} (e^{-ik_5 l_4} + e^{-2ik_5 l_5} e^{ik_5 l_4}). \quad \text{(A4)}$$

Continuity of volume velocity needs to take into account changes in porosity and can be written as

$$\left[U_i^{(4)} + U_r^{(4)} = U_i^{(5)} + U_r^{(5)}\right]_{x = l_4}. \quad \text{(A5)}$$

But $U = Su = Sp/z$, where S is the cross sectional area of the fluid and z is the characteristic impedance of the region. Hence, continuity of volume velocity can be written as

$$(S^{(4)}/z^{(4)})(P_i^{(4)} e^{-ik_4 l_4} - P_r^{(4)} e^{+ik_4 l_4}) = (S^{(5)}/z^{(5)})(P_r^{(5)} e^{-ik_5 l_4} - P_r^{(5)} e^{+ik_5 l_4}). \quad \text{(A6)}$$

Dividing by the cross-sectional area of the empty tube S, defining the porosity $\Omega^{(n)} = S^{(n)}/S$, and further defining the impedance $z_n = z^{(n)}/\Omega^{(n)}$ yield

$$(1/z_4)(P_i^{(4)} e^{-ik_4 l_4} - P_r^{(4)} e^{ik_4 l_4}) = (P_i^{(5)}/z_5)(e^{-ik_5 l_4} - e^{-2ik_5 l_5} e^{ik_5 l_4}). \quad \text{(A7)}$$

Dividing Eq. (A4) by Eq. (A7) and solving for $P_r^{(4)}$ give

$$P_r^{(4)} = e^{-2ik_4 l_4}([A - 1]/[A + 1])P_i^{(4)}, \quad \text{(A8)}$$

where

$$A = \frac{z_5}{z_4} \frac{e^{-ik_5 l_4} + e^{-2ik_5 l_5} e^{ik_5 l_4}}{e^{-ik_5 l_4} - e^{-2ik_5 l_5} e^{ik_5 l_4}}. \quad \text{(A9)}$$

Now we will proceed to the boundary at $x = l_3$:

$$P_i^{(3)} e^{-ik_3 l_3} + P_r^{(3)} e^{ik_3 l_3} = P_i^{(4)} e^{-ik_4 l_3} + P_r^{(4)} e^{ik_4 l_3} \quad \text{(A10)}$$

and

$$(1/z_3)(P_i^{(3)}e^{-ik_3l_3} - P_r^{(3)}e^{ik_3l_3}) = (1/z_4)(P_i^{(4)}e^{-ik_4l_3} - P_r^{(4)}e^{ik_4l_3}), \quad \text{(A11)}$$

so

$$\frac{P_i^{(3)}e^{-ik_3l_3} + P_r^{(3)}e^{ik_3l_3}}{P_i^{(3)}e^{-ik_3l_3} - P_r^{(3)}e^{ik_3l_3}} = \frac{z_4}{z_3}\left(\frac{e^{-ik_4l_3} + e^{-2ik_4l_4}([A-1]/[A+1])e^{ik_4l_3}}{e^{-ik_4l_3} - e^{-2ik_4l_4}([A-1]/[A+1])e^{ik_4l_3}}\right) = B \quad \text{(A12)}$$

and

$$P_r^{(3)} = e^{-2ik_3l_3}([B-1]/[B+1])P_i^{(3)}. \quad \text{(A13)}$$

We can now identify a pattern and write

$$P_r^{(2)} = e^{-2ik_2l_2}([C-1]/[C+1])P_i^{(2)}, \quad \text{(A14)}$$

where

$$C = \frac{z_3}{z_2}\left(\frac{e^{-ik_3l_2} + e^{-2ik_3l_3}([B-1]/[B+1])e^{ik_3l_2}}{e^{-ik_3l_2} - e^{-2ik_3l_3}([B-1]/[B+1])e^{ik_3l_2}}\right), \quad \text{(A15)}$$

and

$$P_r^{(1)} = e^{-2ik_1l_1}([D-1]/[D+1])P_i^{(1)}, \quad \text{(A16)}$$

where

$$D = \frac{z_2}{z_1}\left(\frac{e^{-ik_2l_1} + e^{-2ik_2l_2}([C-1]/[C+1])e^{ik_2l_1}}{e^{-ik_2l_1} - e^{-2ik_2l_2}([C-1]/[C+1])e^{ik_2l_1}}\right). \quad \text{(A17)}$$

Now we must consider the driver. The driver is assumed to deliver a constant displacement l independent of load, $x = le^{i\omega t}$ (provided l is small). In this case, the velocity is $u_0(0,t) = i\omega le^{i\omega t}$. Applying continuity of volume velocity (with the definition of z_n) at $x = 0$,

$$i\omega le^{i\omega t} = \frac{1}{z_1}(P_i^{(1)} - P_r^{(1)})e^{i\omega t} = \frac{1}{z_1}P_i^{(1)}\left(1 - e^{-2ik_1l_1}\frac{[D-1]}{[D+1]}\right)e^{i\omega t}, \quad \text{(A18)}$$

so

$$P_i^{(1)} = i\omega lz_1/[1 - e^{-2ik_1l_1}([D-1]/[D+1])] \quad \text{(A19)}$$

and

$$P_{\text{total}} = P_i^{(1)} + P_r^{(1)} = i\omega lz_1\frac{1 + e^{-2ik_1l_1}([D-1]/[D+1])}{1 - e^{-2ik_1l_1}([D-1]/[D+1])}. \quad \text{(A20)}$$

APPENDIX B: PARALLEL SLITS WITHOUT A TEMPERATURE GRADIENT

Using fundamental concepts from inviscid acoustics, it is easy to show that for plane waves the propagation constant k and characteristic impedance z can be expressed as

$$k^2 = \omega^2 C\rho_f \quad \text{(B1)}$$

and

$$z = (k/\omega)/C. \quad \text{(B2)}$$

In these equations ω is the angular frequency, ρ_f the mean fluid density, and C the compressibility of the medium. One way of defining the compressibility is through the equation of state $p = s/C$, where p is the acoustic pressure and s the condensation. These results must, of course, be modified when considering propagation through porous media to take into account the complications introduced by viscosity and thermal conductivity. The approach commonly taken in porous media analysis is to incorporate the added complexity into the definitions of new parameters, such as the complex density and complex compressibility, leaving the forms of Eqs. (B1) and (B2) unchanged. This analysis is outlined in this appendix. The reader is directed to Refs. 8, 9, and 12 for a more complete analysis.

The average acoustic velocity in the slit formed between two stationary parallel plates separated by $2a$ is[12]

$$\bar{u}_1 = \frac{-1}{i\omega\rho_f}\frac{\partial p}{\partial x}\left(1 - \frac{\tanh[(1+i)a/\delta_v]}{(1+i)a/\delta_v}\right), \quad \text{(B3)}$$

where $\delta_v = (2\nu/\omega)^{1/2}$ and ν is the kinematic viscosity. We define the complex density ρ_c in terms of the pressure gradient and the slit-averaged acoustic velocity such that

$$-\frac{\partial p}{\partial x} = \rho_c\left(\frac{\partial \bar{u}_1}{\partial t}\right). \quad \text{(B4)}$$

To be consistent we should use the slit-averaged pressure gradient in Eq. (B4). However, we have assumed the pressure to be dependent only on x, so this distinction need not be made. Solving Eq. (B3) for $-(\partial p/\partial x)$ and comparing the result to Eq. (B4) give

$$\rho_c = \rho_f\left(1 - \frac{\tanh[(1+i)a/\delta_v]}{(1+i)a/\delta_v}\right)^{-1}. \quad \text{(B5)}$$

The temperature equation is

$$i\omega\rho_f c_p\theta + i\omega p = \lambda_h\frac{\partial^2\theta}{\partial y^2}, \quad \text{(B6)}$$

where λ_h is the coefficient of thermal conduction, θ the difference between slit wall and fluid temperatures, and c_p the isobaric specific heat of the fluid; y is measured perpendicular to the slit wall. Applying the boundary condition that $\theta = 0$ at $y = \pm a$ yields the solution

$$\theta = p/\rho_f c_p\left(1 - \frac{\cosh[(1+i)y/\delta_s]}{\cosh[(1+i)a/\delta_s]}\right). \quad \text{(B7)}$$

A differential form of the ideal gas equation of state is $d\rho/\rho_f = dp/p_m - dT/T_m$. Substituting acoustic quantities for differentials and identifying the condensation as ρ/ρ_f, we have

$$s = p/p_m - \theta/T_m. \quad \text{(B8)}$$

Substituting Eq. (B7) into Eq. (B8) and noting that $p_m/\rho_f c_p T_m = (\gamma - 1)/\gamma$ for an ideal gas give

$$s = \frac{p}{\gamma p_m}\left(1 + (\gamma - 1)\frac{\cosh[(1+i)y/\delta_s]}{\cosh[(1+i)a/\delta_s]}\right). \quad \text{(B9)}$$

Averaging the condensation across the slit gives[12]

$$\bar{s} = \frac{p}{\gamma p_m}\left(1 + (\gamma - 1)\frac{\tanh[(1+i)a/\delta_\kappa]}{[(1+i)a/\delta_\kappa]}\right). \quad \text{(B10)}$$

Zwikker and Kosten[9] define the complex compressibility of the gas in the slit through the slit-averaged equation of state

$$\bar{p} = \bar{s}/C(\omega). \quad \text{(B11)}$$

Substituting Eq. (B10) into Eq. (B11) and keeping in mind that the pressure is assumed constant across the slit, we arrive at the following expression for the complex compressibility:

$$C(\omega) = \frac{1}{\gamma p_m}\left(1 + (\gamma - 1)\frac{\tanh[(1+i)a/\delta_\kappa]}{[(1+i)a/\delta_\kappa]}\right). \quad \text{(B12)}$$

Now that we have the (slit-averaged) complex density and complex compressibility, we can immediately write down the slit-averaged expressions for the propagation constant and impedance. From Eq. (B1),

$$k^2 = \omega^2 C(\omega)\rho_c. \quad \text{(B13)}$$

From Eq. (B2) and the relation $z_n = z/\Omega$ (see Appendix A),

$$z_n = (k/\omega)/\Omega C(\omega). \quad \text{(B14)}$$

To find common ground with those readers familiar with Swift's work, especially Ref. 1, our Eqs. (B3), (B6), and (B7) are identical to (from Ref. 1) the slit-averaged Eq. (A4), and Eqs. (A9) and (A10) in the absence of a temperature gradient, respectively.

[1] G. W. Swift, "Thermoacoustic Engines," J. Acoust. Soc. Am. **84**, 1145–1180 (1988).

[2] J. C. Wheatley and A. Cox, "Natural Engines," Phys. Today **38**, 50 (1985).

[3] N. Rott, "Thermoacoustics," Adv. Appl. Mech. **20**, 135 (1980).

[4] See, for example, S. Temkin, *Elements of Acoustics* (Wiley, New York, 1981), Chap. 3.

[5] J. W. S. Rayleigh, *The Theory of Sound* (1896; reprinted by Dover, Toronto, 1945), Chaps. XI and XII.

[6] K. U. Ingard, *Fundamentals of Waves and Oscillations* (Cambridge U.P., Cambridge, 1988), p. 56, Eq. (9).

[7] F. D. Shields, "Numerical Solution for Sound Velocity and Absorption in Cylindrical Tubes," J. Acoust. Soc. Am. **37**, 724–729 (1965).

[8] K. Attenborough, "Acoustical Characteristics of Porous Materials," Phys. Rep. **82**, 179–227 (1982).

[9] C. Zwikker and C. W. Kosten, *Sound Absorbing Materials* (Elsevier, New York, 1949).

[10] L. S. Han, "Hydrodynamic Entrance Lengths for Incompressible Laminar Flow in Rectangular Ducts," J. Appl. Mech., Trans. ASME **27**, 403–409 (Sept. 1960).

[11] A quadratic equation for the propagation constant can also be derived from Rott's wave equation [Ref. 1, Eq. (A19)]. It can be shown that this equation is identical to Eq. (12) in the limit that ϵ_s and the temperature dependence of f_ν can be ignored.

[12] M. A. Biot, "Theory of Propagation of Elastic Waves in a Fluid-saturated Porous Solid. II. Higher Frequency Range," J. Acoust. Soc. Am. **28**, 179–192 (1956).

THERMOACOUSTIC ENGINES

W. Pat Arnott, Richard Raspet, and Henry E. Bass

Dept. of Physics and Astronomy and the National Center for
Physical Acoustics, University of Mississippi, Univ., MS, 38677

ABSTRACT

Thermoacoustic engines can be used to pump heat using a sound wave or pump a sound wave using a temperature gradient. The basic arrangement is a gas-filled acoustic resonator with appropriately positioned thermoacoustic elements. Two types of thermoacoustic elements are used in these engines: (1) heat exchangers used to communicate heat between the gas and external heat reservoirs; (2) the thermoacoustic engine (TAE), also known as a stack. The TAEs are sections of porous media that support the temperature gradient, transport heat on the acoustic wave between the exchangers, and produce or absorbs acoustic power. Previous results have been developed for TAEs with circular or parallel slit pore geometries. We have extended the theory for gas-filled TAEs to include pores of arbitrary cross-sectional geometry. Included are an introductory section, approximate analysis of energy flow, and acoustical measurements of a thermoacoustic prime mover.

INTRODUCTION

Thermoacoustics is broadly classified as the interaction of heat and sound. The branch of thermoacoustics we consider is heat driven oscillations of gas in a tube and thermoacoustic transport of heat. The basic arrangement is shown in Fig. 1a where thermoacoustic elements of heat exchangers and a TAE are shown in the gas-filled driven resonance tube. The plane wave mode of the resonator is considered to be dominant and pressure and particle velocity have near standing-wave phasing. This arrangement could be used to deliver acoustic power to the TAE for heat transport from cold to hot (for low temperature gradients $(T_H - T_C)/d$) as in a normal refrigerator. Thermoacoustic elements are sections of capillary-tube-type porous media as shown in Fig. 1b. Theory for the system is built from the model for sound in a single arbitrary-perimeter capillary tube as shown in Fig. 1c. Some pore perimeter shapes which have been considered are shown in Fig. 2. Single tube radii are usually designed to equal the frequency-dependent thermal boundary layer thickness δ_T for optimal performance. By removing the acoustic driver and supplying a sufficiently high temperature gradient, the TAE produces acoustic power at the resonant frequency of the system.

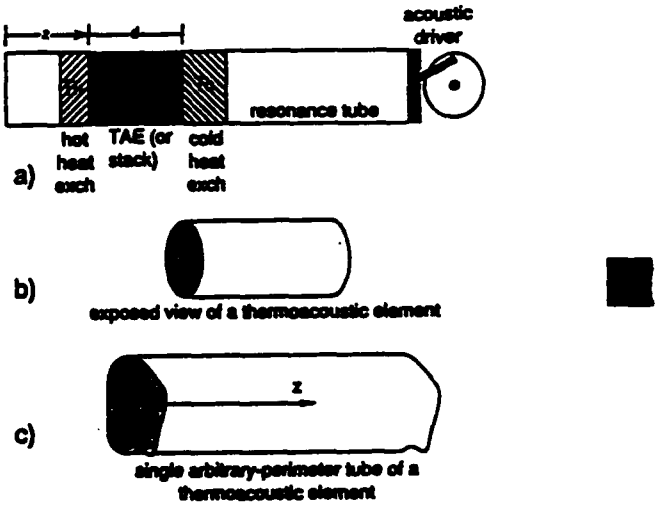

Fig. 1. a) Generic arrangement used in thermoacoustic heat engines. b) An exposed view of a thermoacoustic element consisting of a parallel combination of square capillary tubes. c) A single arbitrary-perimeter capillary tube for use in a thermoacoustic element.

Observations of heat-driven acoustic oscillations date back to at least the eighteenth century. Rayleigh[1] gave a qualitative explanation well-worth quoting: "In almost all cases where heat is communicated to a body, expansion ensues, and this expansion may be made to do mechanical work. If the phases of the forces thus operative be favorable, a vibration may be maintained." Acoustic oscillations were noted to frequently occur in a capillary tube filled with helium vapor with one end of

the tube at approximately 2 K and the other at room temperature and a qualitative explanation similar to Rayleighs was given.[2] A full, linear, theoretical investigation of heat-driven acoustic oscillations was performed first by N. Rott[3] and was explored in a series of papers starting in 1969. Rott has reviewed this work.[4]

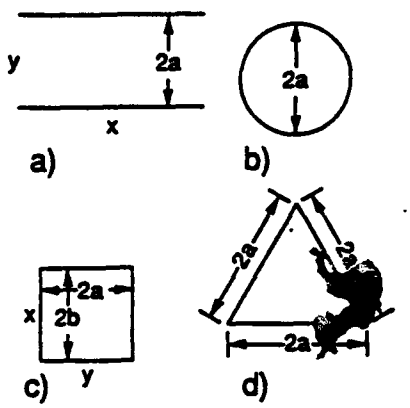

Fig. 2. a) Parallel plate, b) circular, c) rectangular, and d) equilateral triangular capillary tube geometries.

The reciprocal mode of operation, which uses a sound wave in a resonator to transport heat from cold to hot as in a refrigerator, has also been of recent interest. This thermoacoustic streaming has its analogy in acoustic streaming, which is the transport of mass by an acoustic wave.[5] Merkli and Thomann[6] found experimental verification for their theory of thermoacoustic streaming in a driven resonance tube. Wheatley, Swift, Hofler, Garrett and others have developed the notion that the arrangement shown in Fig. 1a can be viewed as a thermodynamic heat engine.[7,8] Swift has expertly reviewed this work.[9] The thermodynamic heat engine point of view enhances the understanding of thermoacoustics and is very helpful in evaluating practical devices. The connection between Refs. 4, 6, and 9 has been briefly explored by Rott.[10] Other references to the early history and practitioners of thermoacoustics can be found in the review articles.[4,9]

A common approach for the theory of sound in porous media is to envision the medium as a collection of circular capillary tubes.[11] The generalization to capillary tubes of arbitrary geometry has recently been explored.[12] The equations and boundary conditions used in porous media modeling and in thermoacoustics are nearly identical (thermoacoustics has an extra term proportional to the ambient temperature gradient that occurs when evaluating the time rate of change of the entropy). It was apparent to us that thermoacoustic theory should be cast in a sufficiently simple form tha analysis of pore geometries other than circles[4] and parallel slits[4,9] would be readily possible.

In particular, we have considered use of extruded ceramic monolithic catalyst supports (for example, the ceramic used in some automobile catalytic convertors) use in thermoacoustics on account of their low thermal conductivity and regular square-pore geometry.[13] This material has main pores of diameter 1.54 mm. In addition, the walls of the main pores are porous as wel with typical wall pores of diameter 25 μm. The frequency-dependent complex propagation constant of sound in the square pore ceramic was measured in relate work.[14] The specific acoustic impedance of a 49 cm long piece was measured both before and after the wall pores were filled. These measurements verified our theory for sound propagation in porous wall porous media.[15] The TAE used in the lecture demonstration w a sample of this ceramic.

We have extended thermoacoustic theory to inclu the acoustic field quantities and the second order energy flow for arbitrary perimeter pores.[16] Heat and work flo were compared in the short stack approximation to investigate the effects of pore geometry. Once the acoustical properties of the separate thermoacoustic elements have been determined the elements must be connected in series inside of a resonator as shown in Fi 1a. Numerical integration of the acoustical equations is used to compute field quantities in the stack since in general a temperature gradient exists from one end to th other.[4,9] The physical parameters of ambient density, viscosity, sound speed, thermal conductivity, etc, are temperature dependent and thus depend on location with the TAE. Specific acoustic impedance and pressure translation theorems were developed[16] to compute all acoustical field quantities and energy flow at each point the resonance tube shown in Fig. 1a.

FLUID PARCEL VIEW OF THERMOACOUSTICS

Figure 3a and 3b depict an inviscid gas parcel oscillating between solid parallel plates at the extremes motion. Heat transfer can usually be neglected in norm low frequency acoustics. However, for parcels near solic surfaces heat exchange is likely to occur. Standing wav phasing is assumed so fluid parcel displacement and

pressure are in phase. The plates have a temperature gradient along them in the direction of oscillation. The location for wall temperature T_0 is nominally the parcel equilibrium location. The magnitude of the temperature gradient determines whether heat is transferred to or from the gas parcel. The right end of the plate faces a pressure antinode and the left end a pressure node. Consider first the heat pump operation in Fig. 3a. The gas parcel is rapidly displaced left a distance d from equilibrium. During displacement parcel pressure and hence temperature diminishes and expansion occurs. At the left-most location, the parcel is momentarily still so the possibility of (slow) heat transfer from the wall occurs. For a small wall temperature gradient, the parcel is now at a lower temperature than the wall so heat flows from the wall to the parcel. After transfer of heat dQ' from the wall to the parcel, the parcel expands to the size shown by the shaded square and work is done by the parcel on the gas to the left. This work discourages vibration of the gas to the left since that gas is in the expansion part of the cycle. The parcel then is displaced to the right a distance 2d. Heat dQ is transferred to the wall from the parcel, and the parcel shrinks to the size shown by the shaded square. The parcel absorbs work from the gas to the right which is in the compressional part of the acoustic cycle. Net heat is transported by the parcel from the wall at temperature $T_0 - \Delta T$ to the wall at temperature $T_0 + \Delta T$. It is now easy to see that heat from an exchanger at the left can be transported up the temperature gradient to a heat exchanger on the right and that acoustic power is absorbed by the parcel.

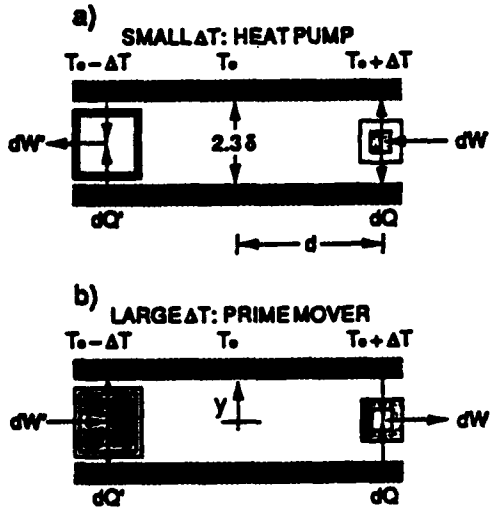

Fig. 3. Lagrangian view of a fluid parcel in a standing wave near a boundary.

Consider next the prime mover in Fig. 3b. The gas parcel is rapidly displaced left a distance d from equilibrium. For a large wall temperature gradient, the parcel is now at a higher temperature than the wall so heat flows from the parcel to the wall. After transfer of heat dQ' from the parcel to the wall, the parcel shrinks to the size shown by the shaded square and work is absorbed by the parcel. This work encourages vibration of the gas to the left since that gas is in the expansion part of the cycle. The parcel then is displaced to the right a distance 2d. Heat dQ is transferred to the parcel from the wall, and the parcel enlarges to the size shown by the shaded square. The parcel delivers work to the gas on the right which is in the compressional part of the acoustic cycle, thus encouraging vibration. Net heat is transported by the parcel from the wall at temperature $T_0 + \Delta T$ to the wall at temperature $T_0 - \Delta T$. It is now easy to see that heat from an exchanger at the right can be transported down the temperature gradient to a heat exchanger on the left and that acoustic power is produced by the parcel.

Viscous and thermal boundary layer thicknesses[9,16] are given by $\delta_\nu = (2\eta/\omega\rho_0)^{1/2}$ and $\delta_\kappa = (2\kappa/\omega\rho_0 c_p)^{1/2}$. We introduce a dimensionless "shear wave number" $\lambda = R(\rho_0\omega/\eta)^{1/2}$ or $\lambda = 2^{1/2} R/\delta_\nu$, where R is a characteristic transverse dimension of the pore in Fig. 1c, and a dimensionless thermal disturbance number $\lambda_T = R(\rho_0\omega c_p/\kappa)^{1/2}$ or $\lambda_T = 2^{1/2} R/\delta_\kappa$. Use of the Prandtl number $N_{pr} = \eta c_p/\kappa$ gives the relation $\lambda_T = \lambda N_{pr}^{1/2}$. For definiteness, take R to be twice the ratio of the transverse pore area to the pore perimeter so for a circular or square pore, R is the pore radius. Consider the *single pore transport function* $F(x,y,\lambda)$ defined by the following partial differential equation[16]:

$$F(x,y;\lambda) + \frac{R^2}{i\lambda^2} \nabla_\tau^2 F(x,y;\lambda) = 1, \qquad (1)$$

subject to the boundary condition that $F(x,y,\lambda) = 0$ at the (arbitrary perimeter) pore wall in Fig. 1c. The average over pore cross-sectional area A is $F(\lambda) = A^{-1} \int F(x,y;\lambda)\, dx\, dy$. All first order acoustic and second order heat equations can be written in terms of $F(x,y;\lambda)$.[16]

HEAT AND WORK FLOW

The short stack approximation was devised by Swift[4] to get an interpretable analytical expression for energy flow using boundary layer theory. For arbitrary pore shapes, see Ref. 16. Figure 1a shows the arrangement for the short stack approximation. Heat exchangers are taken to be of negligible thickness and

thus not to affect near-standing wave phasing. The TAE (or stack) of length d is assumed to be short enough that the empty tube standing wave is marginally affected. The temperature difference between opposite ends of the TAE is assumed to be much less than the average temperature at the TAE center so that the thermophysical quantities are approximately constant and are evaluated at the average temperature. TAE porosity is Ω.

With a rigid termination at z=0 in Fig. 1a, pressure, particle velocity amplitude, particle velocity, and particle displacement amplitude and particle displacement at z are

$$P_1(z) = P_1(0)\ cos\ k_0 z \quad , \tag{2a}$$

$$v_z^s(z) = \frac{P_1(0)}{\Omega \rho_0 c}\ sin\ k_0 z \quad , \tag{2b}$$

$$v_z(z) = i v_z^s(z) \quad , \tag{2c}$$

$$\xi_{sz}^s(z) = \frac{v_z^s(z)}{\omega} \quad , \text{and} \tag{2d}$$

$$\xi_z(z) = -\xi_z^s(z) \quad , \tag{2e}$$

where the wavenumber in the empty tube is k_0, the π phase between pressure and particle displacement is due only to the choice of the coordinate system in Fig. 1a, and the actual pore particle velocity and displacement are shown. When z is less than one quarter of a wavelength, $P_1(z)$, $v_z^s(z)$, and $\xi_z^s(z)$ are all greater than zero. The total time averaged energy flow in the TAE is the sum of heat and work flows, $\dot{H}_2(z) = \dot{Q}_2(z) + \dot{W}_2(z)$.[9,16] Heat flow at the hot end of the TAE (that would flow into a heat exchanger) is

$$\bar{\dot{Q}}_2(z) = -\frac{\Omega A_{res} P_1(z) v_z^s(z)}{2} \beta T_0 \frac{Im\,[F^*(\lambda_T)/F(\lambda)]}{1 + N_{pr}} + \frac{\rho_0 c_p \Omega A_{res} v_z^s(z)}{2} \times \frac{Im\{F^*(\lambda_T) + N_{pr} F(\lambda)\}}{(1 - N_{pr}^2)\,|F(\lambda)|^2} \times \xi_{sz}^s(z) \frac{T_H - T_C}{d} \quad . \tag{3}$$

The first term is due to conversion of acoustic power to heat and this heat flows (in the TAE) *towards* the nearest pressure antinode. The second term is heat transported on account of the temperature gradient and this heat flows in the direction opposite to the positive temperature gradient irregardless of the position of the stack in the standing wave. The terms preceding the temperature gradient are a kind of a dynamical coefficient of thermal conduction. The TAE acts as a refrigerator when the first term is larger than the second. Denote by $T_{0z} = (T_C - T_H)/d$ the temperature gradient across the stack, and denote by Γ the dimensionless critical temperature gradient ratio given by[9,16]

$$\Gamma = -T_{0z} \frac{c_p\ tan\ (k_0 z)}{\omega\ \Omega\ \beta T_0\ c} \quad .$$

In the inviscid approximation for which $N_{pr} = 0$ and $F = 1$,

$$\bar{\dot{Q}}_2(z) = -\frac{A_{res}}{2} \frac{P_1(0)^2}{\rho_0 c} \beta\ T_0\ \frac{sin\ (2k_0 z)}{2} \times Im\ F^*(\lambda_T)\ (1 - \Gamma) \quad .$$

Physically, the term $Im\ F^*(\lambda_T)$ is a measure of the dynamical thermal interaction between the gas and sol If $\Gamma<1$ heat is transported from cold to hot for $2k_0 z <$

No work is done in the region to the left of the stack in Fig. 1a because in this region, pressure and velocity have standing wave phasing. To compute th work done in the stack, use is made of the impedance translation theorem to get the impedance at the right of the stack.[16] Denote by $V_G = A_{res}\,\Omega\,d$ the ambie volume of gas in the TAE. Work flow to first order $k_0 d$ is

$$\bar{\dot{W}}_2(z) = -\omega \frac{V_G P_1^2(z)}{2 \rho_0 c^2} (\gamma - 1)\ Im\ F^*(\lambda_T) - \omega \frac{\rho_0 V_G v_z^{s2}(z)}{2} \frac{Im\ F^*(\lambda)}{|F(\lambda)|^2} + \frac{\Omega A_{res}}{2} P_1(z)\ v_z^s(z)\ \beta \times (T_H - T_C) \frac{Im\{F^*(\lambda_T)/F(\lambda)\}}{1 - N_{pr}}$$

The first and second terms, always < 0, are dissipation of potential and kinetic energy per unit time due to thermal and viscous diffusion processes. The third term, which is > 0 when the hot end faces a pressure antinode, is the acoustic power produced on account of the temperature gradient. When the third term is larger than sum of the first two, the TAE produces net acoustic power. Work flow in the inviscid approximation is

$$\bar{W}_2(z) = -\frac{A_{res}\,\Omega}{2}\,P_1(0)^2\,\frac{T_0\,\beta^2\,\omega\,d}{\rho_0\,c_p}$$

$$\times\, Im\,F^*(\lambda_T)\,cos^2(k_0 z)\,(1-\Gamma)\quad . \qquad (7)$$

Work and heat flow are to be compared for the various pore geometries shown in Fig. 2a-2d. In the inviscid short stack approximation, pores with a large value of $Im\,F(\lambda)^*$ will have the greatest heat and work flows. According to Fig. 4, which shows the real and imaginary parts of $F(\lambda)$ for the various pore geometries, the parallel plate geometry has the largest value of $Im\,F(\lambda)^*$. The value occurs for $\lambda_c = 3.2$ which allows one to compute the optimal operating frequency from the relation $\lambda_c = (\rho_0\,\omega\,c_p/\kappa)^{1/2}\,R$. In other words, you can get about 10% more heat flow and work flow in thermoacoustics by choosing to make your stack from parallel plates rather than the other pore geometries. The functional form of $F(\lambda)$ for the various pore geometries is given in Ref. 16.

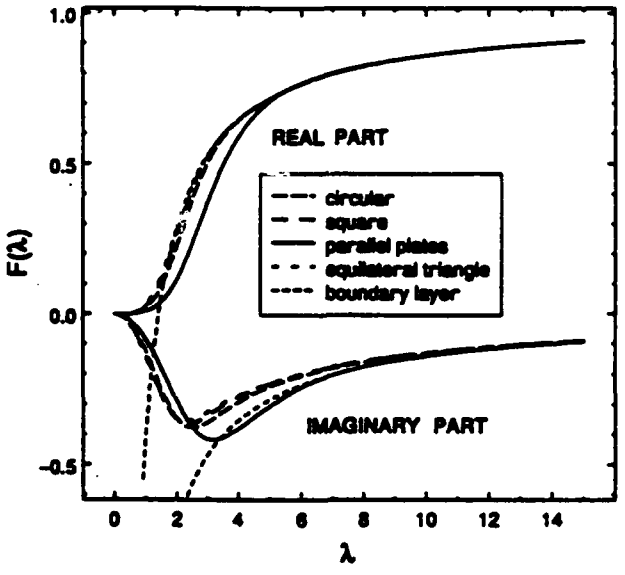

Fig. 4. Real and imaginary part of the $F(\lambda)$ different pore geometries.

AIR-FILLED PRIME MOVER RESULTS

The air-filled thermoacoustic source demonstrated during the lecture is shown schematically in Fig. 5. Heat exchangers were parallel plates of copper and the TAE is a monolithic catalyst support extruded ceramic.[13-15] The two-microphone-technique impedance-tube[17] at the bottom was removed for the demonstration. The nominally quarter-wavelength resonator was capped at the top with a rigid plate and was open at the bottom. Heat tape was wrapped around the hot end (the region including the tube at top and the first heat exchanger) followed by heat insulation. Water was circulated around a jacket surrounding the cold heat exchanger. In this way, a temperature gradient was established across the TAE. For sufficiently high temperature gradients, (ΔT = 176 K) the tube produces sound at 116 Hz. The ambient temperature T_C = 295 K. The location z=0 is nominally a pressure node and particle velocity antinode so the specific acoustic impedance (equal to pressure divided by particle velocity and abbreviated by SAI) is a relative minima for frequencies in the vicinity of the quarter wavelength resonance. All parts were made of copper except the TAE.

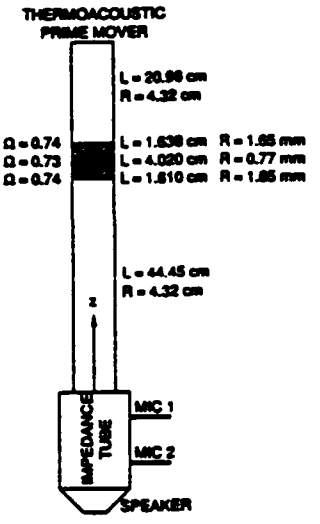

Fig. 5. Demonstration thermoacoustic oscillator and analysis impedance tube.

SAI measurements were made as a function of the temperature gradient across the stack. The real part is shown in Fig. 6 and imaginary in Fig. 7. Among other uses, these measurements are helpful for evaluating the

possibility of using the prime mover as a sound source.[18] One interpretation of Fig. 6 is, for example, that the plane wave reflection coefficient at 80 Hz and ΔT = 160 K is > 1 for waves incident in a tube of the same diameter as the prime mover but in the location of the impedance tube in Fig. 6.[19] Also shown as dashed lines in Fig. 6 and 7 is the expression for radiation impedance for a unflanged tube.[20] The expression is $Z_{rad}(\omega) = -\rho_0 c[(k_0R/2)^2 - i\,0.6\,k_0R]$ where $k_0 = \omega/c$. To determine the frequency of oscillation, we solve for the value of ω such that the complex equation $Z_{rad}(\omega) = Z(\omega)$ measured at z=0. The operating point ΔT = 176 K and f_{res} = 116 Hz of the prime mover demonstrated is shown by the plus symbol in Figs. 6 and 7.

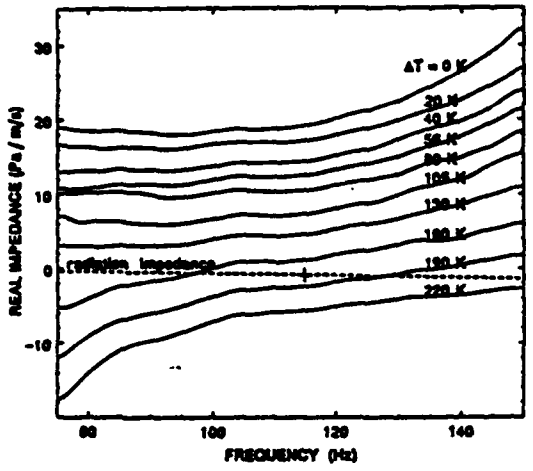

Fig. 6. Real part of the specific acoustic impedance at the mouth of the prime mover.

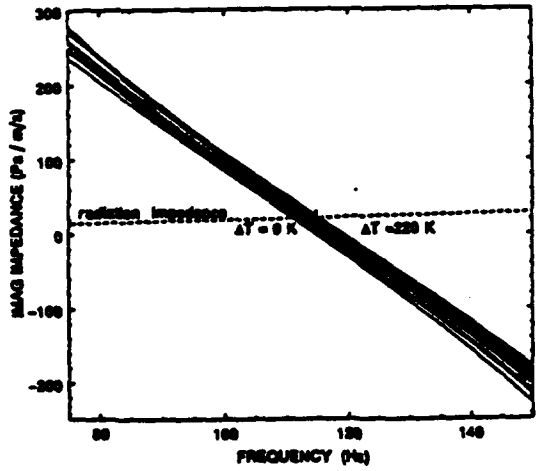

Fig. 7. Imaginary part of the specific acoustic impedance.

To validate the theoretical model, SAI, denoted by $Z(z=0;\omega_c)$ can be calculated at z=0.[16] Most generally, for arbitrary termination impedance $Z_{end}(\omega_c)$ at z=0, the frequency of operation is determined by setting $Z_{end}(\omega_c) = Z(z=0;\omega_c)$.[21] Here $\omega_c = 2\pi f_{res} - i\,\pi f_{res}/Q$ is the complex eigenfrequency of the system where f_{res} is the resonant frequency and Q is the quality factor. Notice that ω_c is a function of the tube geometry and of ΔT. The condition $Q \to \infty$ determines ΔT for onset of acoustic oscillation. The complex eigenfrequency has recently been investigated for a helium or argon-filled prime mover where the resonance tube was sealed at z=0 by a rigid cap.[22] The presence of the strong acoustic wave influences its thermal surroundings[8] by heat transport an in this sense the thermoacoustic oscillation is an exampl of a self-interacting wave process.

With the impedance tube removed in Fig. 5, *measurements* were made of the sound spectrum produce by the prime mover. Figure 8 shows the spectrum for the onset temperature ΔT = 176 K (the peak at 425 Hz was not produced by the prime mover) and for ΔT = 20 K. The ambient temperature was 298 K. A Bruel and Kjaer type 4147 1/2" microphone was placed at z=0 in Fig. 5 for these measurements. The electrical power delivered to the heat tape was 220 watts. The value ΔT 209 K was the steady state equilibrium temperature gradient of the system where heat supplied by the tape was balanced by the sum of the acoustic energy radiated away and dissipated in the resonator, and the heat deposited at the cold heat exchanger due to thermoacous transport plus normal heat conduction down the gradien

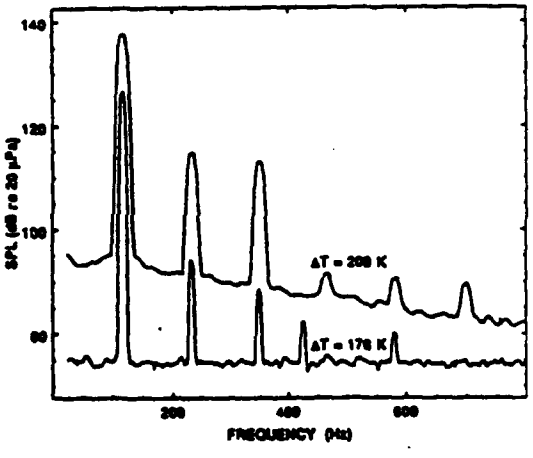

Fig. 8. Prime mover sound spectrum for onset ΔT = K and a higher ΔT = 209 K.

The acoustic power radiated at 116 Hz and $\Delta T = 209$ K was estimated to be 0.25 watts. Some of the applied heat energy goes into the acoustical energy in the band near 116 Hz, in the higher harmonics, and into the steady DC circulation of gas due to acoustic streaming[5,23] that occurs out of the prime mover at the center and returns along the walls.[24] Evidence of acoustic streaming is indicated in Fig. 8 where the generally elevated background level is due to flow induced noise. A flow velocity of 4 m/s was measured for the gas exiting the central part of the prime mover. It is noteworthy that the eigenfrequencies of the quarter wavelength oscillator are given by $f_{res}(2m+1)$ where $m=0,1,...$ and the harmonics of the fundamental due to nonlinear processes[5] are given by $f_h = f_{res}\, n$ where $n = 2,3...$. For example, the peak at 232 Hz does not correspond to any eigenfrequency of the tube, but is predicted by the analysis of strong waves in open tubes.[5] Nonlinearities in closed thermoacoustic oscillators have also been studied.[25]

Figure 9 shows $\Delta T = 209$ K sound produced by the prime mover with the microphone in the opening and 5.7 cm from the bottom (inside of the tube). At the inside point the sound pressure level is 145 dB, 116 Hz. The opening corresponds nominally to a pressure node, so the acoustic pressure $\approx cos(\pi x/2L)$ where x is the distance from the top and $L = 72.7$ cm is the overall length of the prime mover. Consequently the pressure at the top is approximately 8 times the level at 5.7 cm inside, or $\approx$ 163 dB at 116 Hz. The tube radius $R = 4.32$ cm is much less than the acoustic wavelength = 297 cm at 116 Hz, so the prime mover mouth behaves as a point source of spherically expanding waves. Figure 10 shows the sound pressure level for the fundamental at 116 Hz and its harmonics 5.7 cm inside the prime mover, at the mouth, and at distances away from the mouth. Efforts to increase the radiation efficiency of the prime mover in a given direction would result in more radiated acoustic energy and would need to be accommodated by increasing the temperature gradient.

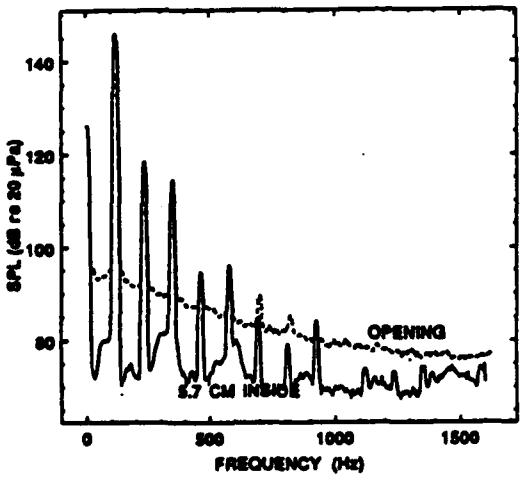

Fig. 9. Prime mover sound spectrum for $\Delta T = 209$ K in the mouth and 5.7 cm inside of the prime mover.

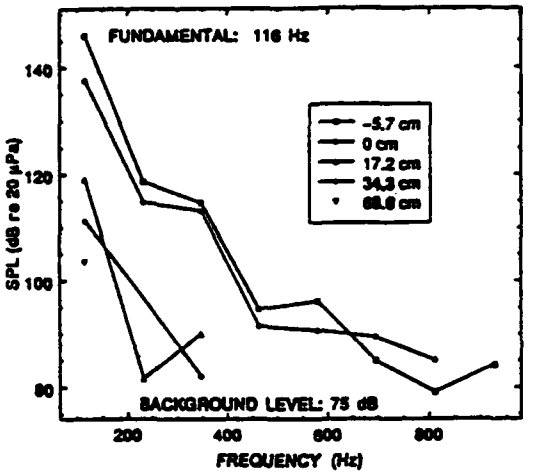

Fig. 10. Spectral peaks as a function of distance from the mouth of the prime mover.

In one experiment the sound production by the prime mover was suppressed and it was super-heated to $\Delta T = 285$ K, well beyond the minimal onset $\Delta T = 176$ K. Figure 11 shows the time evolution of the super-heated prime mover. A microphone was placed = 14 cm from the mouth for this measurement. The top figure shows the first 0.6 seconds. Up to 1.4 seconds the amplitude grows exponentially with time and beyond it begins to level off. The bottom figure is a peak detection of the maximal pressure amplitude, the beginnings of which is shown in the top figure. Between 1.5 and 2 seconds the prime mover flutters as shown on the bottom figure and is apparent to an observer. During this time the built-up heat in the hot end is used up by sound production and thermoacoustic heat transport down the temperature gradient. After 2 seconds the prime mover makes a long transition to a steady-state pressure level and the temperature at the hot end slowly diminishes to the steady state equilibrium value $\Delta T = 209$ K. The time

evolution of a non superheated prime mover has been studied by Muller, et. al.[26]

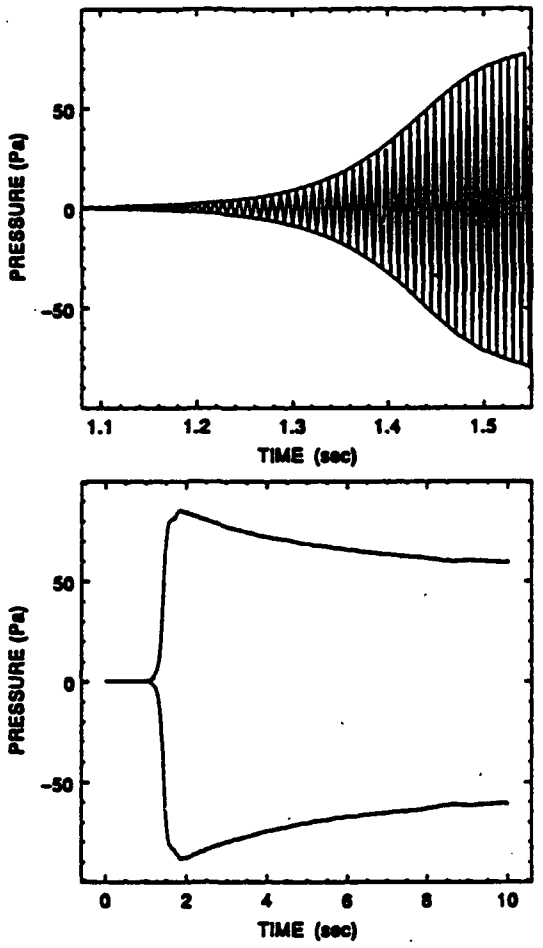

Fig. 11. Time evolution of the superheated prime mover.

ASUNDERY REMARKS

A series of interesting fundamental investigations have been performed using a single circular tube for which the thermal boundary layer thickness was approximately equal to the tube radius.[27-30] Their basic arrangement was a tube closed at one end by a pressure transducer and at the other by varying transducers depending on the particular situation under study. The gaseous helium filled tube was bent to a U-shape and the U-portion was immersed in cold helium gas at temperatures in the range 4.2 to 45 K.[28] The hot end was held at room temperature. They investigated the stability curve of the second tube mode,[30] the stabilit curve of the fundamental mode under a variety of conditions,[29] the universal properties of a thermoacou oscillator at the intersection of the stability curve of th first and second modes,[28] and the universal properties a driven thermoacoustic oscillator.[27] On the practical side, thermoacoustics refrigeration has been a recent to of investigation.[31-34] Traveling wave thermoacoustic engines utilizing the Stirling thermodynamic cycle ha also been of recent interest.[35,36] We acknowledge Of of Naval Research support.

REFERENCES

1. J. W. Strutt Lord Rayleigh, *Theory of Sound* (t volumes), (New York, Dover, 1945 re-issue) V II Secs. 322f and 322g.
2. K. W. Taconis, J. J. M. Beenakker, A. O. C. Nier, and L. T. Aldrich, "Measurements concerning the vapour-liquid equilibrium of solutions of He^3 and He^4 below 2.19 K", Phys 15, 733-739 (1949).
3. N. Rott, "Damped and thermally driven acousti oscillations in wide and narrow tubes," Z. Ange Math. Phys. 20 230-243 (1969).
4. N. Rott, "Thermoacoustics," Adv. Appl. Mech 20, 135-175 (1980).
5. O. V. Rudenko, S. I. Soluyan, *Theoretical Formulations on nonlinear acoustics*, (Plenum, New York, 1977).
6. P. Merkli and H. Thomann, "Thermoacoustic effects in a resonance tube," J. Fluid Mech. 70. 161-177 (1975).
7. J. Wheatley, T. Hofler, G. W. Swift, and A. Migliori, "Experiments with an intrinsicilly irreversible acoustic heat engine," Phys. Rev. L 50, 499-502 (1983).
8. J. Wheatley, T. Hofler, G. W. Swift, and A. Migliori, "An intrinsically irreversible thermoacoustic heat engine," J. Acoust. Soc. A 74, 153-170 (1983).
9. G. W. Swift, "Thermoacoustic engines," J. Acoust. Soc. Am. 84, 1145-1180 (1988).
10. N. Rott, "Thermoacoustic heating at the closed of an oscillating gas column," J. Fluid. Mech. 145, 1-9, (1984). See pg. 5 in particular.
11. C. Zwikker and C. Kosten, *Sound Absorbing Materials* (Elsevier, Amsterdam, 1949).
12. M. R. Stinson, "The propagation of plane soun waves in narrow and wide circular tubes, and generalization to uniform tubes of arbitrary cros sectional shape," J. Acoust. Soc. Am. 89, 550-558, (1991).

13. The ceramics are manufactured by, among others, Corning Incorporated, Industrial Products Division, Corning, New York, 14831. See J. J. Burton and R. L Garten, *Advanced Materials in Catalysis* (Academic Press, New York, 1977) Chapter 10.
14. H. S. Roh, W. P. Arnott, J. M. Sabatier, and R. Raspet, "Measurement and calculation of acoustic propagation constants in arrays of small air-filled rectangular tubes," J. Acoust. Soc. Am 89, 2617-2624, (1991).
15. W. P. Arnott, J. M. Sabatier, R. Raspet, "Sound propagation in capillary-tube-type porous media with small pores in the capillary walls," In press, J. Acoust. Soc. Am.
16. W. P. Arnott, H. E. Bass, R. Raspet, "General formulation of thermoacoustics for stacks having arbitrarily-shaped pore cross-sections," In press, J. Acoust. Soc. Am.
17. A. F. Seybert and D. F. Ross, "Experimental determination of acoustic properties using a two-microphone random-excitation technique," J. Acoust. Soc. Am. 61, 1362-1370 (1977).
18. T. B. Gabrielson, "Radiation from a submerged thermoacoustic source," J. Acoust. Soc. Am. 90, 2628-2636 (1991).
19. A. D. Pierce, *Acoustics: An Introduction to Its Physical Principles and Applications* (American Instutue of Physics, New York, 1989), p. 109.
20. L. E. Kinsler, A. R. Frey, A. B. Coppens, and J. V. Sanders, *Fundamentals of Acoustics* (Wiley, New York, 1982), 3rd ed., p. 202.
21. W. P. Arnott, R. Raspet, H. E. Bass, "Complex eigenfrequency analysis of thermoacoustic heat engines," J. Acoust. Soc. Am. Suppl. 1 89, S2007 (1991).
22. A. Atchley, H. E. Bass, T. J. Hofler, and H. T. Lin, "Study of a thermoacoustic prime mover below onset of self-oscillation," In press, J. Acoust. Soc. Am.
23. N. Rott, "The influence of heat conduction on acoustic streaming," Z. Angew. Math. Phys. 25 417-421 (1974).
24. E. N. Andrade, "On the circulations caused by the vibration of air in a tube," Proc. Roy. Soc. (London) A134, 445-470, (1931).
25. A. A. Atchley, H. E. Bass, and T. J. Hofler, "Development of nonlinear waves in a thermoacoustic prime mover," in *Frontiers of Nonlinear Acoustics: Proceedings of 12th ISNA*, ed. M. F. Hamilton and D. Blackstock (Elsevier, London, 1990) 603-608.
26. V. A. A. Muller, E. Lang, "Experimente mit thermisch getriebenen Gas-Flussigkeits-Schwingungen," Z. Angew. Math. Phys. 36 358-366 (1985).
27. T. Yazaki, S. Sugioka, F. Mizutani, and H. Mamada, "Nonlinear dynamics of a forced thermoacoustic oscillation," Phys. Rev. Lett. 64, 2515-2518 (1990).
28. T. Yazaki, S. Takashima, and F. Mizutani, "Complex quasiperiodic and chaotic states observed in thermally induced oscillations of gas columns," Phys. Rev. Lett. 58, 1108-1111 (1987).
29. T. Yazaki, A. Tominanga, and Y. Narahara, "Experiments on thermally driven acoustic oscillations of gaseous helium," J. Low Temp. Phys. 41, 45-60 (1980).
30. T. Yazaki, A. Tominanga, and Y. Narahara, "Thermally driven acoustic oscillations: Second harmonic," Phys. Lett. 79A, 407-409 (1980).
31. Hofler, T. J., *Thermoacoustic refrigeration design and performance*, Ph.D. Diss., Univ. CA, San Diego, CA, 1986. See also Ref. 9.
32. R. B. Byrnes, *Electronics for autonomous measurement and control of a thermoacoustic refrigerator in a space environment*, Masters Thesis, Naval Postgraduate School, Monterey, CA, 1989.
33. G. A. Bennett, *Active cooling for downhole instrumentation: Miniature thermoacoustic refrigerator*, Ph.D. Diss., Univ. of NM, Albuquerque, NM, 1991.
34. G. W. Swift and R. A. Martin, "First measurements with a thermoacoustic driver for an orifice-pulse-tube refrigerator," J. Acoust. Soc. Am. Suppl. 1 88, S95 (1990).
35. P. H. Ceperley, "Gain and efficiency of a short traveling wave heat engine," J. Acoust. Soc. Am. 77, 1239-1244 (1985).
36. P. H. Ceperley, "A pistonless stirling engine-The traveling wave heat engine," J. Acoust. Soc. Am. 66, 1508-1513 (1979).

Specific acoustic impedance measurements of an air-filled thermoacoustic prime mover

W. Pat Arnott,[a] Henry E. Bass, and Richard Raspet
Physical Acoustics Research Group, Department of Physics and Astronomy, University of Mississippi, University, Mississippi 38677

(Received 24 January 1992; revised 2 July 1992; accepted 10 August 1992)

Thermoacoustic heat engines can be used to produce sound from heat and to transport heat using sound. The air-filled prime mover studied is a quarter wavelength resonator that produces sound at nominally 115 Hz for a temperature difference of $\Delta T = 176$ K. Specific acoustic impedance at the mouth of the prime mover was measured as a function of the temperature difference between the hot and cold heat exchangers. The real part of the impedance changes sign for sufficiently large temperature differences, indicating the possibility of sound production. The theoretically predicted radiation impedance of an open pipe was compared to the measured impedance curves. The operating point was confirmed from the intersection of these experimental and theoretical impedance curves. These measurements allow for analysis of the prime mover as a sound source as discussed in a recent theoretical paper [T. B. Gabrielson, J. Acoust. Soc. Am. **90**, 2628–2636 (1991)].

PACS numbers: 43.35.Ud, 43.85.Bh

INTRODUCTION

Thermoacoustic engines are used to transport heat using sound and to produce sound from heat.[1] The latter application is the focus of this letter. Thermoacoustic sources are also known as prime movers by analogy to heat engines in thermodynamics.[1] Recent work has considered use of thermoacoustic prime movers as underwater sound sources.[2,3] Applications to both gas and liquid-filled prime movers were investigated. A schematic diagram of a prime mover is given in Fig. 1. Starting at the top in Fig. 1, the essential elements are a section of a resonator with a cap on the end to establish a velocity node; a hot heat exchanger, indicated by vertical lines, to inject heat; a heat ionsulating section, shown as the squares region, known as the stack which supports the temperature gradient between the heat exchangers; and a cold heat exchanger to remove excess heat. When the hot heat exchanger faces a velocity node (or pressure antinode), acoustic power can be produced in the stack for sufficiently large temperature gradients. The radiation impedance at the mouth and the length of the resonator determine the conditions for impedance matching the open resonator section and the prime mover.[3] The general utility of the impedance framework was recently developed[4] for the linear theory of thermoacoustics.[5] The utility of impedance measurements for analyzing prime movers is demonstrated experimentally in this letter.

I. PRIME MOVER IMPEDANCE MEASUREMENTS

The experimental arrangement used is shown in Fig. 1. A prime mover was mounted vertically and an impedance tube was attached at the bottom via a flange. The prime mover was built originally for use as a demonstration device and for practice in fabricating the elements. A section of resonator made of copper pipe of length 20.96 cm and inner radius 4.32 cm, and capped at the top, was the first element. High-temperature heat tape was wrapped around the entire section followed by a 1-in. layer of heat insulating material. Heat was transported by conduction to next element which was the hot heat exchanger. A type K thermocouple was placed inside of the hot exchanger to monitor the temperature. The stack (or thermoacoustic engine) that supports the temperature gradient was the next element and will be discussed below. Heat was removed at the cold exchanger by water from the lab sink. Another section of resonator, which was wrapped with water-circulating tubing, was the next element. This section was 44.45 cm long with a radius of 4.32 cm.

The heat exchangers were made by laminating with epoxy copper sheets spaced by aluminum sheets. The copper–aluminum laminate was then turned to a cylindrical shape using a lathe. The cylindrical boundary was cladded with a shell of copper about 2.5 mm thick by using an electroplating technique. The heat exchanger was then machined into a disk form and inserted into a flanged holder for attachment to the other elements. Then the aluminum was etched away using a diluted hydrochloric acid solution. The resulting heat exchanger was made entirely of copper with plate-to-plate spacing of the copper strips equal to 1.65 mm. The cold heat exchanger flange included an open tank for water circulation around the periphery of the plates. The hot and cold exchangers were 1.638 and 1.610 cm long, and had open-to-total volume ratios of $\Omega = 0.74$.

The stack was a ceramic cylindrical sample of a monolithic catalyst support.[6] Reference 7 describes the analysis of some acoustic properties of the catalyst supports. It is a section of a porous medium in which the open pores have square

[a] Current address: Atmospheric Sciences Center, Desert Research Institute, P.O. Box 60220, Sage Bldg., Reno, NV 89506-0220.

 0001-4966/92/123432-03$00.80

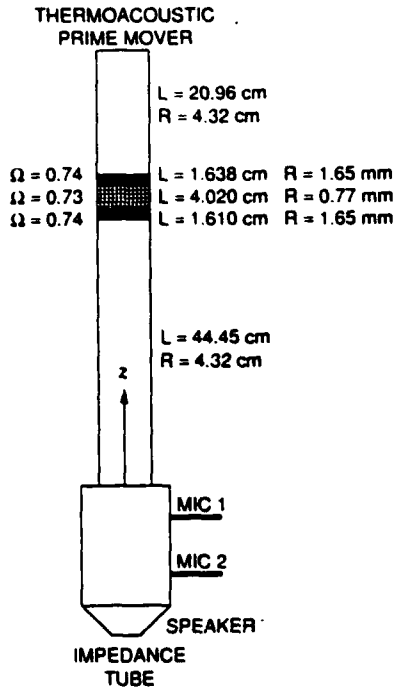

FIG. 1. Air-filled thermoacoustic prime mover ($z > 0$) and impedance tube. Lengths of each thermoacoustic element are given by L, R is the characteristic transverse dimension, and Ω is the porosity. Microphones were separated by 10 cm and were 5 cm from the speaker and prime mover. Impedance tube inner radius was 7.3 cm.

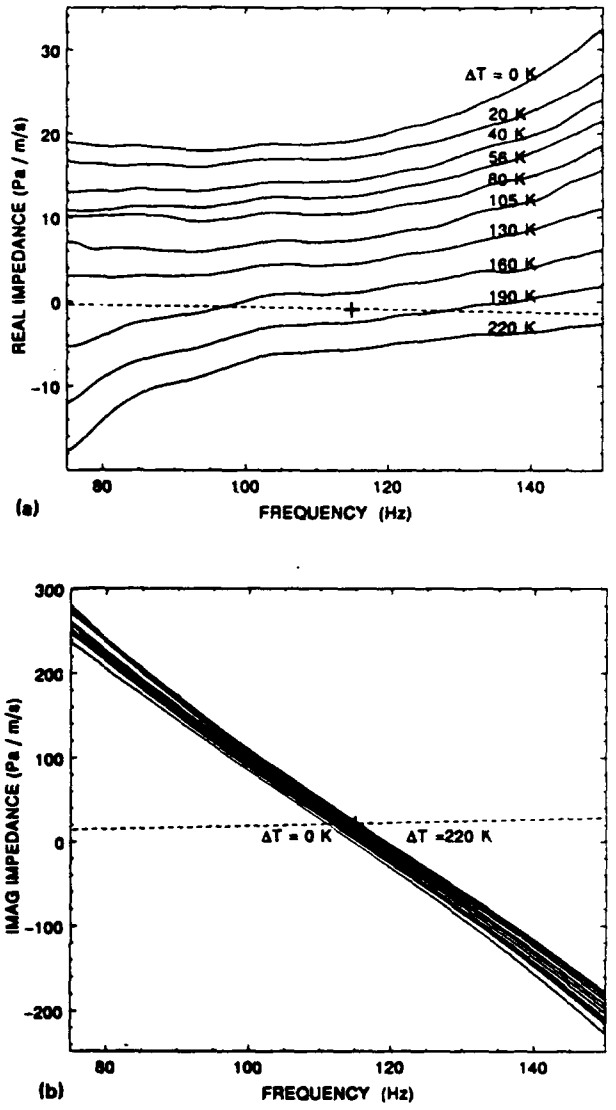

FIG. 2. (a) Real and (b) imaginary parts of the measured specific acoustic impedance (solid lines) as a function of the externally applied temperature difference. The dashed line is the theoretical radiation impedance for the prime mover mouth. The plus symbol locates the operating point of the prime mover at the onset of sound production at 115 Hz and $\Delta T = 176$ K. The ambient temperature was 296 K.

boundaries of semi-width 0.77 mm, and are straight tubes in the z direction (Fig. 1). The ceramic sample had a radius of 7.3 cm. To attach it to the heat exchangers, a ring of inner radius 4.32 cm, outer radius 7.3 cm, and depth 3.2 mm was removed from the ceramic sample. This left a protruding central portion. Copper rings of thickness 3.2 mm, inner radius 4.32 cm, and outer radius of 12 cm were supported between the ends of the ceramic piece using threaded rod stand-offs. Holes were drilled in the copper disks to match the heat exchanger flange holes.

An impedance tube with an inner radius of 7.3 cm was attached at the bottom of the prime mover. Microphones were placed 5 cm from the bottom of the prime mover and the speaker below (10-cm separation). The impedance tube[8] is generally used to determine the specific acoustic impedance (or pressure divided by particle velocity) at $z = 0$ in Fig. 1. Denote by P_1, V_1, and v_1 the pressure, volume velocity, and particle velocity at $z = 0$ in the impedance tube of cross-sectional area $A_1 = 167.5$ cm^2. Denote by subscript 2 the corresponding quantities for the prime mover. Assuming conservation of pressure and volume velocity at the interface, $P_1/V_1 = P_2/V_2$. The quantity measured using the impedance tube was $Z_1 = P_1/v_1 = A_1P_1/V_1 = A_1P_2/V_2 = A_1P_2/(v_2A_2)$. The desired quantity $Z_2 = P_2/v_2$ was thus determined from $Z_2 = Z_1A_2/A_1$. Neglect of interfacial effects of the impedance tube to prime mover radius discontinuity is a low-frequency approximation. The prime mover was evaluated using swept sine wave analysis at sufficiently low amplitudes that negligible heat was transported thermoacoustically. The measured impedance can become a function of the amplitude of driving pressure signal at high levels due to the alteration of the static temperature gradient by thermoacoustic streaming.[9]

The real and imaginary parts of the measured specific acoustic impedance as a function of the temperature difference are shown in Fig. 2(a) and (b). The real part becomes negative at some frequencies, indicating the possibility of having an active system with reflection coefficients greater than one.[10] When the impedance tube is removed, which of course changes the prime mover termination impedance, sound at a nominal frequency of 115 Hz is produced for $\Delta T > 176$ K. The expression for the specific acoustic radiation impedance[11] at the mouth of the prime mover is $Z_{\text{rad}}(\omega) = -\rho_0 c[(k_0R/2)^2 - i\,0.6k_0R]$, where $k_0 = \omega/c$,

ω is the radian frequency, ρ_0 is the ambient air density, c is the adiabatic sound speed of air, and $R = 4.32$ cm is the tube radius. The minus sign occurs because of our choice for the positive direction of z in the coordinated system on Fig. 1. Radiation impedance is represented by the dashed lines in Fig. 2(a) and (b). One immediate check of the measurements is that the initial operating point (115 Hz, $\Delta T = 176$ K) given by the plus symbols occurs, for both the real and imaginary parts of the radiation impedance, at the intersection of the calculated and measured impedance values.

II. CONCLUSION

Specific acoustic impedance measurements were made as a function of the temperature gradient across the stack. Among other uses, these measurements are helpful for evaluating the possibility of using the prime mover as a sound source. Another interpretation of Fig. 2 is, for example, that the plane wave reflection coefficient at 80 Hz and $\Delta T = 160$ K is > 1 for waves incident in an infinite length tube of the same diameter as the prime mover but in the location of the impedance tube in Fig. 1. For prime movers far above the onset of sound production, or for strongly driven thermoacoustic refrigerators, the temperature distribution from hot to cold is not simply the static distribution established by the thermal conductivity of the gas and stack. The presence of the strong acoustic wave influences its thermal surroundings[9] by heat transport and in this sense the thermoacoustic oscillation is an example of a self-interacting wave process.

ACKNOWLEDGMENTS

This work was supported by the Office of Naval Research.

[1] G. W. Swift, "Thermoacoustic engines," J. Acoust. Soc. Am. **84**, 1145–1180 (1988).

[2] G. W. Swift and A. Fusco, "Seawater as a thermoacoustic working fluid," J. Acoust. Soc. Am. Suppl. 1 **84**, S37 (1988).

[3] T. B. Gabrielson, "Radiation from a submerged thermoacoustic source," J. Acoust. Soc. Am. **90**, 2628–2636 (1991).

[4] W. P. Arnott, H. E. Bass, and R. Raspet, "General formulation of thermoacoustics for stacks having arbitrarily shaped pore cross sections," J. Acoust. Soc. Am. **91**, 3228–3237 (1991).

[5] N. Rott, "Thermoacoustics," Adv. Appl. Mech. **20**, 135–175 (1980).

[6] The ceramics are manufactured by, among others, Corning Incorporated, Industrial Products Division, Corning, New York 14831. For a discussion of their properties, see J. J. Burton and R. L. Garten, *Advanced Materials in Catalysis* (Academic, New York, 1977), Chap. 10.

[7] H. S. Roh, W. P. Arnott, J. M. Sabatier, and R. Raspet, "Measurement and calculation of acoustic propagation constants in arrays of small air-filled rectangular tubes," J. Acoust. Soc. Am. **89**, 2617–2624 (1991); W. P. Arnott, J. M. Sabatier, and R. Raspet, "Sound propagation in capillary-tube-type porous media with small pores in the capillary walls," J. Acoust. Soc. Am. **91**, 3299–3306 (1991).

[8] A. F. Seybert and D. F. Ross, "Experimental determination of acoustic properties using a two-microphone random-excitation technique," J. Acoust. Soc. Am. **61**, 1362–1370 (1977).

[9] J. Wheatley, T. Hofler, G. W. Swift, and A. Migliori, "An intrinsically irreversible thermoacoustic heat engine," J. Acoust. Soc. Am. **74**, 153–170 (1983).

[10] A. D. Pierce, *Acoustics: An Introduction to Its Physical Principles and Applications* (American Institute of Physics, New York, 1989), p. 109.

[11] L. E. Kinsler, A. R. Frey, A. B. Coppens, and J. V. Sanders, *Fundamentals of Acoustics* (Wiley, New York, 1982), 3rd ed., p. 202.